

TESIS DE LA UNIVERSIDAD
DE ZARAGOZA

2021

162

Jonathan Pitocchi

Computer Aided Tools for the Design and Planning of Personalized Shoulder Arthroplasty

Director/es

van Lenthe, G. Harry
Pérez Ansón, María Ángeles

<http://zaguan.unizar.es/collection/Tesis>

ISSN 2254-7606



Premsas de la Universidad
Universidad Zaragoza



Universidad
Zaragoza

Tesis Doctoral

COMPUTER AIDED TOOLS FOR THE DESIGN AND
PLANNING OF PERSONALIZED SHOULDER
ARTHROPLASTY

Autor

Jonathan Pitocchi

Director/es

van Lenthe, G. Harry
Pérez Ansón, María Ángeles

UNIVERSIDAD DE ZARAGOZA
Escuela de Doctorado

2021



Instituto Universitario de Investigación
de Ingeniería de Aragón
Universidad Zaragoza

ESCUELA DE DOCTORADO



ARENBERG DOCTORAL SCHOOL
Faculty of Engineering Science

Computer Aided Tools for the Design and Planning of Personalized Shoulder Arthroplasty

Jonathan Pitocchi

Supervisors:

Prof. dr. ir. M^a Angeles Pérez

Prof. dr. ir. G. H. van Lenthe

Dissertation presented in partial
fulfillment of the requirements
for the degree of Doctor from Unizar
and the degree of Doctor of Engineering
Science (PhD): Mechanical Engineering
from KU Leuven

December 2020

Computer Aided Tools for the Design and Planning of Personalized Shoulder Arthroplasty

Jonathan PITOCCHI

Examination committee:

Prof. dr. ir. M^a Angeles Pérez, supervisor

Prof. dr. ir. G. H. van Lenthe, supervisor

Prof. dr. ir. J. M. Garcia Aznar

Prof. dr. ir. J. Vander Sloten

Prof. dr. P. Debeer (UZ Leuven)

Dr. ir. R. Wirix-Speetjens (Materialise NV)

Prof. dr. ir. M. Malvè (University of Navarre)

Prof. dr. E. Audenaert (UZ Gent)

Prof. dr. F. van der Helm (TU Delft)

Dissertation presented in partial fulfillment of the requirements for degree of Doctor from Unizar and the degree of Doctor of Engineering Science (PhD): Mechanical Engineering from KU Leuven

December 2020

© 2020 KU Leuven – Faculty of Engineering Science
Uitgegeven in eigen beheer, Jonathan Pitocchi, Celestijnenlaan 300C box 2419, B-3001 Leuven (Belgium)

Alle rechten voorbehouden. Niets uit deze uitgave mag worden vermenigvuldigd en/of openbaar gemaakt worden door middel van druk, fotokopie, microfilm, elektronisch of op welke andere wijze ook zonder voorafgaande schriftelijke toestemming van de uitgever.

All rights reserved. No part of the publication may be reproduced in any form by print, photoprint, microfilm, electronic or any other means without written permission from the publisher.

Abstract

Shoulder arthroplasty is the third most common joint replacement procedure, after knee and hip arthroplasty, and currently the most rapidly growing one in the orthopaedic field. The main surgical options include total shoulder arthroplasty (TSA), in which the normal joint anatomy is restored, and, for patients with a completely torn rotator cuff, reverse shoulder arthroplasty (RSA), in which the ball and the socket of the glenohumeral joint are switched. Despite the recent progress and advancement in design, the reported rates of complication for RSA are higher than those of conventional shoulder arthroplasty. A patient-specific approach, in which clinicians adapt the surgical management to patient characteristics and preoperative condition, e.g. through custom implants and pre-planning, can help to reduce postoperative problems and improve the functional outcome. The main goal of this thesis is to develop and evaluate novel methods for personalized RSA, using state-of-the-art computer aided technologies to standardize and automate the design and planning phases.

Custom implants are a suitable solution when treating patients with extensive glenoid bone loss. However, clinical engineers are confronted with an enormous implant design space (number and type of screws, contact surface, etc.) and large anatomical and pathological variability. Currently, no objective tools exist to guide them when choosing the optimal design, i.e. with sufficient initial implant stability, thus making the design process tedious, time-consuming, and user-dependent. In this thesis, a Virtual Bench Test (VBT) simulation was developed using a finite element model to automatically evaluate the initial stability of custom shoulder implants. Through a validation experiment, it was shown that the virtual test bench output can be used by clinical engineers as a reference to support their decisions and adaptations during the implant design process.

When designing shoulder implants, knowledge about bone morphology and bone quality of the scapula throughout a certain population is fundamental. In particular, regions with the best bone stock (cortical bone) are taken into account to define the position and orientation of the screw holes, while aiming for an optimal fixation. As an alternative to manual measurements, whose generalization is limited by the analysis of small sub-sets of the potential patients, Statistical Shape Models (SSMs) have been commonly used to describe shape variability within a population. However, these SSMs typically do not contain information about cortical thickness. Therefore, a methodology to combine scapular bone shape and cortex morphology in an SSM was developed. First, a method to estimate cortical thickness, starting from a profile analysis of Hounsfield Unit (HU), was presented and evaluated. Then, using 32 manually segmented healthy scapulae, a statistical shape model including cortical information was created and assessed. The developed tool can be used to virtually implant a new design and test its congruency inside a generated virtual population, thus reducing the number of design iterations and cadaver labs.

Measurements of deltoid and rotator cuff muscle elongation during surgical planning can help clinicians to select a suitable implant design and position. However, such an assessment requires the indication of anatomical landmarks as a reference for the muscle attachment points, a process that is time-consuming and user-dependent, since often performed manually. Additionally, the medical images, which are normally used for shoulder arthroplasty, mostly contain only the proximal humerus, making it impossible to indicate those muscle attachment points which lie outside of the field of view of the scan. Therefore, a fully-automated method, based on SSM, for measuring deltoid and rotator cuff elongation was developed and evaluated. Its clinical applicability was demonstrated by assessing the performance of the automated muscle elongation estimation for a set of arthritic shoulder joints used for preoperative planning of RSA, thus confirming it a suitable tool for surgeons when evaluating and refining clinical decisions.

In this research, a major step was taken into the direction of a more personalized approach to Reverse Shoulder Arthroplasty, in which the surgical management, i.e. implant design and position, is adapted to the patient-specific characteristics and preoperative condition. By applying computer aided technologies in the clinical practice, design and planning process can be automated and standardized, thus reducing costs and lead times. Additionally, thanks to the novel methods presented in this thesis, we expect in the future a wider adoption of the personalized approach, with important benefits both for surgeons and patients.

Resumen

La artroplastia de hombro es el tercer procedimiento de reemplazo articular más común, después de la artroplastia de rodilla y cadera, y actualmente es el de más rápido crecimiento en el campo ortopédico. Las principales opciones quirúrgicas incluyen la artroplastia total de hombro (TSA), en la que se restaura la anatomía articular normal, y, para pacientes con un manguito rotador completamente desgarrado, la artroplastia inversa de hombro (RSA), en la que la bola y la cavidad de la articulación glenohumeral se cambian. A pesar del progreso reciente y los avances en el diseño, las tasas de complicaciones reportadas para RSA son más altas que las de la artroplastia de hombro convencional. Un enfoque específico para el paciente, en el que los médicos adaptan el tratamiento quirúrgico a las características del mismo y al estado preoperatorio, por ejemplo mediante implantes personalizados y planificación previa, puede ayudar a reducir los problemas postoperatorios y mejorar el resultado funcional. El objetivo principal de esta tesis es desarrollar y evaluar métodos novedosos para RSA personalizado, utilizando tecnologías asistidas por ordenador de última generación para estandarizar y automatizar las fases de diseño y planificación.

Los implantes personalizados son una solución adecuada para el tratamiento de pacientes con pérdida extensa de hueso glenoideo. Sin embargo, los ingenieros clínicos se enfrentan a muchas variables en el diseño de implantes (número y tipo de tornillos, superficie de contacto, etc.) y una gran variabilidad anatómica y patológica. Actualmente, no existen herramientas objetivas para guiarlos a la hora de elegir el diseño óptimo, es decir, con suficiente estabilidad inicial del implante, lo que hace que el proceso de diseño sea tedioso, lento y dependiente del usuario. En esta tesis, se desarrolló una simulación de Virtual Bench Test (VBT) utilizando un modelo de elementos finitos para evaluar automáticamente la estabilidad inicial de los implantes de hombro personalizados. A través de un experimento de validación, se demostró que los ingenieros clínicos pueden utilizar el resultado de Virtual Bench Test como referencia para respaldar sus decisiones y adaptaciones durante el proceso de diseño del implante.

Al diseñar implantes de hombro, el conocimiento de la morfología y la calidad ósea de la escápula en toda la población es fundamental. En particular, se tienen en cuenta las regiones con la mejor reserva ósea (hueso cortical) para definir la posición y orientación de los orificios de los tornillos, mientras se busca una fijación óptima. Como alternativa a las mediciones manuales, cuya generalización está limitada por el análisis de pequeños subconjuntos de pacientes potenciales, Statistical Shape Models (SSMs) se han utilizado comúnmente para describir la variabilidad de la forma dentro de una población. Sin embargo, estos SSMs normalmente no contienen información sobre el grosor cortical. Por lo tanto, se desarrolló una metodología para combinar la forma del hueso escapular y la morfología de la cortical en un SSM. Primero, se presentó y evaluó un método para estimar el espesor cortical, a partir de un análisis de perfil de Hounsfield Unit (HU). Luego, utilizando 32 escápulas sanas segmentadas manualmente, se creó y evaluó un modelo de forma estadística que incluía información de la cortical. La herramienta desarrollada se puede utilizar para implantar virtualmente un nuevo diseño y probar su congruencia dentro de una población virtual generada, reduciendo así el número de iteraciones de diseño y experimentos con cadáveres.

Las mediciones del alargamiento de los músculos deltoides y del manguito rotador durante la planificación quirúrgica pueden ayudar a los médicos a seleccionar un diseño y una posición de implante adecuados. Sin embargo, tal evaluación requiere la indicación de puntos anatómicos como referencia para los puntos de unión de los músculos, un proceso que requiere mucho tiempo y depende del usuario, ya que a menudo se realiza manualmente. Además, las imágenes médicas, que se utilizan normalmente para la artroplastia de hombro, contienen en su mayoría solo el húmero proximal, lo que hace imposible indicar los puntos de unión de los músculos que se encuentran fuera del campo de visión de la exploración. Por lo tanto, se desarrolló y evaluó un método totalmente automatizado, basado en SSM, para medir la elongación del deltoides y del manguito rotador. Su aplicabilidad clínica se demostró mediante la evaluación del rendimiento de la estimación automatizada de la elongación muscular para un conjunto de articulaciones artríticas del hombro utilizadas para la planificación preoperatoria de RSA, lo que confirma que es una herramienta adecuada para los cirujanos a la hora de evaluar y refinar las decisiones clínicas.

En esta investigación, se dio un paso importante en la dirección de un enfoque más personalizado de la artroplastia inversa de hombro, en el que el manejo quirúrgico, es decir, el diseño y la posición del implante, se adapta a las características específicas del paciente y al estado preoperatorio. Al aplicar tecnologías asistidas por computadora en la práctica clínica, el proceso de diseño y planificación se puede automatizar y estandarizar, reduciendo así los costos y los plazos de entrega. Además, gracias a los métodos novedosos presentados

en esta tesis, esperamos en el futuro una adopción más amplia del enfoque personalizado, con importantes beneficios tanto para los cirujanos como para los pacientes.

Beknopte samenvatting

Schouderartroplastie is de derde meest voorkomende gewrichtsvervangingsprocedure, na knie- en heupartroplastiek, en momenteel de snelst groeiende op orthopedisch gebied. De belangrijkste chirurgische opties omvatten totale schouderartroplastie (TSA), waarbij de normale gewrichtsanatomie wordt hersteld, en, voor patiënten met rotator cuff arthropatie, omgekeerde schouderartroplastiek (RSA), waarbij de bal en de kom van het glenohumerale gewricht zijn omgekeerd. Ondanks de recente vooruitgang in het ontwerp, zijn de gerapporteerde complicaties bij RSA hoger dan bij conventionele schouderprothesen. Een patiëntspecifieke benadering, waarbij klinici de chirurgische behandeling aanpassen aan de kenmerken van de patiënt en de preoperatieve toestand, b.v. door op aangepaste implantaten en pre-planning, kan het postoperatieve problemen helpen verminderen en het functionele resultaat verbeteren. Het belangrijkste doel van dit proefschrift is het ontwikkelen en evalueren van nieuwe methoden voor gepersonaliseerde RSA, waarbij gebruik wordt gemaakt van de modernste computerondersteunde technologieën om de ontwerp- en planningsfasen te standaardiseren en automatiseren.

Aangepaste implantaten zijn een geschikte oplossing bij de behandeling van patiënten met uitgebreid glenoïdbotverlies. Klinisch ingenieurs worden echter geconfronteerd met een enorme ontwerpruimte voor implantaten (aantal en type schroeven, contactoppervlak, enz.) en een grote anatomische en pathologische variabiliteit. Momenteel bestaan er geen objectieve hulpmiddelen om hen te begeleiden bij het kiezen van het optimale ontwerp, d.w.z. met voldoende initiële implantaatstabiliteit, waardoor het ontwerpproces langdradig, tijdrovend en gebruikersafhankelijk wordt. In dit proefschrift is een Virtual Bench Test (VBT) ontwikkeld met behulp van een eindige-elementenmodel om automatisch de initiële stabiliteit van aangepaste schouderimplantaten te evalueren. Door middel van een validatie-experiment werd aangetoond dat de output van de Virtual Bench Test door klinische ingenieurs kan worden gebruikt als referentie ter ondersteuning van hun beslissingen en aanpassingen tijdens het ontwerpproces

van het implantaat.

Bij het ontwerpen van schouderimplantaten is kennis over botmorfologie en botkwaliteit van de scapula in de hele populatie fundamenteel. In het bijzonder wordt rekening gehouden met de gebieden met de beste botvoorraad (corticaal bot) om de positie en oriëntatie van de schroefgaten te bepalen, waarbij wordt gestreefd naar een optimale fixatie. Als alternatief voor handmatige metingen, waarvan de generalisatie wordt beperkt door de analyse van kleine subgroepen van de potentiële patiënten, worden Statistical Shape Models (SSM's) vaak gebruikt om vormvariabiliteit binnen een populatie te beschrijven. Deze SSM's bevatten echter doorgaans geen informatie over de corticale dikte. Daarom werd een methodologie ontwikkeld om scapulaire botvorm en cortexmorfologie te combineren in een SSM. Eerst werd een methode gepresenteerd en geëvalueerd om de corticale dikte te schatten, uitgaande van een profielanalyse van Hounsfield Units (HU). Vervolgens werd met behulp van 32 handmatig gesegmenteerde gezonde scapulae een statistical shape model met corticale informatie gemaakt en beoordeeld. De ontwikkelde tool kan worden gebruikt om virtueel een nieuw ontwerp te implanteren en de overeenstemming ervan te testen binnen een gegenereerde virtuele populatie, waardoor het aantal ontwerp-iteraties en testen op donorschouders wordt verminderd.

Metingen van spierverlenging in de deltaspijer en rotator cuff tijdens de chirurgische planning kunnen klinici helpen bij het kiezen van een geschikt implantaatontwerp en -positie. Een dergelijke beoordeling vereist echter de indicatie van anatomische oriëntatiepunten als referentie voor de spieraanhechtingspunten, een proces dat tijdrovend en gebruikersafhankelijk is, aangezien het vaak handmatig wordt uitgevoerd. Bovendien bevatten de medische beelden, die normaal gesproken worden gebruikt voor schouderprothesen, meestal alleen de proximale humerus, waardoor het onmogelijk is om die spieraanhechtingspunten aan te geven die buiten het gezichtsveld van de scan liggen. Daarom werd een volledig geautomatiseerde methode, gebaseerd op SSM, voor het meten van de verlenging van de deltaspijer en rotator cuff ontwikkeld en geëvalueerd. De klinische toepasbaarheid ervan werd aangetoond door het bepalen van de nauwkeurigheid van de geautomatiseerde schatting van de spierverlenging voor een reeks artritische schoudergewrichten die worden gebruikt voor preoperatieve planning van RSA. Hiermee werd dat het een geschikt hulpmiddel is voor chirurgen bij het evalueren en verfijnen van klinische beslissingen.

In dit onderzoek werd een grote stap gezet in de richting van een meer gepersonaliseerde benadering van omgekeerde schouderartroplastiek, waarbij de chirurgische behandeling, d.w.z. het ontwerp en de positie van het implantaat, wordt aangepast aan de patiëntspecifieke kenmerken en preoperatieve toestand. Door computerondersteunde technologieën toe te passen in de klinische praktijk, kunnen ontwerp- en planningsprocessen worden geautomatiseerd en gestandaard-

diseerd, waardoor kosten en doorlooptijden worden verminderd. Bovendien verwachten we, dankzij de nieuwe methoden die in dit proefschrift worden gepresenteerd, in de toekomst een breder gebruik van de gepersonaliseerde benadering, met belangrijke voordelen voor zowel chirurgen als patiënten.

List of Abbreviations

ASME	American Society of Mechanical Engineers
ASTM	American Society for Testing and Materials
AVN	Avascular necrosis
CAN	Computer-assisted navigation
CoCr	Cobalt-Chrome
COR	Center of rotation
CT	Computed tomography
CTA	Cuff tear arthropathy
DVRT	Differential variable reluctance transducer
EID	European industrial doctorate
FDA	Food and Drug Administration
FE	Finite element
HU	Hounsfield unit
IQR	Interquartile range
OA	Osteoarthritis
PCF	Pound-force per cubic foot
PSI	Patient-specific instrumentation
PTA	Post-traumatic arthritis
RA	Rheumatoid arthritis
RMS	Root mean square error
ROM	Range of motion
RSA	Reverse shoulder arthroplasty
SLM	Selective laser melting
SSM	Statistical shape model
VBT	Virtual bench test
TSA	Total shoulder arthroplasty
2D	Two-dimensional
3D	Three-dimensional

Contents

Abstract	i
Resumen	iii
Beknopte samenvatting	vii
List of Abbreviations	xi
List of Figures	xvii
1 Introduction	1
1.1 Motivation	1
1.2 Aim	4
1.2.1 Objective 1: Virtual Bench Test for design of custom shoulder implants	4
1.2.2 Objective 2: Assessment of scapular cortical thickness using statistical models	5
1.2.3 Objective 3: Automated landmarking for muscle elonga- tion measurement during RSA	5
1.3 Thesis Outline	6
2 Background	7
2.1 Introduction to the shoulder joint	8

2.1.1	Shoulder Joint Anatomy	8
2.1.2	Shoulder Joint Pathology	12
2.1.3	Shoulder Joint Arthroplasty	15
2.2	Personalized Reverse Shoulder Arthroplasty	18
2.2.1	Custom Glenoid Implants	18
2.2.2	Preoperative Planning	21
3	Virtual Bench Test for design of custom shoulder implants	25
3.1	Introduction	26
3.1.1	Motivation	26
3.1.2	Finite Element Models for Implant Design	27
3.2	Material and Methods	29
3.2.1	Experimental set-up for model validation	29
3.2.2	Generation of Finite Element Models	30
3.2.3	Screw Model	31
3.2.4	Statistical analyses and sensitivity study	34
3.3	Results	35
3.4	Discussion	36
3.4.1	Limitations	40
3.4.2	Conclusion	41
4	Assessment of scapular cortical thickness using statistical models	43
4.1	Introduction	44
4.1.1	Motivation	44
4.1.2	State of the Art	44
4.1.3	Aim	45
4.2	Material and Methods	46
4.2.1	Data	46

4.2.2	Cortical thickness estimation	46
4.2.3	Validation of cortical thickness estimation	47
4.2.4	SSM construction	48
4.2.5	SSM evaluation	48
4.3	Results	49
4.3.1	Cortical thickness estimation	49
4.3.2	SSM analysis	49
4.4	Discussion and Limitations	53
4.4.1	Conclusion	54
5	Automated landmarking for muscle elongation measurement during RSA	55
5.1	Introduction	56
5.2	Material and Methods	57
5.2.1	Data	57
5.2.2	Anatomic landmarks	58
5.2.3	Humerus SSM	60
5.2.4	Automated landmarking	60
5.2.5	Muscle length measurement	61
5.2.6	Evaluation of humerus landmarking accuracy	64
5.2.7	Application to arthritic joints	65
5.2.8	Sensitivity analysis	65
5.3	Results	66
5.4	Discussion	69
5.4.1	Limitations	71
5.5	Conclusions	72
6	General discussion and conclusion	73

6.1	Summary of Key Results	74
6.2	Clinical Application	76
6.3	Suggestions for future works	80
6.4	Conclusion	86
7	Conclusiones	87
	Bibliography	89
	This is curriculum	107

List of Figures

1.1	Workflow	3
2.1	Joints of the Shoulder	8
2.2	Anatomy of the scapula	9
2.3	Anatomy of the humerus	10
2.4	Main shoulder muscles	12
2.5	Shoulder Osteoarthritis	13
2.6	Shoulder Arthroplasty	15
2.7	Glenius system	19
2.8	Glenius process	20
2.9	Materialise shoulder planning software	22
3.1	Implant and experimental set-up	30
3.2	Implant loading condition	32
3.3	Screw model	33
3.4	Experimental and <i>in-silico</i> displacement	36
3.5	Bone-implant nterface micromotion	37
3.6	Peak micromotion map	37
3.7	Sensitivity analysis	38

4.1	Workflow of the cortical thickness algorithm	47
4.2	Shape and cortical thickness variation in the first two modes of variations	51
4.3	Investigation of the SSM quality: outer surface	51
4.4	Investigation of the SSM quality: specificity	52
4.5	Investigation of the SSM quality: generalization trabecular surface	52
5.1	Anatomic landmarks on the scapula	59
5.2	Anatomic landmarks on the humerus	59
5.3	Registration and fitting of the humerus SSM	62
5.4	Shoulder muscles visualization: pre and post-op	63
5.5	Wrapping algorithm for muscle evaluation	64
5.6	Landmark prediction errors	67
5.7	Muscle elongations prediction errors	68
5.8	Muscle elongations prediction errors for arthritic joints	69
6.1	Humeral Planner	78
6.2	In-house loosening set-up	81
6.3	Loosening set-up: preliminary experiment	82
6.4	Screw fixation experiment	84

Chapter 1

Introduction

1.1 Motivation

Shoulder arthroplasty is the third most common joint replacement procedure, after knee and hip arthroplasty, and currently the most rapidly growing one in the orthopaedic field [6]. Since its first application in the 1950s, it has continuously advanced, bringing newly evolved and improved implant designs and techniques to the market and eventually becoming a well-established, pain-relieving procedure.

In this context, Reverse Shoulder Arthroplasty (RSA) was introduced to specifically treat patients with a completely torn rotator cuff, which could not be effectively managed by conventional surgeries [145]. While a conventional shoulder replacement device mimics the normal anatomy of the shoulder, in an RSA, the ball and the socket of the glenohumeral joint are switched. The spherical part of the joint is attached to the glenoid and a plastic cup is fixed to the upper end of the humerus. In this way, the reversed configuration causes the center of rotation (COR) of the prosthesis to move medially and inferiorly, thus allowing for the deltoid to compensate for the injured cuff muscles. Despite the recent progress and advancement in RSA design, the reported rates of complication [14] are higher than the complication rates of conventional shoulder arthroplasty, thus calling for the development of novel methodologies to support clinicians and improve the functional outcome of patients.

Patient-specific preoperative planning can be used to adapt implant choice and positioning to the patient characteristics and preoperative condition, thus reducing the complication risk of RSA [171]. In fact, through the assessment of

patient-related parameters during the preparation of the arthroplasty, clinicians can select the best option for each patient and limit the operating time during surgery.

A high complication rate is also associated to the management of patients with large glenoid defects, a condition that is becoming more frequent as a consequence of the increasing number of revision surgeries in the active elderly population. For those non-standard cases, surgeons are confronted with tougher reconstructive challenges, while still required to provide good clinical outcomes to patients with different pathologies, characteristics and individual needs. Recently, custom implants have been introduced as an alternative to more classic treatments, such as eccentric reaming and bone grafting. Together with patient-specific preoperative planning and design, which allow the prosthesis to be shaped as if the defect never occurred, custom implants allow for proper joint positioning and fixation of the component in the remaining native bone, improving functional outcome and pain relief [17].

Both preoperative planning and custom implants are the result of a development process that is driven by the patient needs, aiming for a personalized approach able to tailor the medical treatment to each patient. The principal elements of such a personalized approach, which would increase the success rate of the surgical therapy and support the clinicians in achieving an enhanced functional outcome for the patient, are shown in Figure 1.1.

The process starts with the acquisition of patient-specific data, i.e. medical images. In particular, CT-scans have been demonstrated to provide better details of bone structures and pathologies compared to plain radiography [131]. Typically, a 3D surface model is reconstructed through segmentation and it is used as input for the planning phase. Subsequently, regardless of the severity of the defect, both for standard and non-standard cases, virtual preoperative planning softwares are used to provide clinicians with an established surgical plan, customized to each patient. In case of non-standard cases, e.g. large glenoid defects or bone loss following revisions surgeries, custom-made implants can be designed and manufactured through 3D printing technology, to fit each patient's anatomy and potentially improve outcomes and postoperative range of motion. Next to plan only solutions, different technologies can be considered to transfer the plan from the virtual platform to the operating room with sufficient accuracy. 3D printed models help surgeons to better visualize bony structures which would not be accessible otherwise, or to perform try-outs of implant positioning. Additionally, patient-specific instrumentation (PSI) or intra-operative navigation, e.g. through computer-assisted navigation (CAN) or robotics, are suitable for supporting surgeons when placing implants, drilling holes, inserting screws or reaming osteophytes.

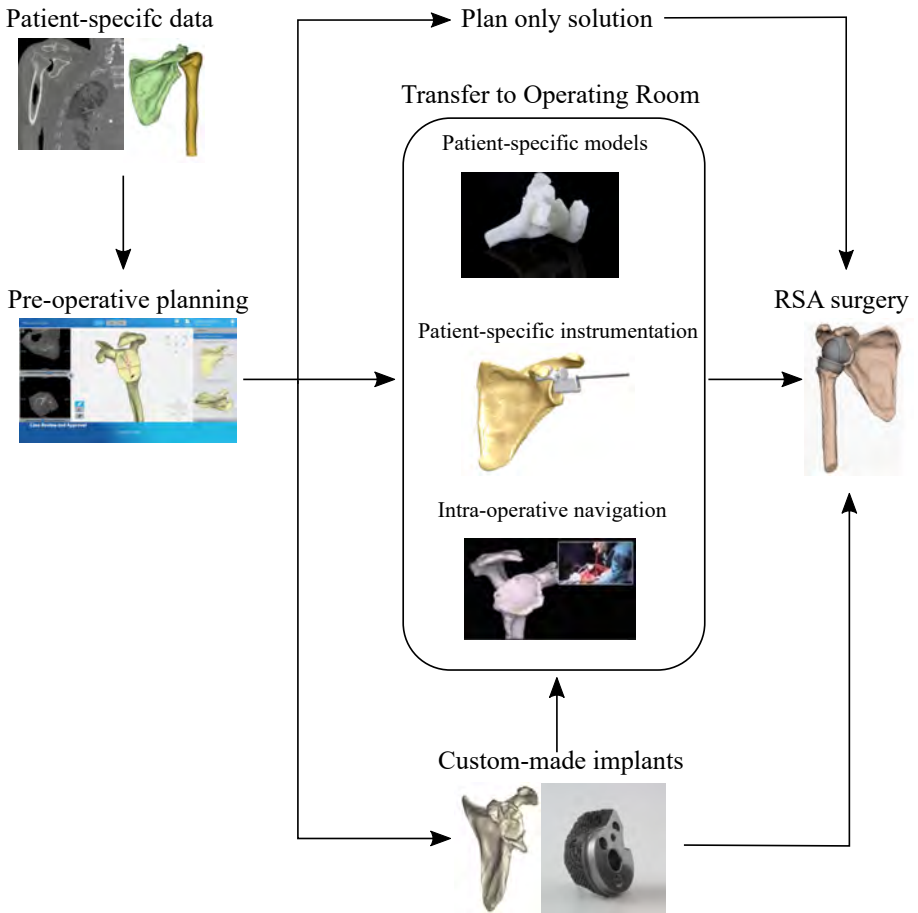


Figure 1.1: Workflow for a personalized shoulder arthroplasty.

Each of the steps presented in Figure 1.1 is based on a complex collection of technologies suffering from a variety of different problems and could benefit from more reliable, robust and automated algorithms to further expand their adoption in a clinical setting. In particular, for non-standard cases, the design of custom shoulder implants is a highly complex procedure which needs to be carried out by experienced biomedical engineers. Currently, no objective tools exist to guide them when choosing the optimal design, thus making this step tedious, time-consuming and user-dependent. Similarly, for standard planning, reliable guidelines are missing to support surgeons when positioning screws and/or implants, mainly due to the large variability among patients. Computer Aided Tools may potentially address the challenges in the design and planning phases while also helping to reduce costs and lead times, ultimately contributing to a wider adoption of the personalized approach.

1.2 Aim

The main goal of this research is to **develop and evaluate novel and automated methods for personalized Reverse Shoulder Arthroplasty (RSA), using state-of-the-art computer aided technologies**. Driven by a patient oriented strategy, three objectives are defined to address unsolved problems in the design and planning of standard and non-standard cases. The motivation and the goals related to each of these main objectives are presented below.

1.2.1 Objective 1: Virtual Bench Test for design of custom shoulder implants

Custom implants are a suitable solution when treating patients with extensive glenoid bone loss. However, clinical engineers are confronted with an enormous implant design space (number and type of screws, contact surface, etc.) and large anatomical and pathological variability. Ideally, the design should be optimized to have sufficient initial implant stability and avoid prosthetic loosening. For custom implants with a unique design for each patient, the use of mechanical testing to verify the stability for each implant is not feasible. Alternatively, Finite Element (FE) analysis has the potential to guide the design process by virtually comparing multiple designs without the need of a mechanical test. Therefore, the first goal of this thesis is to develop a Virtual Bench Test (VBT) simulation that can be used to automatically evaluate the initial stability of custom shoulder implants. Such a tool can ultimately be used

by clinical engineers during the implant design process, thus supporting their design decisions and adaptations.

1.2.2 Objective 2: Assessment of scapular cortical thickness using statistical models

Knowledge about bone morphology and bone quality of the scapula throughout a certain population is fundamental in the design of shoulder implants. In particular, regions with the best bone stock (cortical bone) are taken into account when defining the position and orientation of the screw holes, aiming for an optimal fixation. As an alternative to manual measurements, Statistical Shape Models (SSMs) have been commonly used to describe shape variability within a population. However, these SSMs typically do not contain information about cortical thickness. Therefore, the second goal of this study is to combine scapular bone shape and cortex morphology in an SSM. First, a method to estimate cortical thickness, based on Hounsfield Unit (HU) profile analysis, is presented and evaluated. Then, based on the manual segmentations of 32 healthy scapulae, a statistical shape model including cortical information is created and assessed.

1.2.3 Objective 3: Automated landmarking for muscle elongation measurement during RSA

Adequate deltoid and rotator cuff elongation following RSA is crucial to maximize the postoperative functional outcome and to avoid complications. Measurements of deltoid and rotator cuff elongation during surgical planning can help clinicians to select a suitable implant design and position. However, such an assessment requires the indication of anatomical landmarks as a reference for the muscle attachment points, a process which is often performed manually, thus being time-consuming and user-dependent. Additionally, the medical images, which are normally used for shoulder arthroplasty, mostly contain only the proximal humerus, making it impossible to indicate those muscle attachment points which lie outside of the field of view of the scan. Therefore, the third goal of this thesis is to develop and evaluate a fully-automated method, based on SSM, for measuring deltoid and rotator cuff elongation. First, the SSM based workflow is presented and evaluated against golden truth measurements obtained from manually indicated landmarks. Then, its clinical applicability is demonstrated by assessing the performance of the automated muscle elongation estimation to a set of arthritic shoulder joints used for preoperative planning of RSA.

1.3 Thesis Outline

Chapter 2 introduces the main concepts of anatomy and physiology of the shoulder joint, focusing on the recent development in custom implants and surgical preoperative planning.

Chapters 3, 4 and 5 address the three defined objectives of the thesis, starting with a problem definition and a more detailed description of the motivation driving the developed research. Chapter 3 presents and evaluates the Virtual Bench Test for the design of custom shoulder implants. Chapter 4 presents a new methodology, based on a statistical shape model, to support implant and screw placement. Chapter 5 evaluates the potential of an automated method to indicate humerus anatomical landmarks and include muscle elongation measurements during preoperative planning.

Finally, Chapter 6 presents a general conclusion, with a summary of the main achievements, their clinical impact and suggestions for future research.

Chapter 2

Background

This chapter introduces the reader to the main concepts of the shoulder anatomy, to have a better comprehension of the research work. Particular attention was reserved to the description of the common pathologies leading to shoulder arthroplasty and the possible surgical treatments. Finally, an overview on the state-of-the art of custom implants and preoperative planning, which are the focus of this thesis, is presented.

2.1 Introduction to the shoulder joint

2.1.1 Shoulder Joint Anatomy

The shoulder is considered one of the most mobile parts of the human body [36]. To allow for its wide range of motion, which is critical to the majority of the daily activities, it presents a complex structure with four different joints (Figure 2.1): the glenohumeral, the acromioclavicular, the scapulothoracic and the sternoclavicular. With shoulder arthroplasty technologies being the main topic of this thesis, the anatomical description will focus solely on the glenohumeral joint.

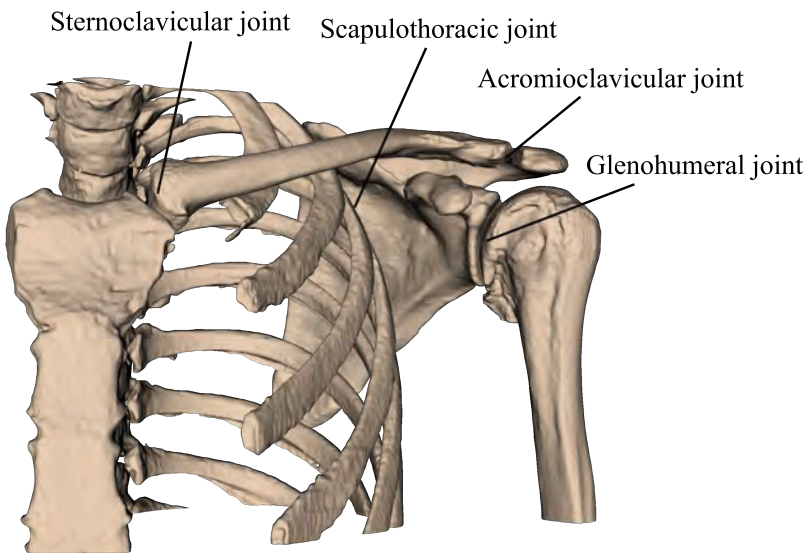


Figure 2.1: Four major shoulder joints: the glenohumeral joint, the acromioclavicular joint, the scapulothoracic joint, and the sternoclavicular joint.

The glenohumeral joint, to which the term "shoulder joint" commonly refers, is responsible for the circular movement of the upper limbs. It consists of a ball and socket joint connecting two bones, the scapula and the humerus, through a cartilaginous articulating surface. The ball is represented by the humeral head, which is inserted into the glenoid cavity (or *fossa*) of the scapula, the socket.

The scapula is a flat, triangular shaped bone, to which several muscles attach (Figure 2.2). The front concavity, called *subscapular fossa*, is an extremely thin region of bone, which is delimited superiorly by an arched structure, the *superior angle*, inferiorly by the *inferior angle*, and laterally by the *lateral angle*. The *suprascapular notch*, which serves as a passage for a critical nerve, the *n. suprascapular*, connects the superior angle to the *coracoid* process, a beak-like protuberance that helps stabilizing the shoulder joint. On the back of the scapula, which is the origin site for most of the rotator cuff muscles, the *spine* divides the bone in two concave areas, the *supraspinatus* and *infraspinatus* fossae. From the spine, the *acromion* process originates towards the glenoid cavity, ultimately forming the acromioclavicular joint.

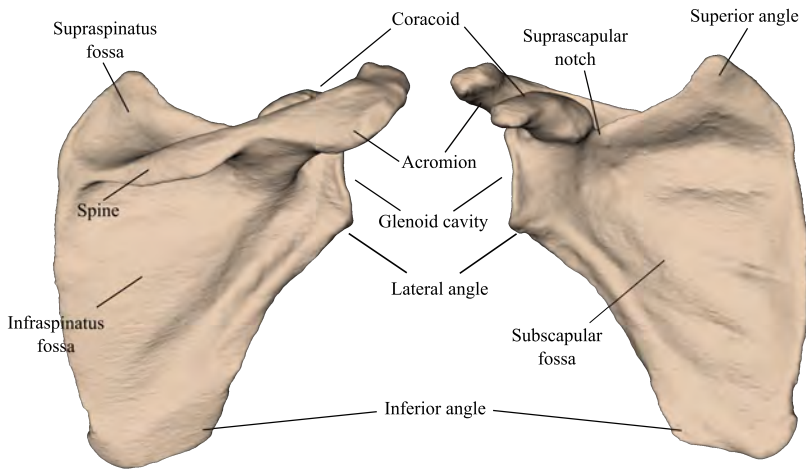


Figure 2.2: Details of the main anatomical structures of the scapula: posterior (left) and anterior (right) view.

The humerus is a long bone that extends from the shoulder to the elbow, where it articulates with the ulna and radius (Figure 2.3).

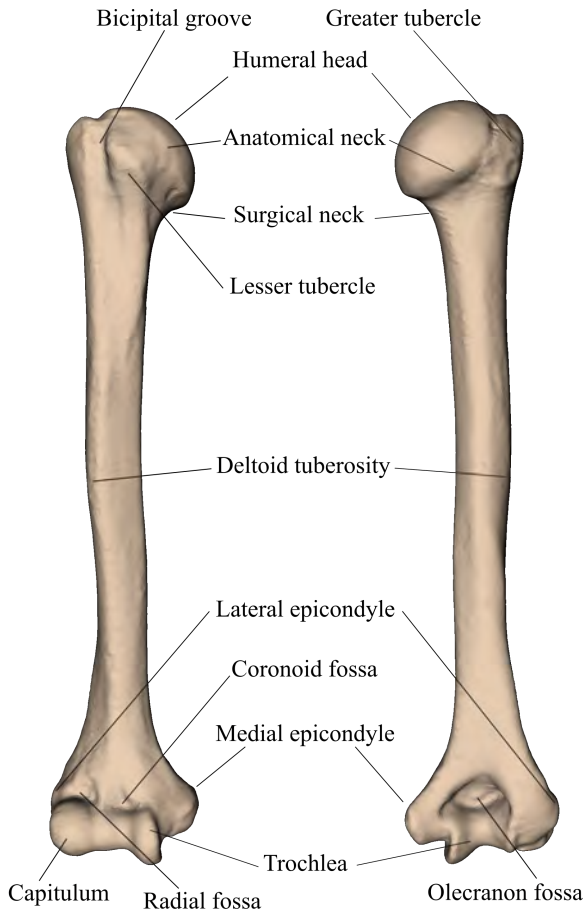


Figure 2.3: Details of the main anatomical structures of the humerus: anterior (left) and posterior (right) view.

In the proximal part, it has a ball-shaped humeral head that inserts into the glenoid cavity. Surrounding the articular surface, the *anatomical neck* divides the head from the *greater* and *lesser tubercles*. The greater tubercle contains the attachment areas of the supraspinatus, infraspinatus and teres minor muscles, which lie on the superior, middle and inferior side, respectively. The lesser tubercle, a smaller protuberance medially located, serves as insertion region for the subscapularis muscle. The two tubercles are separated by the *bicipital groove*, a sulcus extending down to the shaft of the humerus. Just below the head, the *surgical neck* marks the beginning of the diaphysis, which, as with

other long bones, contains a medullary cavity with bone marrow. On the lateral surface of the shaft, the *deltoid tuberosity* is the insertion site for the deltoid muscles.

Continuing distally, the shape of the humerus is characterized by two bony projections, the *lateral* and the *medial epicondyle*, which are normally used as surgical landmarks since they can be easily palpated at the elbow. The distal humerus articulates with the ulna through the *trochlea*, situated below the lateral epicondyle, and with the radius through the *capitulum*, located on the anterior medial surface. Additionally, two other structures belong to the distal joint, the *coronoid* and *radial fossa*, situated respectively above the trochlea and the capitulum on the anterior side. Finally, on the posterior side, the *Olecranon fossa* allows the ulna bone to have enough space during the flexion of the elbow.

One of the reasons explaining the high mobility of the glenohumeral joint is the disproportion in size between humeral head and glenoid vault (4:1 ratio in surface area). To compensate for this difference and avoid an excessive instability, a fibrocartilage rim, called the *glenoid labrum*, deepens the fossa, thus increasing the amount of articulating surface. Additionally, other structures are present to keep in place the bony parts. Together with the ligaments, the rotator cuff muscles and the deltoid are the main actors in this stabilization function, pressing the humeral head against the glenoid. The cuff consists of four muscles (Figure 2.4): the supraspinatus, supporting the abduction of the shoulder, the infraspinatus and teres minor, aiding the external rotation, and the subscapularis, sustaining the internal rotation of the arm.

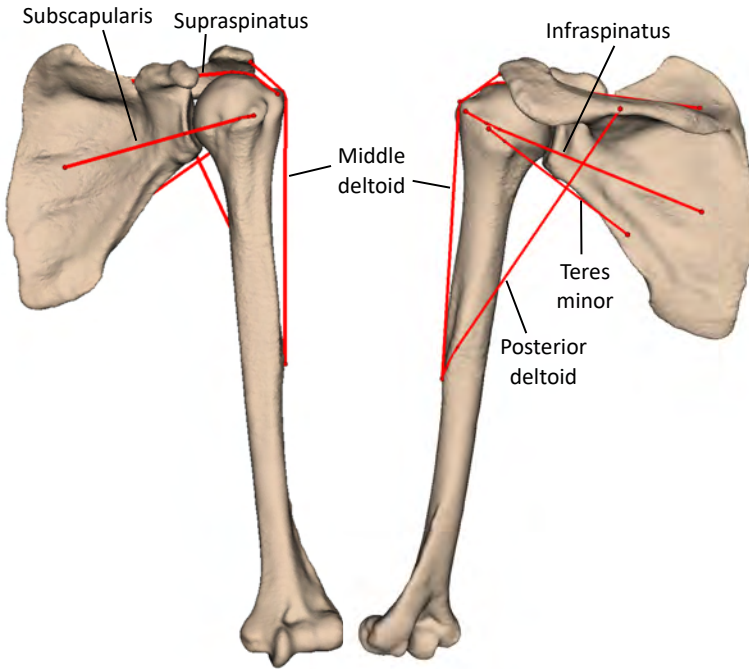


Figure 2.4: Rotator cuff and deltoid visualization: anterior view (left), posterior view (right). Muscles are represented as red lines.

2.1.2 Shoulder Joint Pathology

The causes for shoulder joint problems are multifactorial and include congenital diseases, trauma, malformations, accidental fractures, joint wearing, and muscles infection. The goal of this section is not to give a complete overview of all shoulder joint pathologies, but to briefly introduce common diseases that are most likely to lead to a shoulder arthroplasty.

Osteoarthritis (OA) is a chronic degenerative disease recognized as the leading cause of pain and disability among older adults [89, 146]. Due to the constant growth of the elderly population and the higher prevalence of other risk factors, such as obesity, the incidence of OA is expected to increase. According to the estimation of the World Health Organization [111], by 2050 more than 130 million people, with higher prevalence of women, will suffer from OA worldwide, of whom an approximate 30% will be severely disabled.

OA normally affects different joints throughout the body and its incidence differs by country, age and ethnicity. In a study involving an Asian cohort of over-65 adults [38], the highest prevalence of OA was observed in the spine, followed by the hand, knee, shoulder and hip. In general, although not as prevalent as for other joints, approximately 33% of patients above 60 years old shows radiographical signs of shoulder OA, with the highest prevalence in the female population [92, 103, 120].

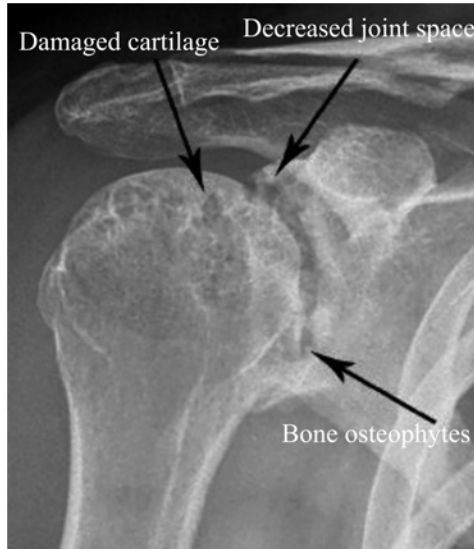


Figure 2.5: X-ray of an arthritic shoulder: the damaged cartilage induces a decrease in the joint space and osteophytes can generate (Figure adapted from [5]).

Shoulder arthritis contributes to the wearing of the cartilaginous layer on the humeral head, ultimately reducing the joint space (Figure 2.5). The lack of an adequate articular surface causes the bones to grind on each other, generally leading to joint pain and limited range of motion. If not treated, the progressive worsening of this condition can be extremely debilitating for the patients, inducing pain during every movement of the shoulder and making it impossible to perform daily activities [105]. There is no consensus over the preferred treatment of shoulder OA, leaving to the clinicians the decision of the medical management, depending on patients characteristics such as age, severity of symptoms and medical comorbidities [37]. Among the nonoperative treatment options, anti-inflammatory drugs and intra-articular injections concur to reduce

the discomfort of the patients. If conservative treatments fail, surgical treatment is normally considered. As for other joints affected by severe OA, arthroplasty, by partially or fully replacing the anatomical joint with a prosthesis, can be a successful solution.

While OA is the most common form of arthritis in the shoulder joint, other distinct forms of arthritis can be identified [1, 25]. Rheumatoid arthritis (RA) is an autoimmune condition, which brings the body to attack its own healthy cells in the articular surface tissues. RA causes the synovium in the joint space to swell, cartilage and ligaments to become damaged and the bone to soften or deform. For 90% of the patients with RA, drug therapies can be used to prevent the progression of irreversible joint damage [9], thus avoiding the need of shoulder arthroplasty.

Fractures and other injuries, e.g. from sport or accidents, can develop the so-called post-traumatic arthritis (PTA). Additionally, given the rather precarious stability of the joint, shoulder dislocations may eventually lead to PTA. Although of different origin, the current management of PTA mirrors that of OA [71].

Avascular necrosis (AVN), or osteonecrosis, is a condition that results in shoulder arthritis when the blood support to the head of the humerus is disrupted, due to fracture or vascular damage, and is responsible for about 3-4% of shoulder arthroplasty [29]. It has also been reported that steroids and alcohol abuse can lead to AVN [80, 108]. In the absence of nutritional substances, the tissues of the humeral head progressively lose strength, causing damage to the overlying cartilage and collapsing. As the pathology worsens, the damage can extend from the head to the glenoid cavity, generating severe pain and making the patient unable to move the arm, a consequence that can manifest several months or even more than one year after the first symptoms [2]. For this reason, if AVN is diagnosed early, nonoperative treatments, such as anti-inflammatory drugs or physical therapy, can be used to reduce pain and restore the mobility of the patient [28]. However, in case of advanced stage and failure of nonoperative solutions, surgical options become necessary [80].

Arthritis can also be present as a collateral effect of severe rotator cuff tendon tear, a degenerative disease that, in certain cases, culminates in cuff tear arthropathy (CTA) [112]. For 90% of patients, in majority adults above 40 years old or athletes, rotator cuff tears emerge after years of repetitive, overhead activities, injuries or trauma [117]. However, there is still very little scientific understanding of the events causing the cuff tear to become arthropathy [59]. Whether caused by nutritional or mechanical factors [112], in CTA patients, mainly women aged >70, the torn weakened rotator cuff is no longer able to constrain the head of the humerus against the glenoid socket, thus leaving the humerus to freely move up and down and grind against the

acromion. The generated debris can damage the surfaces of the bones, ultimately causing arthritis and hence pain and joint dysfunction. The choice of CTA treatment is rather patient-specific. If deltoid and scapular stabilizing muscles are still functional, non-surgical management, including physical therapy or anti-inflammatory drugs, allows the joint to function with minimal pain [67]. Otherwise, operative treatment becomes necessary. Surgical options mainly includes hemiarthroplasty, for patients aged < 70 and with good shoulder elevation, and for those aged ≥ 70 or with no active elevation [59], RSA, which has recently become the preferred solution.

2.1.3 Shoulder Joint Arthroplasty

Shoulder arthroplasty, which aims to restore the functionality of the articulation by partially or fully replacing the anatomical joint with a prosthesis, refers to different surgical procedures: arthrodesis, humerus resurfacing, hemiarthroplasty (or partial arthroplasty), total replacement, reverse replacement. Given the topic of this thesis, the following section will mainly focus on the reverse shoulder arthroplasty (RSA), its applications and limitations.

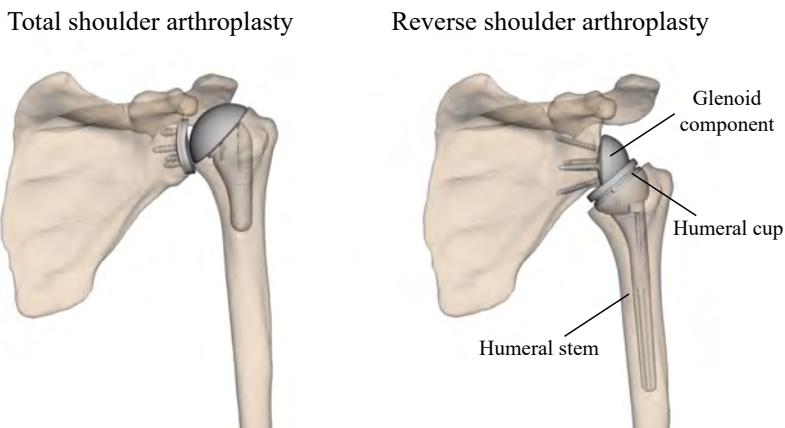


Figure 2.6: Shoulder Arthroplasty: comparison between a traditional and a reverse replacement.

The main innovation behind RSA lies on the switching between the ball and the socket components of the shoulder joint. In fact, while a conventional shoulder replacement device mimics the normal anatomy of the articulation, in an RSA the spherical part of the joint is attached to the glenoid and a plastic cup is fixed

to the upper end of the humerus (Figure 2.6). RSA was successfully introduced for the first time by Grammont in 1985 with the Delta prosthesis [16] and has seen, since then, a continuous growth both in terms of adoption and design development [142]. During 2020, approximately 64'000 people are expected to receive a reverse implant in US, being 25% of the total shoulder arthroplasty procedures. Similar or even higher trends can be seen in Europe [6]. Moreover in 2023, the global shoulder market is forecast to reach a \$2.40 billion value, with RSA being the fastest-growing segment [7].

The large increase in the adoption of RSA is the results of years of design improvements and modifications that, despite still associated with rather high complication rates, significantly improved the clinical benefit for CTA patients. In fact, RSA has proved successful in treating cases with severe cuff tear arthropathy, becoming the preferred alternative to more traditional methods such as hemiarthroplasty, whose outcome failed to provide pain relief and improvement in range of motion (ROM) or function [134, 167]. The reason behind this success is linked to the biomechanics of the reverse prosthesis: the center of rotation (COR) of the glenohumeral joint, which is moved more medially and inferiorly compared to the native COR, leads to tensioning of the deltoid muscle, enhancing the recruitment of the muscle fibers, stabilizing the shoulder and supporting its abduction functionalities [23, 142, 153]. Hence, for patients with CTA, in which all or part of the four rotator cuff muscles are not functional, the reverse configuration allows the deltoid to compensate for the injured cuff.

The literature is rich with studies examining the clinical results of RSA. Favard et al. [64] reported, for a cohort of 506 patients, a survival rate of 89% at ten years, however with clinical score and radiographic changes deteriorating after five years. Other works have shown similar [43, 73] or slightly higher (93%) long-term implant survivorship [154]. Regarding the clinical outcome, in a recent study, sign of pain relief started to occur after 6 months [143]. Additionally, with the advancement in the implant design, surgeons have expanded the application of RSA to fracture care, rheumatoid arthritis, and eventually failed prior surgery, as reported in the literature [70, 133].

Although RSA has improved treatment options for patients with torn rotator cuff, complication rates have been reported from 10% to 47% [57] and from 19% to 68% [63], which are currently higher than those associated with conventional shoulder arthroplasty (10.3%, according to a recent literature review of Bohsali et al. [21]). The large variability of the RSA rates is driven by multiple factors: patients demographics, different levels of CTA severity, surgeons experience, type of implanted prosthesis, proportion of revision procedures, inclusion criteria for reporting complications. For instance, Werner et al. [165] reported a complication rate of 50%, one of the highest in the literature, but considering a

cohort of patients with severe rotator cuff deficiency, including a high ratio of revision cases for failure of previous implants. In contrast, Walch et al. [162] analyzed independently primary and revision cases, reporting an incidence of 19% in primary RSA and 24% in revision and confirming the inconsistency in the literature review of complication rates.

When examining the nature of the clinical complications, instability and infection have the highest incidence [14, 165]. In a clinical analysis of 782 cases, Zumstein et al. [175] reported a 20% rate of postoperative complications, with 4.7% being instability and 3.8% infection, resulting in a 13.4% of patients needing reintervention. Similarly, in the work of Bohsali et al. [21], the main complications after RSA were instability (5%), periprosthetic fracture (3.3%) and infection (2.9%). Additionally, other problems can be associated to failure of the implants, such as humeral and glenoid loosening, acromion fractures and scapular notching [22].

RSA, thanks to its design, has significantly improved the clinical outcome of patients suffering from CTA. However, postoperative complications still represent an obstacle to its widespread adoption. One of the main causes of these complications is the large variability among patients, who can present diverse pathological scenarios. For instance, CTA can lead to severe bone defects at the glenoid vault, thus jeopardizing the surgical operation and calling for a more experienced approach. Related to this, the severity of the pathology can hinder the correct placement of the implant, a condition which is considered necessary to avoid instability and loosening [52]. Depending on the needs of the patients, a personalized approach can be used to reduce the risk of complications. The scope of the next sections is to discuss the state-of-the-art of these patient-specific solutions, which are at the center of the research work of this thesis.

2.2 Personalized Reverse Shoulder Arthroplasty

2.2.1 Custom Glenoid Implants

One of the main challenges in RSA is the presence of bone defects at the glenoid cavity of the scapula. Such bone loss can be the result of a severe CTA or the removal of a previous implant, and surgeons should take it into account when choosing for the best surgical treatment for these non-standard cases. In fact, the low bone stock can lead to a sub-optimal fixation of a standard glenoid component and subsequently implant failure [60]. Depending on the severity of the defects, clinicians can opt for different solutions. In case of moderate loss, reaming the bony structures is a suitable approach to even the contact surface at the implant interface while trying to preserve the residual bone [91].

In contrast, for large defects, the sole reaming is not sufficient to have a stable prosthesis and additional material is necessary to fill the defect. In this context, bone from allograft or autograft can be used as a defect filler to provide a good fixation surface [74, 114]. In a recent clinical study, Hoffelner et al. [79] analyzed the outcome of 17 patients who underwent glenoid reconstruction with autologous bone graft and found significant improvements in patients shoulder functionality, with high satisfaction scores. However, the clinical relevance of these results is questioned by other studies that reported less encouraging outcomes. In particular, major concerns remain on the resorption of the graft due to bone subsidence, which is responsible for loosening and early failure [84, 138]. Following the lack of consensus on the benefits of bone grafting, new methods have been investigated. Nowadays, also thanks to the advancement of the additive manufacturing technologies, custom-implants can be designed and produced to fit the missing bone, opening new doors to the treatment of non-standard cases.

One of the first relevant applications of a custom implant can be found in the hip arthroplasty field, with the Custom Triflange Acetabular Component system, introduced in the 1990 by Biomet (Biomet Inc., Warsaw, IN, US). The acetabular implant, manufactured using conventional milling techniques, has been proved as clinically successful as standard treatment methods, with reliable and long-term results [39]. Only more recently, case reports for shoulder glenoid reconstruction have been published. In 2014, Berger et al. [17] presented a study on the use of a custom component to treat severe glenoid defects with RSA, reporting functional improvement and pain relief in the early follow-up. In the following years, additional studies confirmed the efficacy of patient-specific implants in the glenoid reconstruction setting [35, 55], introducing new designs and techniques and marking the beginning of a new phase for a personalized

RSA.

In this context, Materialise NV developed and introduced Glenius[®], a 3D printed patient-specific device to treat patients with a severe bone loss at the glenoid. The Glenius implant consists of a custom Titanium baseplate together with a matching Cobalt-Chrome (CoCr) glenosphere. The baseplate is composed of two main parts: a defect-filling porous structure and a smooth baseplate (Figure 2.7).

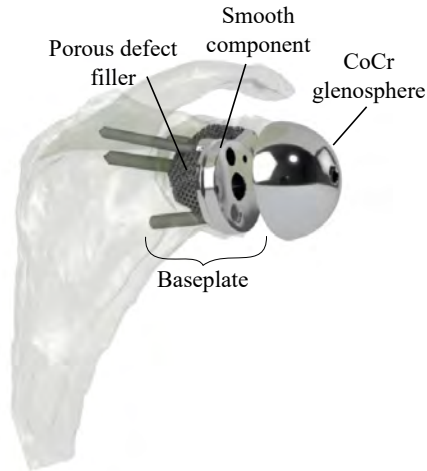


Figure 2.7: Details of the Glenius glenoid reconstruction system (courtesy of Materialise NV).

The combination of CT-based preoperative planning and custom component design allows a unique individual reconstruction of the glenoid. Moreover, thanks to the advantages of the additive manufacturing process, there is maximal freedom in the design shape, enabling the implant to be shaped and positioned as if the erosion never occurred. The presence of a porous scaffold that fills the bone defect promotes bone ingrowth, hence maximizing prosthetic fixation and minimizing the risk of mechanical loosening.

Given the recent introduction of the Glenius system in the market, only studies reporting short and mid-term follow-up results have been published [47, 49, 148]. In one of the first publications [148], a Glenius system was implanted in a 56 years old woman, showing excellent functional outcome at the 30 months follow-up. These results were confirmed in a larger retrospective study of Debeer et al. [49], who evaluated 10 cases from different clinical centers. Overall, at an

average follow-up period of 30.5 months, a high patient satisfaction rate was reached, with adequate pain relief and a reasonable functionality. Although long-term follow-up data are still needed to determine the bony ingrowth and the survivorship of this implant, the early results of the Glenius system are strongly encouraging, confirming the potential of the patient-specific approach.



Figure 2.8: The different steps in the design and manufacturing of the Glenius system (courtesy of Materialise NV).

The current workflow that leads to the manufacturing of a Glenius implant includes multiple steps, from the CT-scans acquisition to the final production through 3D printing (Figure 2.8). First, the images are imported into image processing software (e.g. Mimics [3]) and all bones (and previous implant components in case of a revision surgery) are segmented. The segmentation process is a tedious manual task made even more complex by the high occurrence of metal artefacts, the poor bone quality and the large number of components present from previous operations. At the end of the segmentation, 3D models of the patient's anatomy are obtained, with an accurate representation of the defect scapula.

During the reconstruction phase, a statistical shape model [125] is used to virtually reproduce the defect, by estimating the natural or healthy position and shape of the patient's glenoid. Additionally, the output allows to quantify the amount of bone volume missing and to calculate the anatomical coordinate system of the scapula, which is taken as reference for implant position and orientation.

In the planning phase, the implant position is defined. The position and orientation of the baseplate are defined in the anatomical coordinate system, obtained with the reconstruction: version, inclination and anterior/posterior, medial/lateral and inferior/superior translation. The implant position and

orientation are optimized looking for a trade-off between the predicted natural or neutral position of the joint plane and the existing defect.

After defining the implant position, the design is initiated. First, the fixation screws are planned. On average four screws are used for implant fixation, optimizing both position and orientation to allow for cross-fixation, and preferably looking for bicortical extension in a relatively good amount of bone stock to support grip. The solid baseplate is designed to cover all screw heads and to provide the female taper connection to the CoCr head. The volume between the baseplate and the host bone is then filled with a porous structure. This structure is optimised to balance the need for sufficient contact with the bone and a relatively slim, light structure to allow easy insertion in the surgical incision. The CoCr head does not need patient-specific design. The size and brand-compatibility is discussed with the surgeon and the correct technical drawing is then used in the manufacturing of the head from CoCr blocks.

When all designs are finalised, production begins. The head is shaped from a CoCr block by mostly milling and turning actions. The custom titanium implant is produced via additive manufacturing, more specifically selective laser melting (SLM) [26]. Briefly, a layer of powder is applied on a build plate. A laser beam hardens a path in the powder layer, solidifying it. The build plate is then lowered with the height of one layer and the melting repeated. Patient specific plastic guides are also designed and produced in parallel, to support surgeons with the positioning of the implant, the drilling of the screw holes and their fixation.

2.2.2 Preoperative Planning

As described in subsection 2.1.3, complication rates of RSA are still higher than those of conventional arthroplasty and represent an obstacle to its broader adoption. The large variability among patients, who can present diverse pathological scenarios, is an additional challenge faced from the surgeons and one of the reason for the complexity of shoulder arthroplasty. A successful preoperative planning, able to provide meaningful patient-specific information to the clinicians, is a powerful tool to avoid possible complications. As a consequence, the last few years have witnessed a significant increase in the number of software offering preoperative solutions, like Blueprint (Wright Medical), Trumatch (DePuy Synthes, Materialise) or Match Point System (DJO, Materialise), in part supported by the introduction of novel technology to transfer the plan from the virtual platform to the operating room with sufficient accuracy.

3D preoperative planning originated with early studies examining whether 3D images could support surgeons in identifying key clinical parameters better than 2D imaging [171]. In general, 3D virtual models of the patient's anatomical structures are generated through segmentation and used as input for different analyses. In one of the pioneering works, Kwon et al. [93] demonstrated that measurements from 3D CT images could accurately reflect the true anatomy of the glenoid, when comparing them against cadaveric data. Iannotti et al. [85] proved that, by using virtual templating, a significant improvement could be obtained in achieving the desired implant position within 5° of inclination or 10° of version, when compared to 2D imaging. Similar studies confirmed the superiority of 3D based planning in quantifying glenoid bone loss [137] and guiding surgical decision-making [83, 131]. Building on these results, multiple commercial software allowing preoperative planning have been introduced in the shoulder market in the last decades, making it a growing and innovative business sector.

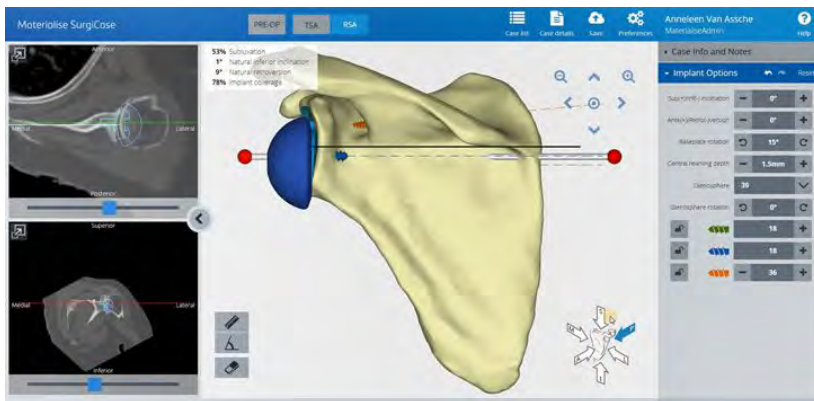


Figure 2.9: Graphic user interface of the Materialise shoulder planning software (courtesy of Materialise NV).

In this context, Materialise NV also offers a solution to help clinicians with the planning of RSA (Figure 2.9). The user-friendly software includes multiple dedicated functionalities, for implant and screws planning, which allow for a fast and accurate measurement of the main surgical parameters: implant size and position, screws position and length, reaming depth. The surgeon can virtually place the prosthesis, e.g. glenoid baseplate, and define the ideal implant location and size to achieve the desired surgical goals. Once the preoperative plan is approved, the planning software generates the location and orientation of the

glenoid guide pin, which is used as a reference in the operating room for placing the implant and can be transferred there through PSI.

Despite the proven success of preoperative planning, recent studies highlighted some controversies. Denard et al. [51] compared the glenoid version and inclination measurements of two commercially available systems and found considerable variability between the obtained values. In a similar but more recent study, Erikson et al. [62] confirmed the limited agreement between preoperative planning software for shoulder arthroplasty, in contrast to surgeons who have high inter-reliability. Therefore, they concluded that attention should be paid when confronting results relying on different planning systems to determine preoperative glenoid deformity measurements. Also the work of Parsons et al. [116] seems to go in this direction. In their study, 49 CT scans from RSA cases were planned by 9 experienced surgeons using the same planner in two time frames, at a 6-12 weeks distance. However, they demonstrated that, even though the inter- and intra-surgeons average differences were relatively small, some cases led to much higher variation, suggesting little consensus on the optimal planning.

Overall, these results highlight one of the main challenges relative to preoperative planning. The advancement of the technologies allow clinician to measure multiple parameters in different ways, but a link to the functional results is still missing. A correlation between preoperative planning and clinical outcomes would not only increase the utility (and possible adoption) of preoperative systems, but also help clinicians to establish guidelines when deciding on the optimal position of an implant.

Chapter 3

Virtual Bench Test for design of custom shoulder implants

This chapter addresses the first objective of the thesis, by presenting a method to support engineers during the design phase of custom implants. The Glenius system (Materialise NV, Leuven, Belgium) is used as a representative case study of custom shoulder implants to demonstrate the applicability of the developed technology.

This chapter was previously published as:

PITOCCHI, J., WESSELING, M., VAN LENTHE, G. H., AND PÉREZ, M. A. *Finite element analysis of custom shoulder implants provide accurate prediction of initial stability*. *Mathematics* 8, 7 (2020), 1113

Jonathan Pitocchi contributed with the development of the automated FE-based method, experimental data interpretation, model validation, sensitivity analysis, statistical analysis and organization of the study steup.

3.1 Introduction

3.1.1 Motivation

Custom implants represent a valuable solution for treating patients with severe glenoid bone loss due to CTA or explant of a previous prosthesis. Thanks to their design, unique for each patient, it is possible to fill the bone defect as if the erosion never occurred. Additionally, a porous titanium scaffold is often used to promote bone ingrowth at the implant interface, hence maximizing fixation and minimizing the risk of loosening. While it has been proven that a patient-specific approach is successful in treating non-standard cases, the unicity of the prosthesis introduces a lot of clinical, regulatory, technological and cost related issues that need to be overcome.

One of the major drawbacks in the production workflow of a custom implant is linked to the complexity of the design phase, which needs to be carried out by experienced engineers. In particular, the high degree of freedom that characterizes the definition of the main parameters of an implant (type and number of screws, contact surface, etc.) lacks of objective measuring tools that could support the decisions and adaptations of the design engineers and reduce the risk of subjectivity during this process. Ideally, the design should be optimized to have sufficient initial implant stability and avoid prosthetic loosening.

Mechanical tests, as required for Food and Drug Administration (FDA) clearance and described in American Society for Testing and Materials (ASTM) standards [33], are normally used to verify the stability. However, for custom implants with a unique design for each patient, the use of mechanical testing to check the adequacy of each implant is not feasible. Alternatively, FE analysis has the potential to guide the design process by virtually comparing multiple designs without the need of a mechanical test. *In-silico* models have been already used in the pre-clinical testing of new devices as part of the planning and design process of implants [149]. For instance, in cardiovascular surgery, personalized FE models were developed to adapt the sizing and positioning of a trans-catheter valve and later introduced in the clinical practice [140].

Therefore, this research aims to develop a Virtual Bench Test (VBT) simulation that can be used to automatically evaluate the initial stability of custom shoulder implants. The output of the VBT should support the engineers when making design decisions and adaptations and should require only a minimal input, thus not adding complexity to the process.

In the proposed method a FE model, starting from parameters that are normally

available during the design phase, is built to replicate a standard mechanical test for implant stability. The model is then validated against experimental data acquired during the development of the thesis. The results section provides a representative picture of the performance and it is followed by a critical interpretation and a comparison with studies that wanted to address similar problems.

3.1.2 Finite Element Models for Implant Design

Since its introduction in the late 1980s, Reverse Shoulder Arthroplasty (RSA) has become a standard treatment for patients with rotator cuff arthropathy. More recently, surgeons have expanded its application to fracture care, rheumatoid arthritis, and eventually failed prior surgery replacements, further increasing the number of surgeries [86, 163]. In many cases, the presence of considerable bone loss at the glenoid side, due to degenerative arthritis or secondary to revision surgeries, may complicate baseplate implantation. This limits the treatment options and jeopardizes the clinical outcomes, as insufficient bone stock can lead to suboptimal component fixation and therefore early implant failure.

Different methods have been described to address glenoid defects, depending on the bone loss severity [169]. Eccentric reaming can be performed in case of moderate bone loss, while bone grafting is more suitable for large defects. However, the results of bone grafting are controversial since not all the studies have reported satisfactory outcomes [79]. More recently, custom implants have been introduced as an alternative treatment. Together with patient-specific preoperative planning and implant design, custom implants allow for proper joint positioning and fixation of the component in the remaining native bone [35, 131].

In order to avoid aseptic loosening of the glenoid component, maximizing implant fixation remains one of the main targets. Fixation screws are used to provide initial mechanical stability (primary fixation) which subsequently can lead to biological fixation by bone ingrowth (secondary fixation). To enable bone ingrowth, custom implants have a porous titanium structure (spray-coated or 3D printed) [55, 148]. However, micromotion at the bone-implant interface above $150\ \mu\text{m}$ has been shown to inhibit this mechanism and lead to an unstable fibrous tissue layer between the metallic porous layer and the host bone [87]. Therefore, implant design should be optimized to minimize micromotion at the time of initial fixation, thus leading to a better osseointegration.

For patient-specific shoulder implants, the enormous design space, which allows the glenoid component to be adapted to the patient anatomy, represents a challenge to the evaluation of the mechanical stability. While mechanical tests

can be performed extensively to assess the stability of standard implants [68, 76, 150], for custom implants with a unique design for each patient, it is not practical to use mechanical testing to verify the stability. Alternatively, Finite Element (FE) analysis has been widely used to evaluate the influence of different implant configurations on the initial fixation of an implant [32, 50, 61, 82, 151, 152, 160].

Chae et al. analyzed the bone-implant interface micromotion of an inferiorly tilted glenoid component virtually implanted in a scapula model and found that the tilted fixation compromised initial mechanical stability [32]. Suarez et al. investigated how different type and number of screws impacted the initial stability of a cementless glenoid component, reporting higher interface micromotions when the same implant was tested in poor quality bone [152], even when more physiological loads (e.g. from musculoskeletal model) were applied [151]. Elwell et al. [61] reported similar results, showing that the use of only two fixation screws could amplify the negative effect of baseplate lateralization, thus jeopardizing implant stability and worsening its functional outcome. Hopkins et al. examined multiple standard designs with different screw angles inclination, concluding that increasing the screw inclination enhanced stability more than using longer and thicker screws [82]. Other studies explored instead the effect of the prosthesis repositioning (using different glenosphere sizes or bone grafting) and found that a lateralization of 10 mm was mechanically acceptable for osseointegration [50, 160].

However, the effect of different loading direction, which in case of a custom implant cannot be neglected due to the asymmetry of the design shape, was never systematically investigated. It is evident that, since the main parameters (number and type of screws, baseplate dimensions, etc.) are unique for each custom implant, FE analysis has the potential to guide the design process by virtually comparing multiple designs without the need of a mechanical test.

Therefore, the aim of this Chapter is to develop an automated workflow to evaluate the initial stability of custom shoulder implants during the design phase, by simulating a fixation experiment based on ASTM F2028-14 [13]. To our knowledge, this is the first study to automate, evaluate and validate a full *in-silico* modeling of the ASTM F2028-14 for a custom-made prosthesis. Moreover, the FE model can be used to predict the relative motion at the bone-implant interface, which cannot be quantified by the current mechanical tests.

3.2 Material and Methods

A custom reverse shoulder implant was designed and 3D printed to comply with ASTM standards [13]. To evaluate the pre-clinical stability of the implant, displacement of the glenoid baseplate was measured in response to axial and shear loading, after insertion in a bone substitute. The experimental baseplate displacement was compared to the model estimation to validate the virtual bench test. A more detailed explanation regarding the mechanical test and the *in-silico* model is presented in the following sections.

3.2.1 Experimental set-up for model validation

The ASTM F2028-14 [13] is a standard method commonly used for assessing the risk of glenoid loosening in shoulder implants. The test protocol includes three subsequent steps: (1) an initial static analysis to measure the baseplate displacement, (2) a fatigue phase in which the implant is cyclically rotated around an axis loaded with a compressive axial force, and (3) an additional static phase to measure the glenoid fixation, similarly to step 1.

The custom implant was inserted into a 20 PCF polyurethane block (Sawbones Europe AB, Sweden), which is normally used as substitute of glenoid bone in mechanical tests [97]. Two locking and two non-locking (compression) screws were used to fix the implant to the artificial bone (Figure 3.1-a). Compression screws are able to close the gap at the bone-implant interface, by pressing the metal component towards the bone. For this reason, non-locking screws were inserted first, followed by the locking screws, which instead lock the implant in place thanks to the threaded head mating the threaded holes of the implant.

An axial compressive load of 430 N was applied perpendicular to the glenoid plane by a flat polyacetal load applicator. An additional shear load of 350 N was applied parallel to the baseplate via a horizontal loading fixture (Figure 3.1-b). Shear and axial forces were defined in a worst-case loading scenario, being respectively the 42% and 51% of the body weight (assumed to be 86 kg) [13].

Contrary to standard baseplates, which normally have a symmetric round shape, custom implants can present an asymmetric design, consequently the shear load was applied along the four main directions of the implant: anterior, posterior, superior, inferior (Figure 3.1-a). Dial indicators (MTS System, USA) were placed to measure the displacement of the baseplate. For each loading direction, both axial and shear baseplate displacements were measured, resulting in a total of 8 measurements. Each measurement was performed three times and

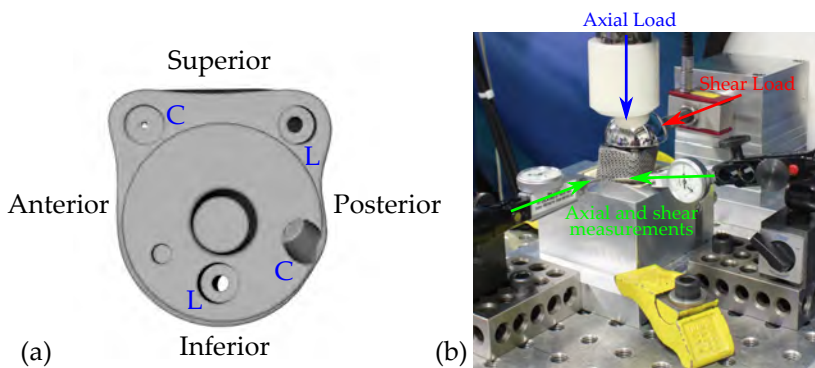


Figure 3.1: Left (a), top view of the custom implant with the four main directions: anterior, posterior, superior, inferior. Four screws were used to fix the implant: two locking (L) and two non-locking (compression, C). Right (b), experimental set-up with a shear load (red arrow) applied inferiorly via a horizontal loading fixture. Axial load was applied through the glenosphere (blue arrow). Axial and shear components of the baseplate displacement were measured superiorly with two dial indicators (green arrows).

averaged value was obtained. The test was repeated for 6 identical samples under the same conditions.

3.2.2 Generation of Finite Element Models

An automated workflow was developed to set-up FE simulations of a virtual bench test. To obtain a virtual bench test that can be run multiple times by the design engineers to support possible design decisions and adaptations, the computational time of the simulation needs to be limited. For this reason, the finite element model was created to simulate only the static step of the experimental test, without considering the fatigue aspect, similarly to the work of Virani et al.[160].

The geometry files (STL) of the implant were imported into the design software 3-matic™(v 14.0, Materialise N.V., Leuven, Belgium), that includes a Python scripting interface to automate processes (Figure 3.2). The bone substitute, which had to match the non-flat contact surface at the interface with the implant, and the loading box were created through a series of Boolean operations. The 3D FE models were meshed with tetrahedral C3D4 elements. For the loading box, a coarse mesh was used, with element edge lengths ranging from 2 to 4 mm.

The bone block was meshed with non-uniform elements, using a more fine mesh at the interface. A mesh convergence study was performed upfront by evaluating the impact of different mesh size on the interface micromotion. Ultimately, an average element edge length of 0.5 mm at the baseplate-bone interface was considered as the converged mesh. Non-manifold nodes were created at the bone-implant interface, to facilitate the micromotion calculation and the convergence of the contact analysis. Due to this operation the elements nodes in the contact surface were shared between implant and bone. The implant was meshed with an average edge length of 0.5, for a total of approximately 630'000 elements, consistent with the dimensions of the prosthetic components and necessary to capture the complexity of the custom design. Ultimately, the glenosphere was meshed with an average element size of 0.5 mm.

All components were modeled with linear elastic material properties, which is an assumption commonly made under these experimental conditions [54]. The loading box and baseplate were assigned with a Young's modulus of 110'000 MPa and a Poisson's ratio, ν , of 0.3 (corresponding to Titanium Ti-6Al-4V, [20]). The porous structure of the baseplate, mainly consisting of 3D printed Titanium, was modelled as a solid part and characterized by a lower stiffness. A Young's modulus equal to 2'000 MPa and a Poisson's ratio of 0.3 were used, consistently with the values reported in literature for titanium porous scaffolds [15]. The glenosphere was modeled using Cobalt-Chromium-Molybdenum material properties ($E = 220'000$ MPa, $\nu = 0.3$, [11]). The material properties of the foam block, representative of human glenoid trabecular bone, were taken as reference for the bone substitute ($E = 200$ MPa, $\nu = 0.3$, [12]).

Contact surfaces were tied or were modelled as a hard contact with friction, depending on the interaction of the component. The interface between glenosphere and baseplate, and loading box and bone block, were considered completely tied, with no relative motion. Coulomb friction contact was implemented at the bone-implant interface. In the literature, values ranging from 0.5 to 0.7 are reported for the friction coefficient between bone and porous metal [54, 152, 160, 173], thus an average friction coefficient of 0.6 was selected for the presented model.

3.2.3 Screw Model

In order to assess the impact of different screw types (compression and locking) on fixation, particular attention was paid to the screw modeling. A recent study showed that an excessive simplification of the screw shaft model has an impact on the micromotion in RSA implant design analysis [54]. Hence, the validity of the simplification assumptions has always to be evaluated against experimental

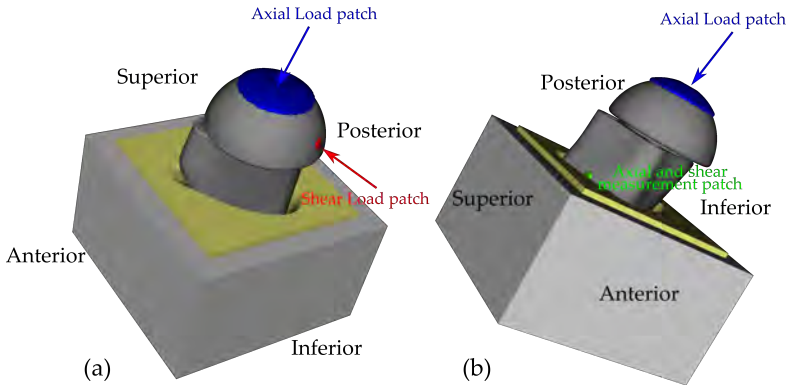


Figure 3.2: Left (a), isometric view of the FE model with a shear load applied inferiorly. In blue the patch defined for the application of the axial load, in red the shear load patch. Right (b), superior view of the FE model. In green the measurement patch defined to calculate the baseplate displacement.

measurements, aiming for a trade-off between acceptable computation times and prediction accuracy.

Screws were modeled following a previously described approach [168]. This approach uses structural elements for the connection to the bone, which avoids the need of meshing screw holes and the associated computational cost related to additional contact analysis (Figure 3.3-a). A script was implemented in Python 3.7 to automate the modeling process and include the screws in the Abaqus input file. As output of the design planning phase, five screw parameters could be extracted: position (head coordinates), length, direction, outer diameter and root diameter.

Each screw was modeled as a wire connecting the head point (input parameter) to the endpoint (obtained with the length and direction vector) and penetrating the elements of the bone (Figure 3.3-b,c). All the nodes of the bone elements lying around the wire and at a maximum distance equal to the outer screw radius were connected perpendicular to the wire with rigid connector elements. Screw head was fixed to the implant in a similar way, by connecting the node representing the head with the nodes within the baseplate holes. To mesh the screw wire, beam elements (B32, three-node) with a circular cross section equal to the root radius were used, imposing as nodes the calculated intersection points between wire and connector elements. Since Titanium screws were used, a Young's modulus of 110'000 MPa and a Poisson's ratio of 0.3 were assigned as material properties.

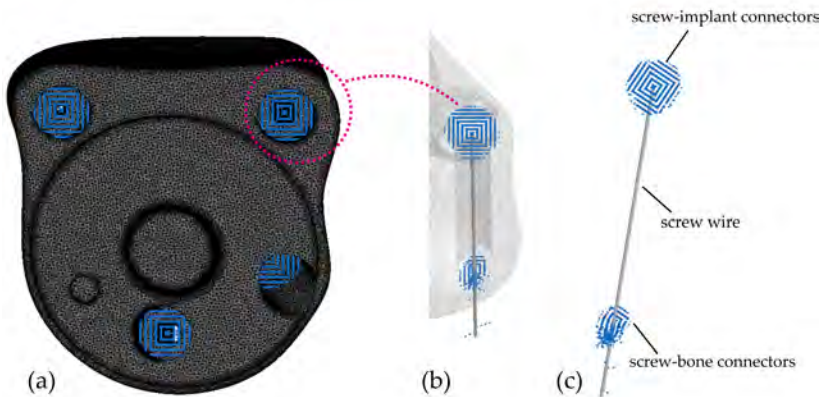


Figure 3.3: Left (a), top view of the model and the four screws. In blue the connectors between screw head and implant. Right (b), detail of one screw (implant transparent). Right (c), the generated screw model.

To differentiate the mechanical behavior between locking and compression screws, additional assumptions were made. To model the loose connection between the unthreaded head of a compression screw and the implant, the stiffness of the first 2 mm of the screw shaft was set to 200 MPa, a value equal to the elastic modulus of the bone substitute [152].

Moreover, non-locking screws provide an initial compression that constrains the implant towards the bone. The impact of this aspect on FE analysis was already examined in literature, demonstrating that the inclusion of preload in the model is a key parameter when investigating interface micromotion [53]. For this reason, preload was explicitly modeled using the pre-tension section of Abaqus at the intersection of the screwed and non-screwed portion of the shaft, similarly to the study of Virani et al. [160]. For the current model, the input values of the insertion force were estimated based on experimental data [124]. Briefly, a custom made load sensor was built to measure the compression force generated by the screw head. Screws with different lengths were inserted into synthetic bone blocks (Sawbones; Malmö, Sweden) of 20 PCF and the force was acquired until failure of the bone substitute. This resulted in a maximum compression of 370 N and 420 N for the two screws used in the loosening test. Since those values were measured at failure loads, the pre-tensions in Abaqus were set to 260 N and 300 N, by taking 70% of the force to failure [152].

3.2.4 Statistical analyses and sensitivity study

Predicted implant stability values were calculated as the average of the displacements for the nodes lying in the measurement patch. Both the shear and axial components of the displacements were taken into account. A Spearman's rank order correlation test was used for comparing the consistency of results between the experimental and *in-silico* analysis, with a significance level set to 0.05. Correlation coefficients whose magnitude were lower than 0.7, between 0.7 and 0.9 and higher than 0.9, indicated respectively a moderate, high and very high correlation [109].

Besides the baseplate displacement, shear and axial micromotion at the bone-implant interface were calculated using the FE method. These micromotions comprised the displacement values for all nodes on the contact surface. Since non-manifold nodes were created at the bone-implant interface, micromotion was defined as the relative motion between the corresponding nodes after application of the loads. In particular, for each contact node on the implant surface, micromotion U_P was calculated as:

$$U_P = R_P - R_B \quad (3.1)$$

where R_P and R_B are the vector positions of the node on the prosthesis (P) and its corresponding one on the bone surface (B), respectively. Shear (U_t) and axial (U_n) micromotion were then calculated by projecting the total micromotion on the corresponding loading direction vectors, as follows:

$$U_t = U_P \cdot \hat{t} \quad (3.2)$$

$$U_n = U_P \cdot \hat{n} \quad (3.3)$$

where \hat{t} and \hat{n} respectively represent the unit vector of the directions along which shear and axial load were applied. The total relative micromotion between glenoid baseplate and bone, is further referred to as peak micromotion [65] and was visualized as a color map on the back of the prosthesis.

To evaluate the impact of changes in the model parameters on the FE output interface micromotion, a sensitivity analysis was performed. In particular, changes in the bone substitute material properties, the friction coefficient and the screw pre-load were investigated. A summary of these numerical tests is presented in Table 3.1. Each parameter was modified independently, for a total of 24 simulations (6 for each loading condition).

For the stiffness of the bone surrogate, the Young's modulus was modified to mimic the properties of 15 PCF (osteoporotic bone) and 30 PCF foam blocks, corresponding to 150 MPa and 553 MPa respectively [50, 12]. The Coulomb's coefficient was adapted to simulate local changes at the bone-implant interface by imposing values of 0.5 and 0.7, which are representative of the friction ranges found in literature.

Finally, a change in the pre-load of the compression screws was applied, modifying by $\pm 20\%$ the baseline pre-tension value. A paired t-test was used to compare the peak micromotion of the baseline model with each sensitivity model, with a significance level set to 0.01, following a Bonferroni correction of the alpha value ($\alpha=0.05$, $n=6$: $\alpha/n \approx 0.01$).

Parameter	Baseline Value	Sensitivity Values
Elastic Modulus Bone	200 MPa	150 MPa, 553 MPa
Coefficient of Friction (CoF)	0.6	0.5, 0.7
Screw pre-load	260 N, 300 N	$\pm 20\%$

Table 3.1: Parameter variation for the sensitivity analysis.

3.3 Results

FE results for the baseplate displacement were within the variability of the experimental measurements for all loading directions (Figure 3.4). The smallest displacements were found when the shear load was applied inferiorly to the baseplate. The Spearman's rank order test revealed a statistically significant ($p < 0.05$) high correlation ($\rho_s = 0.81$) between the experimental results and FE results.

The maximum interface micromotion was found for the anterior shear load (Figure 3.5). For all the loading directions, the median peak micromotion was lower than $50 \mu\text{m}$. A 95th percentile of $141 \mu\text{m}$, $80 \mu\text{m}$, $73 \mu\text{m}$ and $25 \mu\text{m}$ was reported for the anterior, posterior, superior and inferior loading respectively. When looking at the axial and shear components, the median shear micromotion was always higher than the axial. For none of the loading directions, micromotion above $150 \mu\text{m}$ was reported (Figure 3.6).

The sensitivity of the model to input parameters showed a peak micromotion for the baseline model which was significantly different ($p < 0.01$) when compared to the model with reduced and increased elastic moduli of bone substitute, for all the loading directions (Figure 3.7). For the anterior loading, which reported

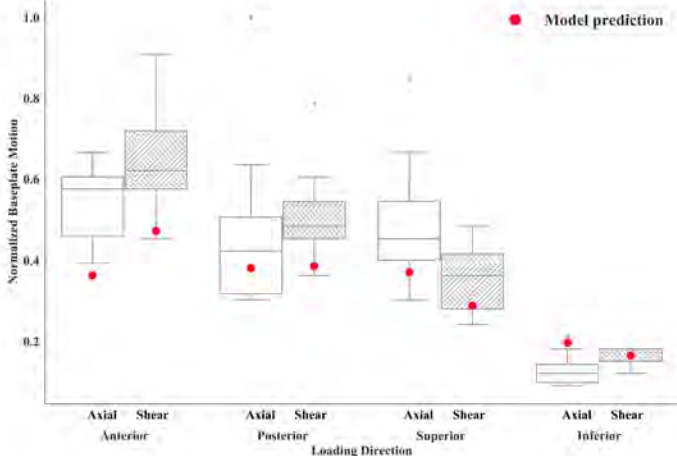


Figure 3.4: Baseplate displacement measured experimentally (boxplot) and determined from the FE analysis model (red dots). For the FE analysis, predicted values were calculated as the average of the displacements for the nodes lying in the measurement patch. Data were normalized to the largest micromotion measured in any of the tests. For each of the four main implant directions, both axial and shear displacements were measured. Gray points represent outliers in the measurements.

the highest micromotion values, significant differences were also found between the baseline model and the one with reduced/increased compression screws pretension.

3.4 Discussion

In this study, an automated workflow to evaluate the pre-clinical stability of a shoulder implant through FE simulations was presented and validated. To our knowledge, this is the first work to report a full *in-silico* modeling of the ASTM F2028-14 for a custom-made prosthesis. Although previous studies [54, 152, 160] reported FE analysis for a similar experimental set-up, the effect of different loading directions, which in case of a custom implant cannot be neglected due to the asymmetry of the design shape, was never systematically investigated.

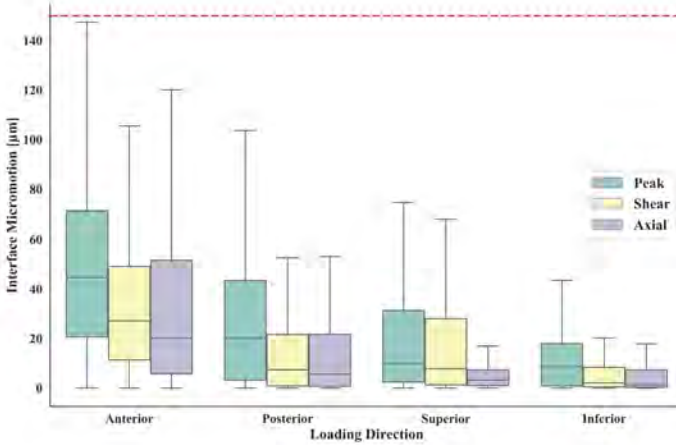


Figure 3.5: Interface micromotion. Shear and axial components of the total micromotion (peak) was evaluated for all the loading directions. The red dashed line represents the 150 μm threshold.

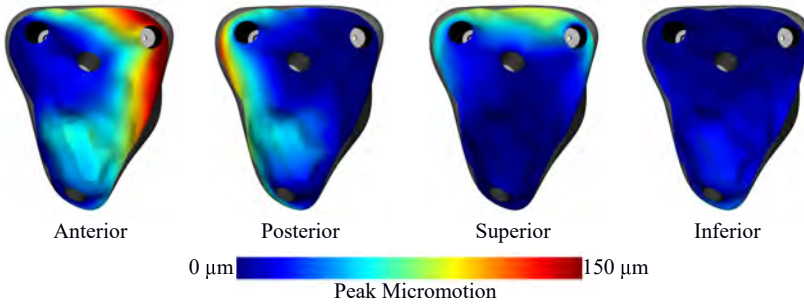


Figure 3.6: Back view of the implant. Peak micromotion map at the bone-implant interface for all the loading directions.

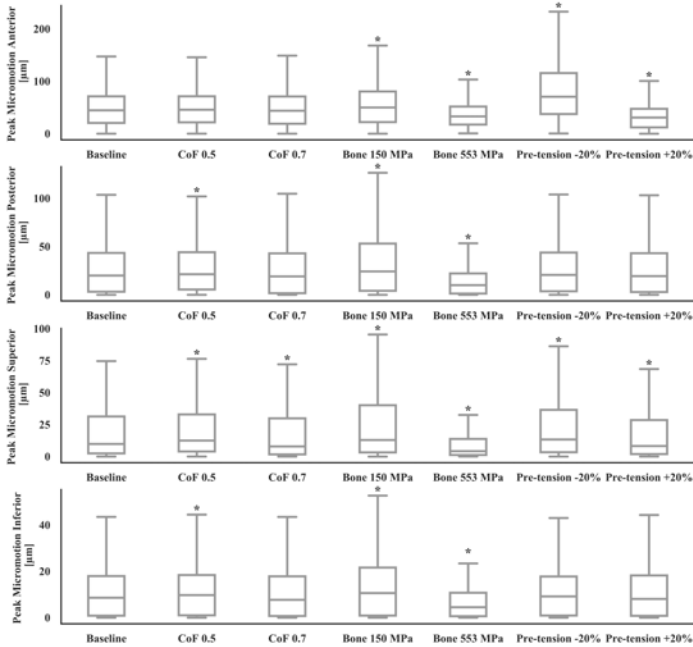


Figure 3.7: Change of the interface peak micromotion due to modification of different model parameters: bone Young’s modulus (150 and 553 MPa), coefficient of friction (CoF = 0.5 and 0.7) and screw pre-tension (load $\pm 20\%$). *: paired t-test, $p < 0.01$.

This approach resulted in a total of 8 measurements that were used to support the FE predictions.

The results of the mechanical test showed an influence of the loading direction on the implant stability. In particular, the presented design reported the lowest displacements when the shear load was applied inferiorly to the glenosphere. This is mainly due to the presence of two screws, one locking and one compression, in the superior part of the baseplate, which are almost perpendicular to the direction of the inferior load and opposite to its application point. Instead, the highest displacements were instead measured for the anterior loading directions, due to the absence of a good screw fixation at the anterior side. These results further corroborate the idea that each new implant should be tested in those different conditions.

All the experimental measurements showed a high variability. Although one unique design was tested with 6 samples, this variability is likely to reflect the variations that occurred during the production of the implants and the assembly of the different components. The 3D printed technique used for the fabrication could introduce inaccuracies, especially in the porous structure, which influenced the mechanical measurements. Similarly, the bone substitute blocks were artificially carved to match the non-flat baseplate surface, possibly causing additional variation. Direct comparison of the experimental outcomes with previous studies is not possible due to major methodological divergences. Higher mechanical loads were used to test standard implants (750N both in axial and shear) and only the shear displacement was measured when the load was applied superiorly [76, 82, 160]. Under this configuration, the presented work reported slightly higher shear values (Figure 3.4, inferior direction), meaning that the effect of a smaller applied load was compensated by the use of a custom implant with non-standard design (e.g. non flat contact surface, asymmetry of the shape).

The good agreement between experimental and FE predicted micromotions was confirmed by a Spearman's rank test, resulting in a correlation coefficient of 0.81 (high), which is lower than the one reported by Virani et al. (0.96, [160]). The lower correlation coefficient can be explained by the use of a custom design, which leads to additional complexity in the simulation. Similar to Virani et al. [160] over-stiffening of the model was observed, which, in the context of this study, can be partially explained by the use of linear tetrahedral elements in the meshing process, a choice justified by the need of low computational cost.

One limitation of the standard mechanical test presented here is related to the lack of micromotion measurements at the bone-implant surface. In contrast, FE modeling can provide a valuable insight on the interface behavior (Figure 3.5), although their accuracy cannot be directly evaluated against experimental

outputs. As previously described, micromotion above $150\ \mu\text{m}$ can jeopardize bone ingrowth and lead to an unstable fixation [87]. Design engineering should take into account this aspect when looking for possible design adaptations. For this reason, interface micromotion was estimated through the FE model. When evaluating the two separated components, higher median values were reported for the shear component. These results are in accordance with previous studies indicating that micromotion of reverse implants occurs mainly in shear [78]. For none of the loading directions peak micromotion was found to be higher than $150\ \mu\text{m}$, suggesting that the implant design is not jeopardizing bone ingrowth. Additionally, the highest values were calculated at the edge of the interface, where osseointegration is less likely to happen.

The interface micromotions predicted by the FE model were sensitive to changes in some of the input parameters: the FE model was sensitive under all the loading directions to a change in bone quality ($150\ \text{MPa}$ and $553\ \text{MPa}$), similarly to what has been reported in the literature [152]. Moreover, this study corroborates the idea that the impact of an adequate modeling of the compression screws cannot be neglected [53]. A change in the screw pre-tension can lead to very different micromotion, thus suggesting that pre-tension should always be included in the simulation and its value estimated or derived through experimental measurements.

3.4.1 Limitations

The generalizability of these results is subject to certain limitations which need to be addressed. Major assumptions were made during the creation of the *in-silico* model, looking for a trade-off between accuracy and computational cost. The bone substitutes were modeled with homogeneous isotropic material properties, a simplification commonly accepted and implemented in literature [50, 54, 152, 160], although not fully representative of the behavior of the bone substitute. The porous structure of the implant was not explicitly modelled to reduce the complexity of the model. As an alternative, a lower elastic modulus was used for the corresponding elements. While this assumption impacts the frictional behavior at the interface, the sensitivity showed that a change in this parameter did not substantially influence the micromotion estimations (at least in the configurations where highest values were reported).

While $150\ \mu\text{m}$ is the ASTM accepted threshold to promote osseointegration [13], its application has been challenged in literature. Other studies [66, 82] referred to lower values ($20\ \mu\text{m} - 50\ \mu\text{m}$) during the evaluation of interface micromotion. When lowering the threshold, the presented model would still predict bone

ingrowth in the inner region of the prosthesis, however these results should be interpreted carefully and always considering the simplifications of the study.

The automated workflow was built to replicate only the static analysis described in the ASTM standard and additional efforts should be made to include the dynamic loading, which are probably not compatible with the requirement of a low computational workflow. However, it can be assumed that minimizing the initial static displacement with an optimized design, will also lead to better fatigue outcome.

Validation of the model was obtained only for a single design and under relatively limited degree of freedom. It is believed that a more complete experimental set of tests is necessary, at least to assess the impact of additional design changes (e.g. number and type of screws) and to ensure the validity of the assumptions made. To further strengthen the predictive power of the simulation, alternative micromotion metrics would be necessary since the current mechanical set-up fails to provide a direct measure of the full-field interface micromotion [53, 66].

3.4.2 Conclusion

Summarizing, the automated workflow presented in this study was able to replicate the mechanical condition of a standard test for a patient-specific shoulder implant. The finite element analysis can potentially support the engineers during the design phase, by virtually comparing different implants. Additionally, the presented tool could be used to define which configurations need to be tested when looking for worst case scenarios, thus reducing the amount of required mechanical experiments.

Chapter 4

Assessment of scapular cortical thickness using statistical models

This chapter addresses the second objective of the thesis, by presenting a methodology to integrate information on the cortical thickness in an SSM of the scapula. First, an automatic method to estimate cortical thickness, based on HU-profile analysis, is described and validated. Then, a benchmark analysis is performed to assess the quality of the created SSM.

The work in this chapter was previously published in the Journal of Computer Methods in Biomechanics and Biomedical Engineering. Only minor adaptations have been made.

PITOCCHI, J., WIRIX-SPEETJENS, R., VAN LENTHE, G. H., AND PÉREZ, M. Á. *Integration of cortical thickness data in a statistical shape model of the scapula*. Computer Methods in Biomechanics and Biomedical Engineering (2020), 1–7

Jonathan Pitocchi contributed with the development of the automated method for cortical bone thickness estimation, the creation and evaluation of the SSM, data processing and interpretation.

4.1 Introduction

4.1.1 Motivation

During the design phase of standard shoulder implants, regions with the best bone stock (cortical bone) are commonly taken into account when defining the position and orientation of the screw holes, aiming for an optimal fixation. Therefore, knowledge about bone morphology and bone quality of the scapula throughout a certain population is fundamental to develop prosthesis that can fit to patients with different bone characteristics.

Commonly, manual measurements on medical images [100] or on cadaveric samples [104] are performed to extract anatomical dimensions. Unfortunately, this information not only is obtained through a tedious and time-consuming process, but it is also limited, since derived from the analysis of small sub-sets of the potential patients.

As an alternative to those measurements, SSM's have been often used to describe shape variability within a population. However, explicitly including cortical thickness information in an SSM of the scapula still remains a challenge. As part of this research, a methodology to integrate information on the cortical thickness in an SSM of the scapula is presented. The ideal application of the presented SSM is to be used as a tool by orthopaedic companies to virtually implant a new design and test its congruency inside a generated virtual population, thus reducing the number of design iterations and cadaver labs [4].

4.1.2 State of the Art

Statistical Shape Models (SSMs) provide a valuable way to describe shape variability within a training dataset. Since their introduction [42], these models have been used for multiple applications: to automatically segment bone structures [96, 98], to study the shapes of human anatomy [30, 132, 135, 144], to virtually reconstruct large bone defects [8, 125, 127, 157], to build 3D models starting from 2D information [72, 110].

The main concept behind SSM techniques is to perform principal component analysis (PCA) on corresponding landmarks derived from the dataset objects and to extract the main modes of variation. Thus, each subject in the training dataset can be described by a linear combination of principal components (PC's), corresponding to these modes of variation. Moreover, new instances, representative of the population, can be generated by varying the PC [42].

In addition to quantifying shape variation, SSMs may be combined with bone quality information (such as image intensities, cortical thickness, etc.) in order to create combined models. Such information can be used in population studies to explore cortical variation in the main region of interest for implant and screw placement. This way, guidelines that function for the overall population, can be defined for the design of robust implant and the positioning of the screws [56].

In a previously published study [24], a statistical appearance model of the femur, combining both shape and image intensities variation, was created using two workflows (an image-based and a mesh-based approach) to generate ready-to-run finite element model that can be used in the *in-silico* assessment of bone quality and strength. In a recent work [172] Zhang et al. demonstrated, on a large population of femur, that cortical information can be integrated to create statistical models with cortical thickness. In their study, cortical bone mapping [155] was used to automatically detect cortical thickness over the entire femoral surface.

Few studies have tried to create a combined model for the scapula. Burton et al. [27] developed an SSM and a statistical intensity model (SIM) to explore the variation in shape and material property distribution throughout a certain population. In their study, volumetric meshes were created to include the bone quality information in the statistical shape model. Only the layer of elements in the surface (size 1.0 ± 0.2 mm) was used to represent the cortical bone, thus their approach was limited in describing the variation in cortical thickness within and between subjects.

In order to explicitly include subject-specific cortical thickness information on the SSM, additional efforts must be done. The scapula morphology is complex and the trabecular region is not one continuous region. For other anatomies (e.g. femur), where often a clear trabecular structure is present, it is possible to use standard SSM workflows (where point correspondence between outer and inner surface is obtained by warping). For the scapula this is not a viable option, but the sparse trabecular information can be included in the model through cortical scalar values.

4.1.3 Aim

The goal of this Chapter is to combine scapular bone shape and cortex morphology in an SSM. First, an automatic method to estimate cortical thickness, based on HU-profile analysis, is developed and validated, as an alternative to the one used in [155]. Second, a technique is presented to include cortical thickness in the SSM of the scapula. The quality of the created

SSM is then evaluated by assessing the generalization, the specificity and the compactness of the resulting model.

4.2 Material and Methods

4.2.1 Data

A set of 32 scapulae, 17 males and 15 females, was selected by an experienced surgeon for the construction and evaluation of the SSM. All computed tomography scans were visually inspected and only scapulae without glenohumeral arthropathy signs were included. The average age was 59 ± 12 years. The youngest patient was 28 years old and the oldest 74. The dataset was already used in [125] for the creation of an SSM to virtually reconstruct glenoid bone defects. The scapula scans were segmented in the image processing software Mimics v.20 [3] and converted to 3-dimensional models, with a mean triangular edge length of 1.5 mm. The 3D models were obtained using the approach described in a previous work [156]. In the study, a segmentation workflow for the construction of 3D models from clinical CT-scans, was validated for medical applications.

4.2.2 Cortical thickness estimation

An algorithm was developed in Python 3.5 to automatically estimate sampled cortical thickness (Figure 4.1) starting from the initial 3D model. For each point in the model surface, HU values were sampled along the line passing through that point and perpendicular to the surface, with a sampled distance of 0.1 mm. As a result, a HU profile was obtained for each point in the surface. First, a threshold of 226 HU was applied to detect the cortical bone in the profile and separate cortical and trabecular values. The full-width at half maximum method (FWHM) [128] was used to estimate the cortical thickness by setting the 10th percentile of the trabecular intensities as the value for the trabecular bone. Using a Variable Wrapped Offset algorithm, it was possible to build the inner surface (representing the trabecular bone) by setting the measured cortical thickness as local offset for each point of the outer surface. The algorithm makes use of a `vtkContourFilter` to generate the Isosurface mesh from the scalar values [139].

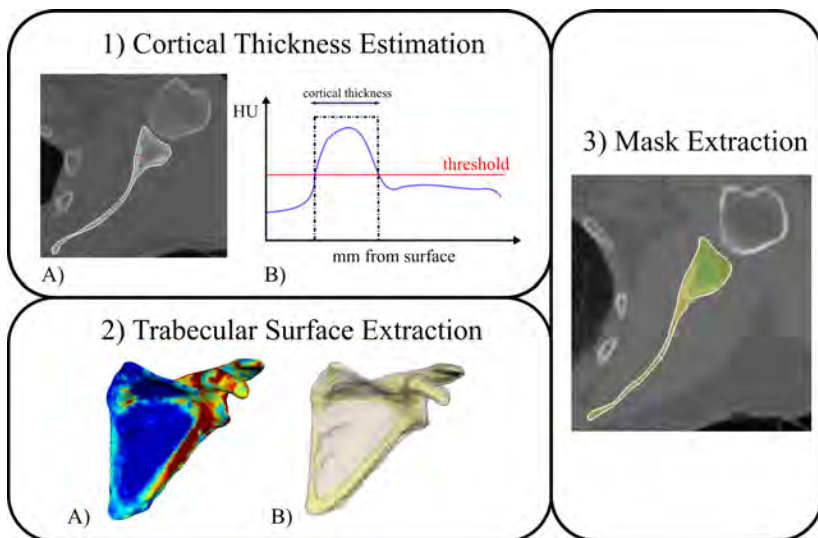


Figure 4.1: The subsequent steps in the estimation of the cortical thickness: Cortical Thickness is estimated for each surface point (1A) by sampling HU values along lines perpendicular to the surface and using a threshold-based method (1B). The cortical values (2A) are set as local offset of a Variable Wrapped Offset algorithm to build the trabecular surface (2B). Finally, from the surface a mask is extracted on the image for comparison against manual segmentation (3).

4.2.3 Validation of cortical thickness estimation

The cortical thickness algorithm was evaluated by comparing its results with manually segmented cortex, for a random subset of 10 scapulae. First, starting from the surface obtained through the automatic algorithm, a mask on the original CT-image was extracted. Then, to take into account for inter-operator variability, three operators were asked to manually segment the same dataset of scapulae. Using the ITK implementation of the STAPLE algorithm [164], the ground truth was generated from the three expert segmentations for each case.

The STAPLE algorithm treats segmentation as a pixel-wise classification, which leads to an averaging scheme that accounts for systematic biases in the behaviour of experts in order to generate a ground truth volume and a simultaneous accuracy assessment of each expert. Thus, accuracy parameters (sensitivity, specificity and Dice Coefficient, DC) could be extracted for each operator by comparing the golden truth obtained with the STAPLE algorithm to the

original manual segmentation. Then the accuracy of the automatic algorithm was evaluated against the golden truth and the performance was compared to that of the manual segmentation (mean \pm standard deviation of the three operators).

4.2.4 SSM construction

An SSM was created in 3 subsequent steps, similarly to the workflow presented in Vanden Berghe et al. [157]. First, one model of the dataset was registered to all other models to obtain corresponding surfaces. Second, the models were aligned to exclude all translational and rotational variations. No scaling was performed to maintain the size information of the models. Similarly to a previously described approach [172], the cortical thickness value of each surface point was directly integrated in the data matrix to produce a model of shape variation correlated with cortical thickness variations. In this way, each column X_i of the data matrix contained the concatenated point coordinates of the training dataset and the corresponding cortical thickness values [42]:

$$X_i = \{x_{i,1}, x_{i,2}, \dots, x_{i,n}, y_{i,1}, y_{i,2}, \dots, y_{i,n}, z_{i,1}, z_{i,2}, \dots, z_{i,n}, s_{i,1}, s_{i,2}, \dots, s_{i,n}\}^T \quad (4.1)$$

where x_i , y_i , z_i are the three dimensional coordinates of node i and s_i are the corresponding cortical thickness values. Finally, PCA was applied to the data matrix.

4.2.5 SSM evaluation

To assure the construction of a high quality SSM, we applied different tests [46]. A visual inspection of the SSM modes of variation was done to ensure that no unnatural shape and cortical variation were present in the model. Compactness was evaluated in order to assess how efficiently the variation in the dataset can be represented by the model. Two fundamental properties that are commonly used to assess the good quality of a model, were measured: specificity and generalization ability.

The specificity ability can be used to quantify how much new cases generated through the SSM differ from the cases included in the training set. It is implied that a good SSM should generate only models representative of the described anatomy. Specificity was evaluated by sampling new instances with a certain

number of modes, and comparing them to the most similar cases of the training set.

The generalization ability of an SSM measures how well new data samples can be represented by the model for a certain number of modes of variation. Generalization was evaluated by performing a Leave-One-Out (LOO) test. To evaluate the ability of the model to generalize the cortical information, the trabecular surface was reconstructed and the Euclidean distance between the original trabecular surface and the reconstructed one was calculated. Finally, we evaluated the generalization of the model on an image level. We extracted a mask from the two trabecular surfaces (the test case and the reconstructed one) and for this we evaluated the accuracy of the generalization by calculating the Dice score.

4.3 Results

4.3.1 Cortical thickness estimation

The results of the inter-operator analysis and the accuracy of the automatic algorithm are presented in Table 4.1. For each case, the mean and the standard deviation of the performances of the three operator is reported for sensitivity, specificity and Dice score. In the last column, the mean and the standard deviation is reported for all the dataset, both for manual and automatic segmentation. All the accuracy parameters of the manual segmentation show a higher standard deviation when compared to that of the automatic algorithm. The performances of the automatic algorithm remain inside the inter-operator variability: 93.8 ± 1.2 vs 95.4 ± 4.4 for the sensitivity, 88.6 ± 1.9 vs 94.9 ± 8.8 for the specificity and 94.7 ± 0.8 vs 96.7 ± 2.5 for the Dice coefficient.

4.3.2 SSM analysis

The average cortical thickness of the SSM was 2.0 ± 0.6 mm. The shape and the cortical thickness variation in the first two modes of variation are represented in figure 4.2. The first mode mainly models the scaling variation of the model set. When considering a large scapula (-2σ), greater thickness values are expected, whereas while considering a small scapula ($+2\sigma$), lower thickness values are observed. The second mode shows a variation in the glenoid inclination and acromion orientation, with no visible relation to the cortical thickness variation.

		Sensitivity	Specificity	Dice Coefficient
Inter-operator	Case 1	93.9 ± 6.3	99.0 ± 0.9	96.6 ± 3.5
	Case 2	95.7 ± 4.4	93.4 ± 8.1	96.3 ± 2.3
	Case 3	96.0 ± 2.9	93.3 ± 8.3	96.7 ± 2.2
	Case 4	94.8 ± 3.9	96.3 ± 2.1	96.7 ± 1.9
	Case 5	95.6 ± 5.0	97.9 ± 0.7	97.3 ± 2.5
	Case 6	96.0 ± 3.1	97.6 ± 1.4	97.3 ± 2.0
	Case 7	94.3 ± 5.1	98.7 ± 0.7	96.7 ± 2.8
	Case 8	95.5 ± 2.8	85.5 ± 20.4	95.7 ± 3.3
	Case 9	95.5 ± 4.5	92.5 ± 6.8	96.3 ± 1.8
	Case 10	94.5 ± 4.7	97.8 ± 0.9	96.7 ± 2.6
		Mean	95.4	94.9
	Std	4.4	8.8	2.5
Automatic Algorithm	Case 1	94.3	90.3	95.7
	Case 2	95.8	87.5	95.1
	Case 3	94.5	89.1	95.2
	Case 4	94.8	87.1	95.2
	Case 5	93.8	92.7	95.7
	Case 6	93.7	87.7	93.8
	Case 7	93.4	87.1	94.0
	Case 8	94.4	87.0	94.8
	Case 9	91.9	86.8	93.5
	Case 10	91.6	90.2	94.1
		Mean	93.8	88.6
	Std	1.2	1.9	0.8

Table 4.1: Accuracy results of the cortical segmentation for a random subset of 10 scapulae. For the Inter-operator, mean ± standard deviation was obtained by evaluating the segmentation of 3 operators against the golden truth generated with the STAPLE algorithm. The accuracy of the automatic algorithm was evaluated against the same golden truth.

The first mode of variation explained 77% of all data variation and the SSM explained more than 95% of all data variation with 12 modes (Figure 4.3-A). The results of the generalization for the outer surface are represented in Figure 4.3-B. At the first mode, the median error for the outer surface was about 3 mm while it reached a plateau in performance around 1.5 mm.

A random sample of 1000 new instances was generated to measure the specificity both for the outer surface and the cortical thickness values (Figure 4.4). For the outer surface, the specificity started to converge after 25 modes, reaching a root-mean-square-error (RMSE) of 3.1 ± 0.54 mm when using all 32 modes to generate the new cases (Figure 4.4-A). For the cortical values, although fully convergence was not reached, a RMSE of 0.67 ± 0.12 mm was measured with 32

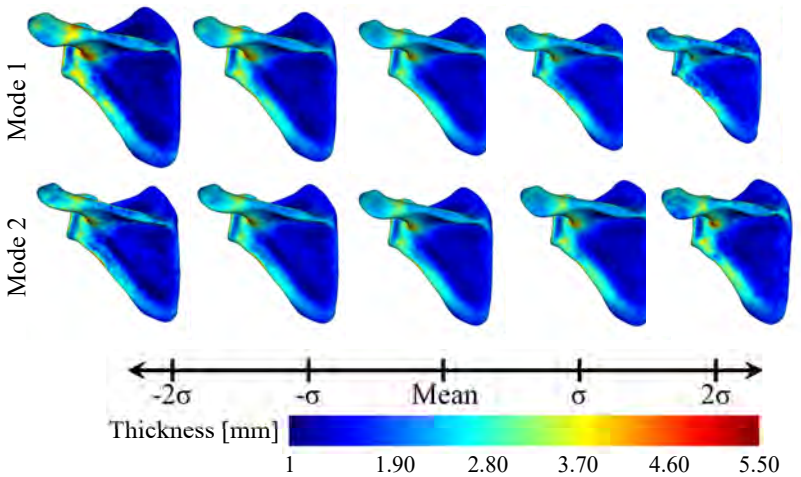


Figure 4.2: Shape and cortical thickness variation in the first two modes of variations. For mode 1 (top), when passing from a large scapula (-2σ) to a small scapula ($+2\sigma$), a decrease in cortical thickness is visible. Mode 2 (bottom) shows a variation in the glenoid inclination and acromion orientation, with no visible relation to the cortical values.

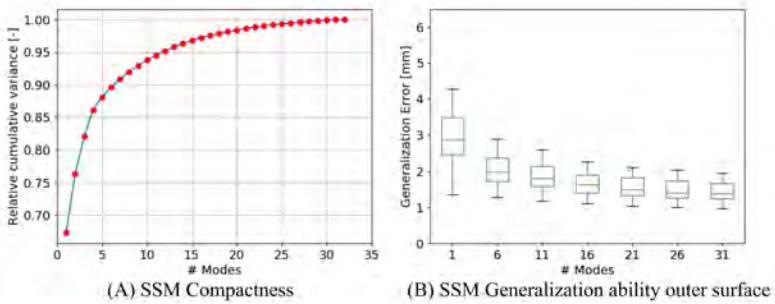


Figure 4.3: Analysis of the SSM quality. (A) Compactness of the SSM. (B) Generalization ability for the shape variation of the outer surface.

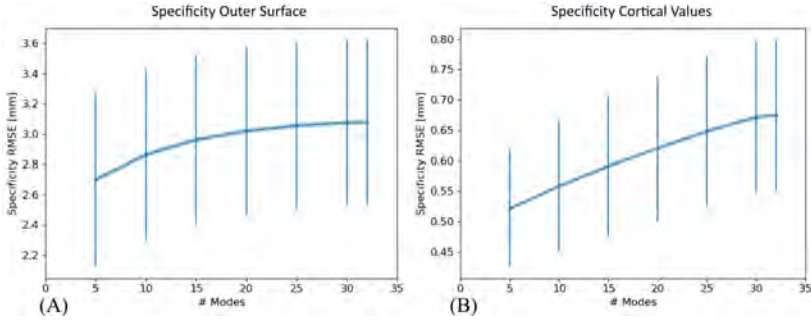


Figure 4.4: Analysis of the SSM quality. Specificity ability of the SSM evaluated for the Outer Surface (A) and the Cortical Values (B). A random sample of 1000 new instances was generated to measure the specificity.

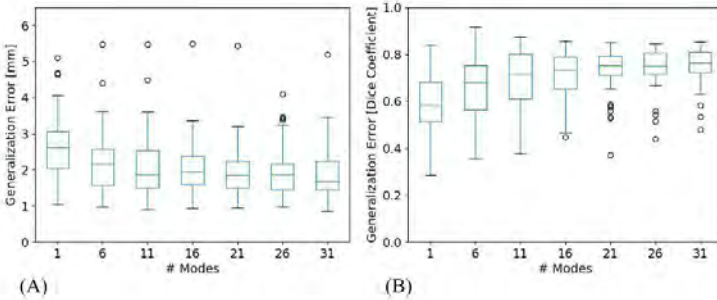


Figure 4.5: Distance (A) and Dice score (B) performances for the generalization of the trabecular surface. The distance error represents the RMSE of the Euclidean distance between the original and the reconstructed trabecular surfaces. The Dice score is calculated on the masks extracted from the two trabecular surfaces (original and reconstructed).

modes (Figure 4.4-A).

Figure 4.5 shows instead the results of the generalization for the trabecular surface. The median error decreased from 3 mm at the first mode to 1.5 mm for the plateau zone. The Dice coefficient, calculated as the overlap between the mask of the original trabecular surface and the reconstructed one, increased from a value of almost 0.6 at the first mode, to a value slightly below 0.8.

4.4 Discussion and Limitations

The main objective of this study was to provide a statistical description of the morphology and cortical bone thickness of the scapula by using statistical shape modelling techniques. It is well established that cortical bone distribution plays a fundamental role in the assessment of the fixation of shoulder implants, in particular for screw placement and orientation [40, 44].

In the current study, an automatic algorithm for cortical thickness estimation was developed and validated against manual segmentations. The inter-operator analysis demonstrated a high variability of the output (Table 1). This result underlines that the segmentation of cortical bone in the scapula remains a difficult task also for expert operators. The automatic algorithm shows results comparable to the inter-operator variability, thus making the algorithm itself a suitable alternative to perform this task. Thicker cortical regions were present in the scapular notch and spine, lateral border of the scapula and junction of glenoid neck, similarly to DiStefano et al. [56]. The presented method was able to describe the subject-specific variation of cortical bone and to provide meaningful information to include in the SSM.

In future, other techniques to segment cortical bone may be investigated and integrated in the current workflow, such as cortical bone mapping (CBM) or machine learning based approaches [155, 106]. In particular, our approach did not consider the impact of the CT-resolutions on the cortical estimation. On the contrary, CBM has proven to be able to estimate very thin cortices that are well within the resolution of the CT scanner through an optimization methods. Its application to the scapula morphology would have required validation against high-quality images, which were not available for the presented dataset.

Furthermore, a workflow was presented and validated to include bone quality information in an SSM and subsequently applied to a training dataset of 32 patients. The compactness and generalization error for the outer surface (1.5 mm) is comparable to the one of similar studies [27]. The specificity analysis results in a good convergence for the outer surface RMSE, while fully convergence could not be reached for the cortical values, possibly due to the limited number of training cases.

When looking to the generalization ability for the trabecular surface, both the Euclidean distance and the Dice score show good performances of the combined SSM. In general, the results demonstrates a high variability of the cortical distribution throughout the population, suggesting that any implant must be designed to accommodate the variation in bone quality. In a clinically relevant application, shoulder standard implants could be virtually implanted in the mean shape of the model to check for congruency between the screws position

and the distribution of cortical thickness. Similarly, through a population study, the cortical thickness distribution could be assessed for different subgroups of the population (based on gender, sex, age) thus allowing for designs that best fit a specific subgroup.

Some limitations to this study need to be acknowledged. During the construction of the SSM, cortical thickness values and point coordinates were concatenated without any normalization to build the data matrix, following the approach described in [172]. Hence, the difference in scales could bias the model. Although a thorough evaluation of the SSM was performed, further analysis is necessary to evaluate the possible impact of the bias on our analysis.

The modes of variation captured in the statistical models are strongly dependent on the training dataset. One of the main limitation of this study is the number of training subjects. A dataset of 32 scapulae may probably be not enough to fully represent the global population. Moreover, the workflow was applied to a dataset of healthy scapulae. However, the study was primarily focus on describing an automatic method to integrate cortical thickness information in an SSM of the scapula. Future work may include the extension of the dataset as well as the application to non-healthy populations that are of interest from a shoulder replacement perspective.

4.4.1 Conclusion

In this work we integrated for the first time, to our knowledge, information on the cortical thickness in an SSM for the scapula. The results demonstrate that this methodology is a valuable tool for automatically generating a large population of scapulae and deducing statistics on the cortex. Moreover, based on this pipeline, a FE model, which includes an explicit model of the cortical bone, could be automatically created to perform statistical analysis of biomechanical performance across a given population.

Chapter 5

Automated landmarking for muscle elongation measurement during RSA

This chapter addresses the third objective of the thesis, by presenting a novel method to automatically indicate humeral landmarks on medical images and allow muscle elongation quantification during preoperative planning. Validation is performed against measurements obtained from manually indicated landmarks. The usability in a clinical setting is then proved by applying the workflow to a set of arthritic shoulder joints.

This chapter was previously published as:

PITOCCHI, J., PLESSERS, K., WIRIX-SPEETJENS, R., DEBEER, P., VAN LENTHE, G. H., JONKERS, I., PÉREZ, M. A., AND VANDER SLOTEN, J. *Automated muscle elongation measurement during reverse shoulder arthroplasty planning*. *Journal of Shoulder and Elbow Surgery* (2020)

Jonathan Pitocchi and Katrien Plessers equally contributed to this manuscript. Jonathan Pitocchi contributed with data screening, landmark indication, humerus SSM creation, development of SSM registration and fitting method, leave-one-out evaluation and data processing.

5.1 Introduction

Adequate deltoid and rotator cuff tensioning in RSA is crucial to maximize the postoperative functional outcome and to avoid complications [48, 88, 95]. Insufficient muscle tensions can lead to instability problems and limited range-of-motion [31, 77, 94]. Overtensioning the deltoid muscle can result in acromion fractures, a complication with an incidence of 1 to 7% [21, 58, 75, 166]. Since muscle tensions are affected by the muscle lengths, deltoid and rotator cuff elongations should be taken into account during preoperative planning of RSA procedures.

Implant design and position, but also patient anatomy have an important impact on the muscle elongations following RSA procedures [95]. Several studies have investigated the effects of implant design and positioning on muscle elongations. Roche et al. [130] evaluated the impact of implant design and placement on muscle elongations using a musculoskeletal shoulder model and reported more anatomic muscle tensions with a lateralization of the humerus. Wright et al. [170] quantified deltoid elongation for three different baseplate positions during a cadaver test and found that inferior baseplate position increases the deltoid muscle length. Lädemann et al. [94] showed that rotator cuff lengthening is affected by the glenoid implant configuration while observing the largest rotator cuff elongation when using RSA with bone grafting. Although the impact of implant design and positioning on muscle elongations has been studied, a high level of uncertainty still exists among surgeons on how to ensure adequate muscle elongation during preoperative RSA planning [130]. Indications of deltoid and rotator cuff elongations as part of preoperative RSA planning can support surgeons evaluating the muscle tensions and refining their surgical plan accordingly [48].

To measure deltoid and rotator cuff elongations during preoperative planning, an accurate, and preferably automated measurement method is desired. Therefore, accurate identification of patient-specific muscle attachment and wrapping points is required. Manual indication of muscle attachment sites on the images or 3D models is time-consuming and subjected to inter-observer variability [48, 77]. Automated methods have been reported that transfer the muscle attachment and wrapping points from one bone model to another by defining a transformation matrix between the bone models [90, 99, 119, 129]. However, the accuracy of these transformation or morphing methods can be limited for bone models with more distinct shapes [119]. Also, the reported morphing algorithms have difficulties with incomplete bone shapes. This is problematic in the case of preoperative shoulder arthroplasty planning, as the medical images typically only contain the proximal humerus [90, 119]. More recently, machine learning based methods have been introduced to automatically detect multiple

landmarks in medical images [113, 118, 174]. While showing promising results, the accuracy of these approaches is dependent on the amount of data used for training. Additionally, only landmarks actually present on the images can be identified, thus limiting their applicability to medical images with muscle attachment points within the field of view of the scan.

Several studies have shown the potential of statistical shape modelling for automated landmark prediction based on partial or complete bone models [125, 126, 141, 157]. Statistical shape models SSM's are fitted to a target bone model, thereby better maintaining point correspondence and being less dependent on bone shape in comparison to morphing methods. Salhi et al. [132] evaluated the prediction accuracy of muscle attachment regions on the scapula and humerus using a statistical shape modeling approach. Although a good accuracy was reported, the study used only a limited evaluation dataset and did not report the errors that can be expected on muscle elongation measurements.

Therefore, the goal of this Chapter is to develop and evaluate the accuracy of an automated method for measuring deltoid and rotator cuff elongation during preoperative planning of RSA, based on a statistical shape modelling approach. The presented method consists of a landmarking algorithm to identify the muscle attachment points, and a wrapping algorithm to identify the path of each muscle around the bones and implants. Once the muscle paths are known, muscle elongation is defined as the change in muscle length relative to the preoperative joint state. Since preoperative shoulder arthroplasty images typically only contain the proximal humerus, the accuracy of the muscle attachment points and muscle elongation measurements is evaluated for both complete and partial humerus models. Additionally, the automated workflow accuracy is evaluated for a dataset of arthritic shoulder joints, used for preoperative planning of shoulder arthroplasty. Finally, a sensitivity study is performed to demonstrate the effect of implant positioning on muscle elongations.

5.2 Material and Methods

5.2.1 Data

A set of 40 CT-scans with a complete scapula and humerus was selected for evaluating the muscle elongation measurements. The average slice spacing of the acquired images was 0.5 mm. The set included 25 males and 15 females, with an average age of 63 years. All selected scapulae and humeri showed no significant signs of bone defect or arthropathy. The scans were manually segmented in the image processing software Mimics v.20 (Materialise, Leuven,

Belgium) and converted to 3-dimensional models, with a mean triangular edge length of 1.5 mm for the scapulae and 2 mm for the humeri. To simulate the presence of an incomplete humerus on the scan and evaluate its impact on the presented method, partial humerus models were created from the 40 complete humerus models by artificially cutting the bone to 30% length from the top.

For indication of the muscle attachment points, SSM's of the scapula and humerus were required. A scapula SSM was already presented in a previous study [125]. This SSM included 66 three-dimensional models of healthy scapulae and was used to successfully reconstruct glenoid bone defects. The scapula models were segmented from CT-scan images and showed no signs of bone defect or arthropathy (cysts, osteophytes, or sclerosis). For the humerus, a new SSM was built based on the same 40 complete humerus models that were used for evaluation. The creation of the SSM is described below.

To assess the accuracy of the automated workflow on arthritic joints, 50 CT-scans were randomly selected from a dataset of images used for preoperative planning of shoulder arthroplasty. All scapulae and humeri showed signs of bone defect or arthropathy. The scans had an average slice spacing of 0.6 mm and were acquired with different machine parameters. Using Mimics v.20 (Materialise, Leuven, Belgium), the scapula and proximal humerus were converted to 3-dimensional bone models with a mean triangular edge length of 1.5 mm and 2 mm, respectively.

5.2.2 Anatomic landmarks

Eleven and six anatomic landmarks were identified on the scapula and humerus respectively. On the scapula, the subscapularis, supraspinatus and infraspinatus attachment points are located centrally and close to the medial side of the subscapularis, supraspinatus and infraspinatus fossa, respectively (Figure 5.1). The teres minor attachment point was defined in the middle of the scapula's lateral rim. The middle and posterior deltoid attachment point are located at the tip of the acromion and at the middle of the scapular spine, respectively. Furthermore, the scapula coordinate frame was defined by the glenoid center point (center of mass of all points on the glenoid surface), trigonum spinae (midpoint of triangular surface on the medial border) and angulus inferior (most inferior point) [69, 125]. To compute the wrapping of the muscles, two additional landmarks were identified, the acromion and coracoid neck point.

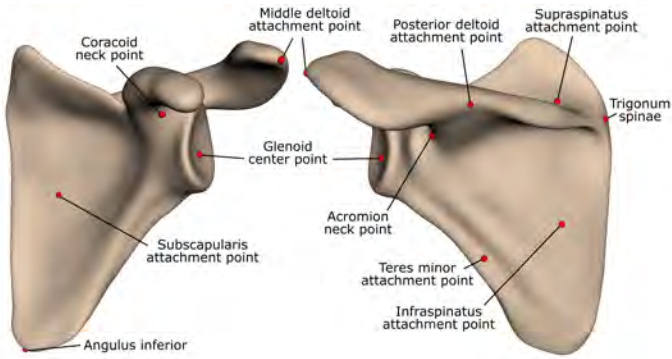


Figure 5.1: Anatomic landmarks on the scapula.

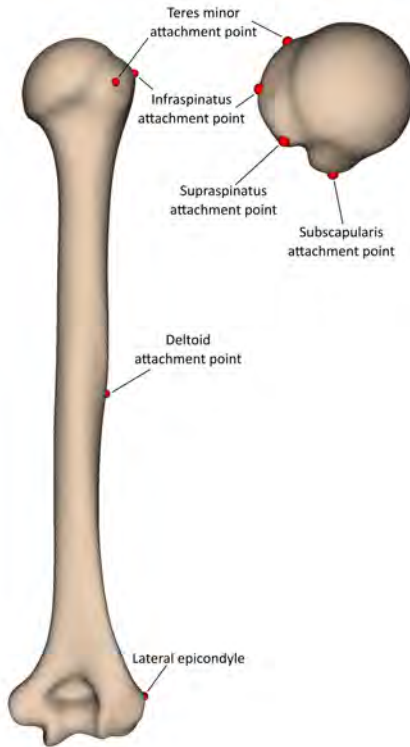


Figure 5.2: Anatomic landmarks on the humerus.

On the humerus, the supraspinatus, infraspinatus and teres minor attachment points are located on the anterior, lateral and posterior side of the greater tubercle, respectively (Figure 5.2). The subscapularis attachment point was defined on the middle of the lesser tubercle. Since the deltoid tuberosity is not clearly visible on the humerus model, the deltoid attachment point was identified at 50% of the humerus length and above the lateral epicondylar point, consistent with what is reported in cadaveric studies in literature [107, 115]. The deltoid attachment point on the humerus is the attachment point for both the middle and posterior deltoid.

5.2.3 Humerus SSM

To create a humerus SSM, muscle attachment points and epicondylar points were manually indicated on the 40 complete humerus models, by two experts (JP, KP). The deltoid attachment point was derived from the lateral epicondylar point, as described previously. The mean landmark positions of the two observers were projected to the surface of the humerus model to obtain the final landmark positions. These final landmarks served as input for the humerus SSM creation. Inter-observer variability was computed for all muscle attachment points as the distance from the observed landmark position to the mean landmark position [159].

Based on the 40 complete humerus models and indicated landmarks, an SSM was created (Python 3.7). In order to capture the variation between the models, all humerus models required corresponding points. To solve the corresponding point problem, one model of the data set was registered as a template to all other models [125, 157]. First, the template was aligned to the other models using an iterative closest point algorithm without scaling [19]. Then, a Thin Plate Spline (TPS) registration algorithm [147] was applied using the manually indicated landmarks, to guide the shape deformation of the template to the other models. Next, the elastic surface registration algorithm of Danckaerts et al. [45] was applied to fine-tune the shape deformation. After registration, all models were aligned by excluding the translational and rotational variations, using a Procrustes algorithm without scaling. Finally, a Principal Component Analysis was performed to extract the mean shape and the different modes of variation [41].

5.2.4 Automated landmarking

Muscle attachment points and coordinate frames can be automatically identified on a target shape using an SSM [125, 157]. The required landmarks are manually

indicated on the mean SSM shape and then transferred to the target shape by registering and fitting the SSM. For the scapula, the registration and fitting method was described in a previous study [126]. Using an iterative approach, the mean SSM shape is registered to the target scapula shape, corresponding points are identified, and the SSM coefficients are computed by adapting the SSM shape to match the identified corresponding points (Python 3.7).

For the humerus, the registration and fitting methods were adapted to account for the axisymmetric shape of the humerus and to include scans that only contain the proximal humerus. The adapted registration method consists of two steps (Figure 5.3). Firstly, the mean shape of the SSM is cut by planes at different heights and each resulting proximal mean shape is aligned to the target shape using an inertia registration. A uniform scaling is applied to count for the difference in size. Between all the cutting planes, the one that minimizes the root mean square (RMS) of the distances between the proximal mean shape and the target shape, is selected. Secondly, the selected proximal mean shape is iteratively rotated around its long axis and registered to the target model through an Iterative Closest Point (ICP) algorithm to find the rotation angle that minimizes the RMS of the distances. This second step enforces a good alignment, despite the axisymmetric shape of the humerus.

After the registration, the SSM is fitted to the target humerus shape. The fitting method, as described in a previous study [126], was adapted to ignore points that are lying under the selected cutting plane, as obtained from step one of the registration. Hence, these points are excluded from the corresponding point search of the fitting method, so that only the information present in the scan is taken into account.

After fitting the SSM, the muscle attachment points are projected from the fitted SSM shape to the target scapula and humerus shape. Since the CT scan of some patients only contained the proximal part of the humerus, the deltoid attachment point cannot always be projected to the target humerus because in these cases the corresponding surface is not available. Therefore, the deltoid attachment point is only projected to the target humerus shape if it lies above the cutting plane obtained from the registration method (Figure 5.3). This means that the deltoid attachment point can be floating if only the proximal humerus is present in the scan.

5.2.5 Muscle length measurement

Once the muscle attachment points are identified, the rotator cuff and deltoid paths can be computed. Similar to existing musculoskeletal models [81, 136], each muscle is represented by a line trajectory (Figure 5.4). The rotator

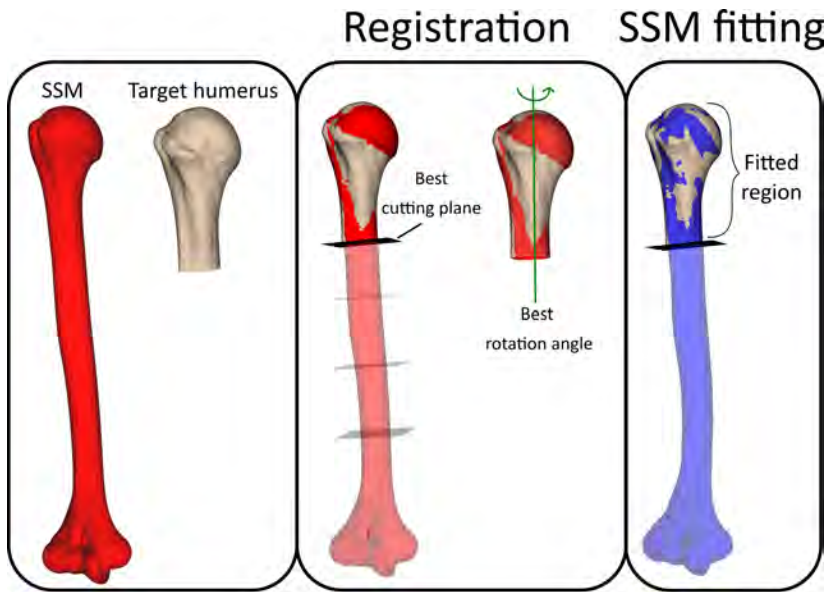


Figure 5.3: Workflow for registration and fitting of the humerus SSM to a target humerus shape. The target humerus shape can contain the complete humerus or only the proximal part (left). First, the best cutting plane and best rotation angle are selected to register the SSM to the target humerus shape (middle). Second, the SSM is fitted to the target humerus shape, while ignoring all SSM points that are below the selected cutting plane (right).

cuff is visualized by four line trajectories, the supraspinatus, infraspinatus, subscapularis and teres minor. The deltoid muscle is shown by two line trajectory, the middle deltoid and the posterior deltoid. The anterior deltoid is excluded in this study, to avoid the need of a 3D model of the clavicle.

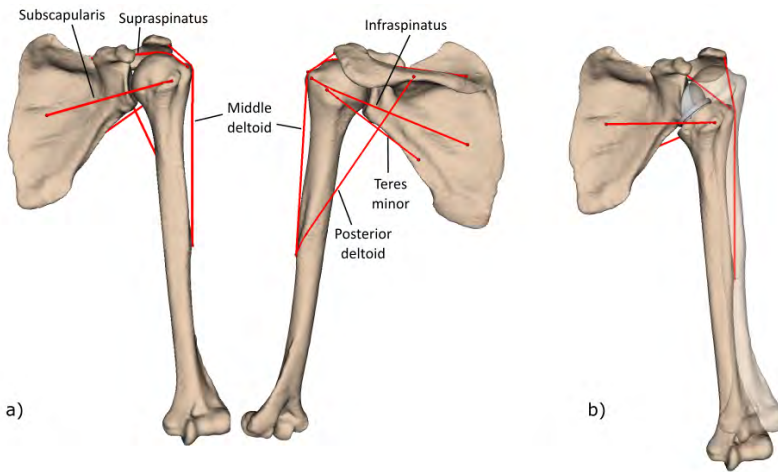


Figure 5.4: Rotator cuff and deltoid visualization for the preoperative situation (a) and with a planned shoulder arthroplasty (b). Muscle elongation is defined as the difference in length between the planned and preoperative situation.

A wrapping algorithm is used to identify the wrapping points forcing the muscle to wrap around the bones and potential implants (Python 3.7) (Figure 5.5). This wrapping algorithm is a recursive algorithm that identifies the most distant point from the muscle line segment in a specific direction. This direction is obtained as follows. First, a fixed wrapping direction is defined for each muscle (Figure 5a). For the supraspinatus, infraspinatus, subscapularis, teres minor, middle deltoid and posterior deltoid, the fixed wrapping directions are superior, posterior, anterior, posterior, lateral and posterolateral respectively, relative to the scapular coordinate frame. Then, this fixed wrapping direction is projected to the plane, perpendicular to the muscle line (Figure 5.5-b). Hence, the wrapping algorithm looks for the most distant point on the bones or implants along this projected wrapping direction. After identifying this wrapping point, the muscle is split in two separate line segments and the algorithm is applied to both segments separately, until no more points can be found along the projected wrapping direction (Figure 5.5-c).

To avoid wrapping of the supraspinatus and subscapularis around the acromion and coracoid, the acromion and coracoid surfaces are cut off before starting the wrapping algorithm. All points of the scapula model that lie superior and posterior to the acromion neck landmark or superior, anterior and lateral to the coracoid neck landmark, measured in the scapula coordinate frame, are not

taken into account in the calculation.

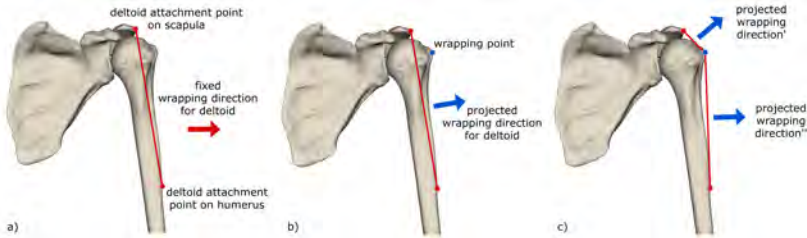


Figure 5.5: Wrapping algorithm: (a) for every muscle a fixed wrapping direction is defined, (b) the fixed wrapping direction is projected to the plane perpendicular to the muscle line and the furthest point along this projected wrapping direction is identified as a wrapping point, (c) the muscle line is split in two separate line segments and the wrapping algorithm is recursively applied on each of these segments.

When the muscle path is known, the muscle length is computed as the sum of the lengths of the different line segments. Muscle elongation is defined as the difference in muscle length between the preoperative situation (no implants) and the postoperative or planned situation, in which a shoulder arthroplasty has been (virtually) implanted (Figure 5.4).

5.2.6 Evaluation of humerus landmarking accuracy

The accuracy of the automatically identified humerus landmarks and their effect on muscle length and elongation measurements were evaluated by comparing the manually indicated landmarks with the automatically identified ones for the set of 40 scapula and humerus models.

First, the muscle attachment points on all 40 scapula and humerus models were automatically identified by fitting the SSM's and projecting the landmarks, as previously explained. Since the humerus SSM was created from the same data used as evaluation dataset, a leave-one-out cross-validation was performed. For each selected humerus, a new 'sub'-SSM was created from all the 39 remaining humeri while excluding the selected one. This evaluation was repeated for all 40 humeri.

After identifying the muscle attachment points, additional wrapping points were determined and the muscle lengths were computed. Next, a reverse humerus and glenoid implant were virtually implanted (DePuy Synthes, Warsaw, United

States). For all subjects, glenoid and humeral implants (38 mm glenosphere) were positioned in a fixed position. The glenoid metaglene was positioned 5 mm below the glenoid center point, in 0° inclination and version relative to the mediolateral axis of the scapula [18, 31]. The humeral implant was positioned along the humeral shaft, with 30° retroversion. The muscle lengths were recomputed and the muscle elongations relative to the preoperative situation were calculated. Finally, the muscle length and elongation measurements were repeated for all subjects using the manually indicated landmarks and compared to the results with the automatically indicated landmarks.

To evaluate the accuracy for patients with incomplete humerus on the scan, each humerus was cut to 30% length from the top and the automated landmark indication and muscle measurements were repeated. A paired t-test was performed to investigate if there was a statistical significant ($p < 0.05$) difference between the results for the complete and partial (30%) humerus.

Since the scapula SSM and fitting method showed a good accuracy for the prediction of anatomic landmarks in a previous study [125] (a mean error of 1.8 mm on the glenoid center point), the accuracy of scapula muscle attachment points and its effect on the muscle measurements were not evaluated in this study.

5.2.7 Application to arthritic joints

To assess the accuracy of the muscle elongation measurements on arthritic joints, the automated workflow was evaluated for a set of 50 arthritic scapula and humerus models. Since the humerus models only contained the proximal part of the humerus, the middle and posterior deltoid were excluded from the evaluation. First, the muscle attachment points on all humerus models were manually indicated by two experts (JP, KP) reaching consensus and automatically indicated by fitting the SSM's and projecting the landmarks, as previously explained. Then, all bone models were virtually implanted with a reverse humerus and glenoid implant (DePuy Synthes, Warsaw, United States). Finally, muscle elongations were measured with the manually indicated landmarks and with the automatically indicated landmarks, and the results were compared between both methods.

5.2.8 Sensitivity analysis

To demonstrate the use of muscle length measurements during preoperative planning, a sensitivity study was performed on the set of 40 complete scapula

and humerus models. The effect of implant positioning on muscle elongation was evaluated by subsequently translating the glenoid baseplate 5 mm more lateral and the humeral implant 5 mm more superior. Also, the effect of implant orientation was investigated by subsequently rotating the glenoid baseplate 10° more retroverted and the humeral implant 10° more anteverted (resulting in 20° of humeral retroversion). For each position and orientation of the implants, muscle elongations were measured for the four rotator cuff muscles and the two deltoid muscles. Since RSA is more and more used with an intact rotator cuff, no muscles were excluded from the sensitivity analysis [34, 102].

5.3 Results

The inter-operator error for the subscapularis, supraspinatus, infraspinatus and teres minor attachment points on the humerus showed a median and interquartile range (IQR) of 0.8 mm [0.4 mm, 1.2 mm], 0.5 mm [0.3 mm, 0.7 mm], 1.2 mm [0.6 mm, 2.0 mm] and 1.2 mm [0.6 mm, 3.0 mm], respectively (Figure 6). The deltoid attachment point, which is derived from the lateral epicondylar point, resulted in an inter-operator variability of 0.1 mm [0.0 mm, 0.2 mm] for the median and IQR.

When automatically indicating the landmarks on the complete humerus models using the SSM, errors with a median and IQR of 1.8 mm [1.1 mm, 2.9 mm], 1.9 mm [1.3 mm, 2.7 mm], 2.2 mm [1.1 mm, 4.0 mm], 3.5 mm [1.8 mm, 5.0 mm] and 0.8 mm [0.6 mm, 1.2 mm] were observed for the muscle attachment points of the subscapularis, supraspinatus, infraspinatus, teres minor and deltoid. For the partial humerus models, the errors resulted in a median and IQR of 1.8 mm [1.2 mm, 2.8 mm], 1.6 mm [1.2 mm, 2.3 mm], 2.1 mm [1.5 mm, 3.3 mm], 3.0 mm [2.0 mm, 4.9 mm] and 8.6 mm [5.3 mm, 11.9 mm], respectively. Only for the deltoid attachment point, a significant ($p < 0.05$) difference was found between the results for the complete and partial (30%) humerus.

Using the complete humerus models, muscle elongations after reverse shoulder arthroplasty implantation, were predicted by the SSM with an error (median and IQR) of 0.3 mm [0.1 mm, 0.4 mm], 0.6 mm [0.3 mm, 1.0 mm], 0.2 mm [0.1 mm, 0.6 mm] and 0.4 mm [0.1 mm, 0.8 mm] for the subscapularis, supraspinatus, infraspinatus and teres minor, respectively (Figure 5.7). For the middle and posterior deltoid, the median and IQR of the errors were below or equal to 0.1 mm. When using the partial humerus models, no significant ($p < 0.05$) differences were observed in the muscle elongation errors, except for the deltoid. The median and IQR of the errors on the middle and posterior deltoid elongation increased to 0.1 mm [0.0 mm, 0.2 mm] and 0.8 mm [0.5 mm, 1.7 mm], respectively.

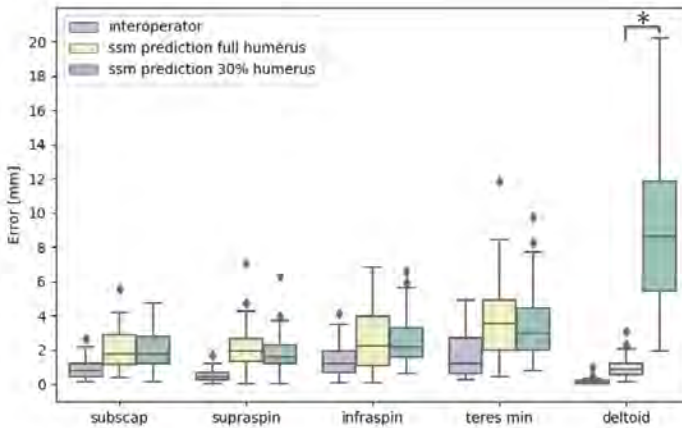


Figure 5.6: Inter-operator and SSM prediction errors on the muscle attachment points of the subscapularis (subscap), supraspinatus (supraspin), infraspinatus (infraspin), teres minor (teres min) and deltoid. The SSM prediction errors are computed for a complete humerus and partial (30%) humerus.

When applying the automated workflow to arthritic shoulder joints, muscle elongations were predicted by the SSM with an error (median and IQR) of 0.5 mm [0.2 mm, 1 mm], 1.1 mm [0.6 mm, 1.9 mm], 0.5 mm [0.2 mm, 1.1 mm] and 0.6 mm [0.3 mm, 1.2 mm] for the subscapularis, supraspinatus, infraspinatus and teres minor, respectively (Figure 5.8).

As shown by the sensitivity study, muscle elongations were affected by implant positioning (Table 5.1). With the initial position of the glenoid and humeral implants, the subscapularis, infraspinatus and teres minor showed a shortening or negative elongation compared to the preoperative situation, with a median of respectively -15 mm, -23 mm and -26 mm. The middle and posterior deltoid were elongated in all subjects, with a median of 19 mm. The supraspinatus showed a median of 0 mm elongation. Translating the glenoid implant 5 mm more lateral stretched the rotator cuff muscles compared to the default implant position, with a median of 4 to 5 mm. Deltoid elongation only slightly increased with the lateral translation of the glenoid implant. When positioning the humerus implant 5 mm more superior, corresponding to an inferior offset of the humeral bone, deltoid elongation increased from a median of 19 mm to 24 mm compared to the initial implant positions. Rotator cuff elongations, however, were only minimally affected by a more superior humerus implant position.

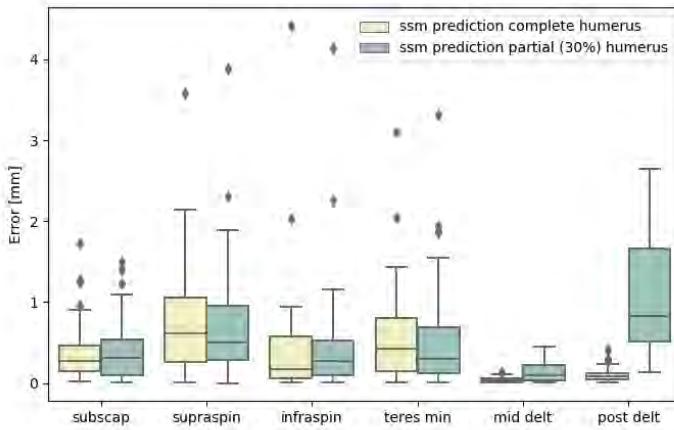


Figure 5.7: SSM prediction errors on the muscle elongations of the subscapularis (subscap), supraspinatus (supraspin), infraspinatus (infraspin), teres minor (teres min) and deltoid. The SSM prediction errors are computed for a complete humerus and partial (30%) humerus.

Finally, changing the retroversion of the humeral and glenoid implant showed a limited effect on the muscle elongations.

	Subscapularis	Supraspinatus	Infraspinatus	Teres minor	Middle deltoid	Posterior deltoid
Initial implant positions	-15 [-21, -13]	0 [-8, 2]	-23 [-27, -21]	-26 [-29, -24]	19 [15, 23]	19 [16, 22]
+5 mm lateral glenoid implant	-10 [-17, -8]	4 [-4, 6]	-19 [-23, -16]	-22 [-25, -19]	20 [17, 24]	22 [17, 24]
+5 mm superior humerus implant	-15 [-21, -12]	3 [-5, 6]	-23 [-28, -21]	-27 [-31, -25]	24 [20, 28]	24 [20, 27]
retroversion humerus implant -10°	-16 [-22, -12]	-1 [-9, 3]	-22 [-26, -19]	-25 [-28, -22]	18 [15, 22]	19 [16, 22]
retroversion glenoid implant +10°	-15 [-21, -13]	0 [-8, 2]	-23 [-27, -21]	-26 [-29, -24]	19 [15, 23]	19 [16, 22]

Table 5.1: Effect of implant position on muscle elongation measurements. Median and interquartile distance are reported in millimeter.

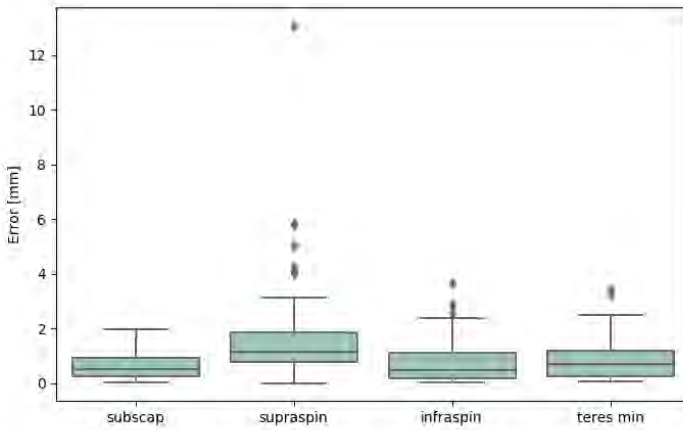


Figure 5.8: SSM prediction errors on the muscle elongations for the arthritic joints: results are reported for the subscapularis (subscap), supraspinatus (supraspin), infraspinatus (infraspin) and teres minor (teres min), being the deltoid attachment point on the humerus out of the scan.

5.4 Discussion

Estimates of deltoid and rotator cuff elongation can support surgeons during preoperative shoulder arthroplasty planning in selecting an implant design and position resulting in adequate muscle tensions. Therefore, this Chapter presented and evaluated a fully-automated method to accurately measure deltoid and rotator cuff elongations, thus eliminating the need of time-consuming manual interactions. Since preoperative shoulder arthroplasty images typically only contain the proximal humerus, the method was evaluated for both complete and partial humeri. To evaluate its use in a clinical setting, the method was additionally applied on a set of arthritic shoulder joints.

First, the method was evaluated for automated identification of muscle attachment points on a set of 40 complete humerus models. The errors on the automatically identified landmarks were higher than the interoperator errors for all landmarks. This was partly due to the accuracy of the SSM landmarks being limited by the 2 mm SSM mesh size. To clarify, the landmarks on the SSM are linked to the nodes of the SSM mesh, while the operators were allowed to put landmarks in between the nodes. Furthermore, a correlation

was observed between the inter-operator errors and the automatic landmarking errors. Landmarks that were indicated less consistently, like the teres minor and infraspinatus, showed higher automatic landmarking errors compared to other landmarks.

For the partial humerus models, the automatic landmarking errors slightly decreased for the subscapularis, supraspinatus, infraspinatus and teres minor attachment points. Since the SSM is fitted to a smaller surface, it better optimizes its shape towards this small surface, resulting in a more accurate indication of the landmarks. However, for the deltoid attachment point the automatic landmarking errors largely increased when only the proximal humerus was available. These large errors are due to the lack of information related to the distal humerus, which is not taken into account when fitting the SSM. Since the deltoid attachment point is defined by the lateral epicondylar point and the humerus length, the distal shape of the humerus is important for accurately predicting its position.

The SSM-based landmarking algorithm performs better than alternative methods reported in literature. Pellikaan et al. [119] investigated the accuracy of a morphing method to transform the muscle attachment regions between two cadaver legs. They reported morphing errors with a median > 10 mm for all muscle attachment regions, which is higher than the median of 0.8 to 3.5 mm that we measured on the muscle attachment points. Kaptein et al [90] evaluated a similar morphing method on the muscle attachment regions of the shoulder bones. They obtained a median of > 7 mm on the morphing errors. Other methods to transform muscle attachment points from one bone to another, include linear or non-linear scaling [101]. Also these methods were found to perform less accurate than the SSM-based landmarking algorithm presented in this study [101, 119]. Our results are comparable to other SSM-based landmarking methods described in literature. Salhi et al. [132] investigated the prediction accuracy of subject-specific muscle attachment regions, using a healthy scapula and humerus SSM. For the humerus, they reported an average RMS error between 0.4 mm – 1.7 mm and a Hausdorff distance between 1.6 mm – 4.8 mm for all muscle attachment regions. Similar to our results, the muscles followed the same descending order of accuracies, going from subscapularis, supraspinatus, infraspinatus to teres minor. In contrast to our study, Salhi et al. [132] did not evaluate the prediction accuracy when only 30% of the humerus was available in the scan.

Next, the presented method was evaluated for measuring muscle elongations following RSA. When virtually implanting an RSA, muscle elongations were predicted with errors below 1 mm, for 75% of the subjects. These errors are lower than the errors on the muscle attachment points. As a result, the relative changes in muscle lengths between the planned and preoperative situation can

be computed more accurately than the exact location of the muscle attachment points. Hence, the muscle elongation measurements are insensitive to errors on the muscle attachment points. Since the impact of implant positioning on muscle elongations is generally larger than 1 mm, we conclude that the muscle elongation measurements are sufficiently accurate for use during preoperative shoulder arthroplasty planning. For the partial (30%) humerus models, the errors on the rotator cuff and middle deltoid elongation remained below 1 mm for 75% of the subjects. Only for the posterior deltoid, the errors (median and IQR) increased to 0.8 mm [0.5 mm, 1.7 mm], when having a partial humerus model. When applied to the set of 50 arthritic shoulder joints, the automated workflow reported slightly higher error predictions, with values still below 2 mm for 75% of the subjects. As we believe that these errors are still acceptable for clinical decision making, muscle elongation measurements can be applied in a clinical setting in which scapula and humerus can show signs of bone defect and in which no complete model of the humerus needs to be present.

Finally, the sensitivity analysis confirmed the effects of implant positioning on muscle elongation measurements, in line with other studies in literature. As reported by Roche et al. [130], lateralization of the glenoid component increases the length of the rotator cuff muscles, which was also seen in our study. Lädermann et al. [94] observed approximately 8 mm more elongation for all muscles when using a Bony Increased Offset RSA with 10 mm lateral offset instead of a normal RSA. Similar to our results, Wright et al. [170] observed an increased deltoid elongation when using increasing inferior offsets. The fact that glenoid and humeral implant retroversion had limited effect on the muscle elongation measurements, can be explained by the unaltered orientation of the humerus relative to the scapula. Although retroversion changes the orientation of the implant in the bone, the orientation of the humerus relative to the scapula remained the same.

5.4.1 Limitations

This study has some limitations. While the automated workflow was tested on arthritic joints, the accuracy of the middle and posterior deltoid muscle could not be assessed since its attachment point on the humerus was out of the scan field of view. Second, we did not evaluate the accuracy of the automatically indicated scapula landmarks. Since the scapula SSM and fitting method showed a good accuracy for the prediction of landmarks and measurements in previous studies [125, 157], we did not re-evaluate this ability for the current muscle attachment points. Also, as demonstrated by Salhi et al. [132], the muscle attachment points on the scapula are expected to be indicated with a higher

accuracy than the muscle attachment points on the humerus, because of the more distinct anatomic regions of the scapula.

As a third limitation, we defined muscle attachment points, instead of using the complete muscle attachment regions. Although muscle attachment regions are a more accurate representation than points, muscle attachment points are required in order to represent the individual line trajectory of the muscle. This approach is comparable to other studies that measure muscle lengths [48, 130]. Also, the exact location of the muscle attachment point has a limited impact on the muscle elongation measurements, as demonstrated in this study.

A last limitation of this study is that the quality of the soft tissues is not taken into account. Therefore, it might be that the preoperatively selected elongations are not feasible and that the muscles do not accept this elongation during surgery. Despite this limitation, measuring muscle elongations during preoperative planning of shoulder arthroplasty is a first step towards integrating soft tissue information and to support surgeons in selecting a suitable implant design and position.

5.5 Conclusions

This study presents an automated method for accurately measuring muscle elongations during preoperative planning of shoulder arthroplasty. The method was able to measure rotator cuff and deltoid elongation with an error below 1 mm for 75% of the subjects. Only the errors on the posterior deltoid increased when 30% of the complete humerus was present in the scan. Muscle elongation errors for the arthritic joints were lower than 2 mm for 75% of the subjects. As a result, the presented method can be applied in a clinical setting, despite the fact that medical images for shoulder arthroplasty typically only contain the proximal humerus and bones can show signs of arthropathy. Moreover, the sensitivity analysis showed that the measurements are affected by implant positioning and thus can support surgeons to evaluate and refine their surgical plan during preoperative planning of shoulder arthroplasty. Even though the optimal values for muscle elongation are not yet known, the measurement method allows an objective comparison of muscle elongations for different implant designs and positions, as well as patient anatomies. Furthermore, the method facilitates processing large datasets and investigating the impact of muscle elongations on postoperative outcomes.

Chapter 6

General discussion and conclusion

In the final chapter of this thesis, the main conclusions are summarized. In section 6.2, the relevant clinical applications of the proposed work are presented. Finally, suggestions for future studies are illustrated.

6.1 Summary of Key Results

The main goal of this thesis was to develop and evaluate novel and automated methods for a personalized Reverse Shoulder Arthroplasty (RSA), using state-of-the-art computer aided technologies. In particular, driven by a patient oriented strategy, the research focused on overcoming some of the limitations affecting the design of custom implants and the preoperative planning for shoulder arthroplasty, by translating the goal into the three research objectives defined in Chapter 1. The level of completion of these research objectives is discussed in detail in the remainder of this section.

Virtual Bench Test for design of custom shoulder implants

The design of custom implants is currently a complex task, which requires the definition of different parameters through extensive manual labor. A major drawback is the lack of objective measuring tools to support design decisions and adaptations, thus increasing the risk of subjectivity during the multiple steps carried out by trained engineers. Ideally, those parameters should be optimized to have sufficient initial implant stability, but the use of mechanical tests is not practical.

For this reason, in Chapter 3, an automated method to evaluate the initial stability of custom shoulder prosthesis was presented. Through the development of a FE workflow, the Virtual Bench Test aimed to replicate a standard experimental set-up normally required for FDA clearance of new implants. To the author's knowledge, this was the first study to automate, evaluate and validate a full *in-silico* modeling of the ASTM F2028-14 for a custom-made prosthesis.

The proposed method, starting from parameters that are normally available during the design phase, is able to provide a tool to guide the engineers during their decisions without any additional manual input. In particular, the bone-implant interface analysis, which results in the calculation of the micro-motion map, can be used as a reference during the design of the implants, always looking for a trade-off between stability (with a bone ingrowth threshold set at 150 μm) and clinical requirements.

The model was validated against experimental data acquired during the development of the thesis and showed good agreement, with a correlation coefficient of 0.81 (high). Although lower than other reported correlations, the validation outcome is the result of a trade-off between accuracy and computational cost. Computational cost should be kept low for the purpose of using the VBT in the current design workflow.

Assessment of scapular cortical thickness using statistical models

The design of standard shoulder implants, which can fit patients with different pathology and bone characteristics, requires knowledge about bone morphology and bone quality of the scapula throughout a certain population. In particular, regions with the best bone stock (cortical bone) are taken into account when defining the position and orientation of the screw holes, aiming for an optimal fixation. Commonly, manual measurements on medical images or cadaveric bones are performed to extract this anatomical information, but the process is tedious, time-consuming and limited by the numerosity of the input sample sets.

In Chapter 4, an SSM of the scapula was built to integrate both morphological and cortical thickness information. First, a method to estimate cortical thickness, based on HU profile analysis, was developed and validated. Then, based on the manual segmentations of 32 healthy scapulae, a statistical shape model including cortical information was created and evaluated. Generalization, specificity and compactness were calculated in order to assess the quality of the model. The average cortical thickness of the SSM was 2.0 ± 0.63 mm. Generalization, specificity and compactness performances confirmed that the combined SSM was able to capture the bone quality changes in the healthy population.

To the author's knowledge, this was the first study to integrate cortical thickness information in an SSM of the scapula. The results demonstrated that this methodology is a valuable tool for automatically generating a large population of scapulae and deducing statistics on the cortex. Finally, this workflow represents an alternative to manual measurements for orthopaedic companies that, by virtually implanting novel devices on the SSM, can verify their congruency inside a generated virtual population, thus reducing the number of design iterations and cadaver labs.

Automated landmarking for muscle elongation measurement during RSA

In order to integrate muscle elongation measurements in the preoperative planning of RSA, which has the potential to support surgeons in the selection of a suitable implant design, an accurate and automated method to indicate landmarks, i.e. muscle attachment points, is necessary. Additionally, since medical images often do not contain the distal humerus, such a method should be flexible enough to give meaningful results even when only the proximal humerus is present on the scans, a goal that state-of-the art technologies currently fail to achieve.

For this reason, in Chapter 5 a method to automatically measure deltoid and rotator cuff elongation relative to the preoperative situation was developed

and evaluated. First, a humerus SSM was created using 40 full humeri to automatically indicate muscle attachment points. Then, a wrapping algorithm was developed to identify the muscle paths and measure the muscle elongations following virtual RSA implantation. The accuracy of the muscle elongation measurements was evaluated by comparing the automatically indicated muscle attachment points with manually indicated points. Finally, the effect of implant positioning on muscle elongations was assessed.

For 75% of the subjects, deltoid and rotator cuff elongations following virtual RSA implantation were predicted with an error below 1 mm, even when only 30% of the humerus was available. To demonstrate its clinical applicability, the automated workflow was applied to a set of 50 arthritic joints, resulting in muscle elongation errors below 2 mm for 75% of the cases, which was considered to be sufficient for its use in the clinical evaluation process.

Additionally, as shown by the sensitivity analysis, the effects of implant positioning on muscle elongations were in line with other studies in literature. As a conclusion, using the muscle elongation measurements, surgeons are able to evaluate and refine clinical decisions during preoperative RSA planning.

6.2 Clinical Application

The methods developed during this thesis have the potential to overcome some of the limitations in the personalized shoulder care. Clinical exploitation is an important aspect for any research applied to medical practice and also in the context of this work, meaningful steps have been taken in its direction.

Virtual Bench Test for design of custom shoulder implants

The past few years have witnessed a growing interest on the applications of *in-silico* models to the medical field. Computational simulations are now emerging as paradigm shifting technologies in the development of medical therapies and devices and, additionally, in the replacement of animal experimentations or bench test set-up [158]. As a confirm of the importance of this topic, the American Society of Mechanical Engineers (ASME) started publishing different standards to regulate the use of computer models in the pre-clinical or clinical phase of a novel medical product [161].

The presented work on the automation of a bench test for custom shoulder implants perfectly fits to the new concept of *in-silico* trials, in which patient-specific modelling is part of the regulatory evaluation of new medical devices. Evidently, to be safely applied in a setting in which there could be potential risk for the patients, an extensive validation and verification of the workflow

is necessary, in order to assess the credibility of the predictive model. Aiming for this goal, future research on this subject should focus on the acquisition of additional experimental evidences, as discussed more in detail in section 6.3. However, a first 'low-risk' application of the VBT in a pre-clinical context was already possible and it is here reported as another contribution brought by this thesis.

In the process of FDA clearance of the Glenius system, which would allow for the custom implant to be commercialized in US, various evidences (mechanical, clinical, etc.) need to be gathered. One of the necessary mechanical tests [13] is described in Chapter 3 and is used for assessing the risk of glenoid loosening in shoulder implants. While for standard prosthesis with few or no design variations mechanical experiments can be performed in an agile manner, for patient-specific devices, testing all the possible variations is not possible.

Therefore, the implant-bone construct test needs a validation on the worst case implant of the design space. However, the design space of Glenius is so wide that it is impossible to parametrize, which makes the definition of a worst case implant extremely complicated. To overcome this issue, the developed VBT was used in an extensive sensitivity analysis, similarly to what is reported in Chapter 3 of this manuscript, to narrow the design space, by evaluating the impact on the initial implant stability of changing input parameters.

Together with clinical and hardware engineers, multiple worst case configurations were identified, by varying some of the prosthesis specifications, e.g. number and position of screws, type of screws, flat or non-flat contact surface, etc. The FE workflow was used to discriminate the most promising designs, for which the simulation predicted good initial stability, from the 'bad' ones, which had a higher risk of failing the test. After some iterations, in which mechanical tests were also performed, the synergy between *in-silico* models and experimental evaluation resulted in a final worst case configuration, which ultimately passed the test requirements, by still remaining representative of the possible population of Glenius devices.

The reported application is a clear example of how computer simulations can be used in a pre-clinical setting, by supporting and accelerating the development of new medical devices. In fact, the VBT contributed to reduce the number of experimental iterations necessary in the definition of a worst-case design, with significant benefits in terms of cost and time savings.

Automated landmarking for muscle elongation measurement during RSA

In the last few years, the research and development of preoperative planning platforms has moved towards the extension of the information available to the

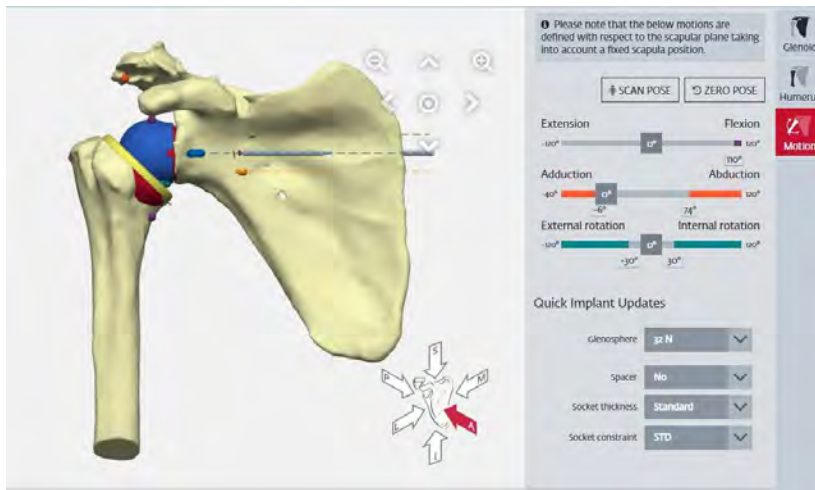


Figure 6.1: Humeral positioning in Materialise preoperative planning software for shoulder arthroplasty (courtesy of Materialise NV).

surgeons, mainly to provide them with additional tools in support of their clinical decisions. For instance, while initially the planning systems allowed only for a guided placement of the implants, which could have been then transferred into the operating room through PSI, the more recent versions are becoming more sophisticated, with innovative functionalities and extended capabilities. Taking that into consideration, the automated workflow presented in Chapter 5 has the potential to bring novel applications in the current Materialise planner.

The research carried out during the development of the humeral SSM, although not described in this manuscript, was at the base of the integration in the Materialise product of the humeral implant planning, a feature that was previously lacking. In particular, the created SSM is used to automatically detect the anatomical neck of the humeral head, a surgical landmark taken as reference for default implant positioning (Figure 6.1). This functionality also goes in the direction of shifting from a glenoid only planning approach towards a total shoulder joint (glenoid + humeral component) planning approach, a trend that is also seen in other commercial software.

Additionally, as reported in Chapter 5, the clinical applicability of the automated workflow was demonstrated on a representative set of 50 arthritic joints, resulting in an error below 2mm for 75% of the subjects. This will soon lead, thanks to the joint effort of the shoulder research group of Materialise, to the integration of the muscle elongation measurements into the planning software. The innovative

and meaningful feature, presented in this thesis, will provide surgeons with an objective tool to extract patient-specific deltoid and rotator-cuff muscle information when evaluating the optimal position or comparing different designs.

6.3 Suggestions for future works

In the path towards a complete personalized approach to RSA, this thesis contributed to overcome some of the limitations affecting the design of custom implants and the preoperative planning for shoulder arthroplasty, as reported in Section 6.1. Additional research and significative efforts are still necessary to further prove the added values and extend the adoption of such technologies. During the development of the project, some initial work has been already carried out regarding the extension of this research, as discussed in detail in the remainder of this section.

Virtual Bench Test for design of custom shoulder implants

Currently, the generalizability of the VBT results is subject to certain limitations which need to be addressed. In particular, one of the stricter is the lack of an extensive validation, which was initially obtained only for a single design and under relatively limited degrees of freedom. The current mechanical tests were performed on commission of Materialise, in an external laboratory, certified for FDA clearance, thus limiting the possibility to conduct more experiments in which different design parameters were varied. For this reason, in the last part of the project, an in-house set-up was built, in collaboration with KU Leuven, to acquire additional mechanical evidences on the Glenius system (Figure 6.2).

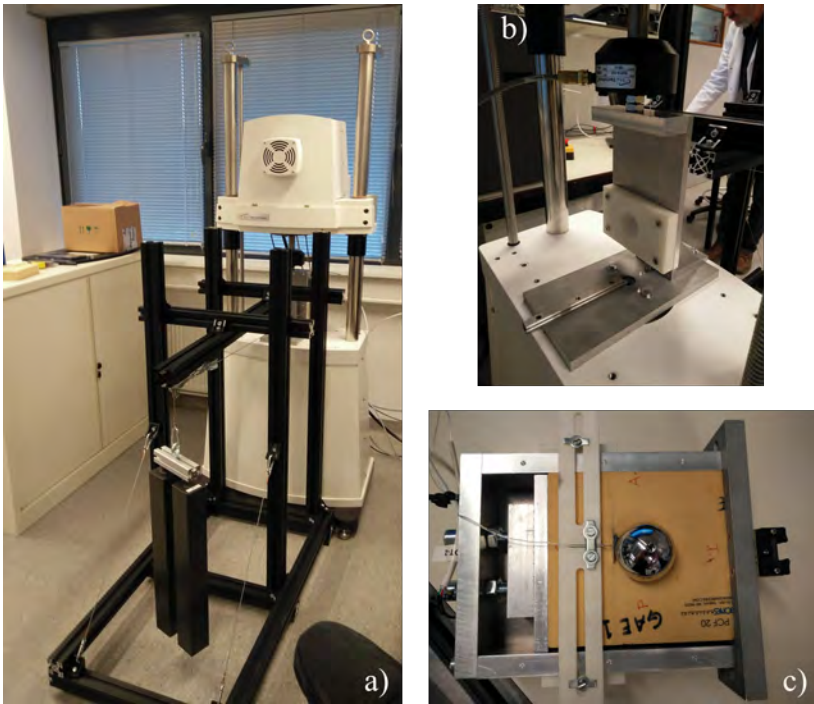


Figure 6.2: Details of the in-house set-up for shoulder loosening test. a) A pulley-mass system was used to generate the compressive load. b) The uniaxial testing machine applied the shear load through a custom-made actuator. c) A DVRT transducer was positioned inferiorly at the baseplate for displacement measurement along the S-I direction.

The custom-made set-up was inspired by the so-called Harman test, whose purpose is to mimic the rocking-horse phenomenon, thought to clinically contribute to glenoid loosening [10]. Briefly, the RSA glenoid component is inserted into a foam block, typically Sawbones, with material properties comparable to those of the human bone. A 756 N compressive force is applied while a fully reversed, cyclic transverse (shear) force of ± 756 N is applied in the superior-inferior (S-I) direction for a duration of 1000 cycles at a frequency of 0.05 Hz. A displacement sensor is then used to measure the baseplate motion relative to the foam block, along the S-I direction [76].

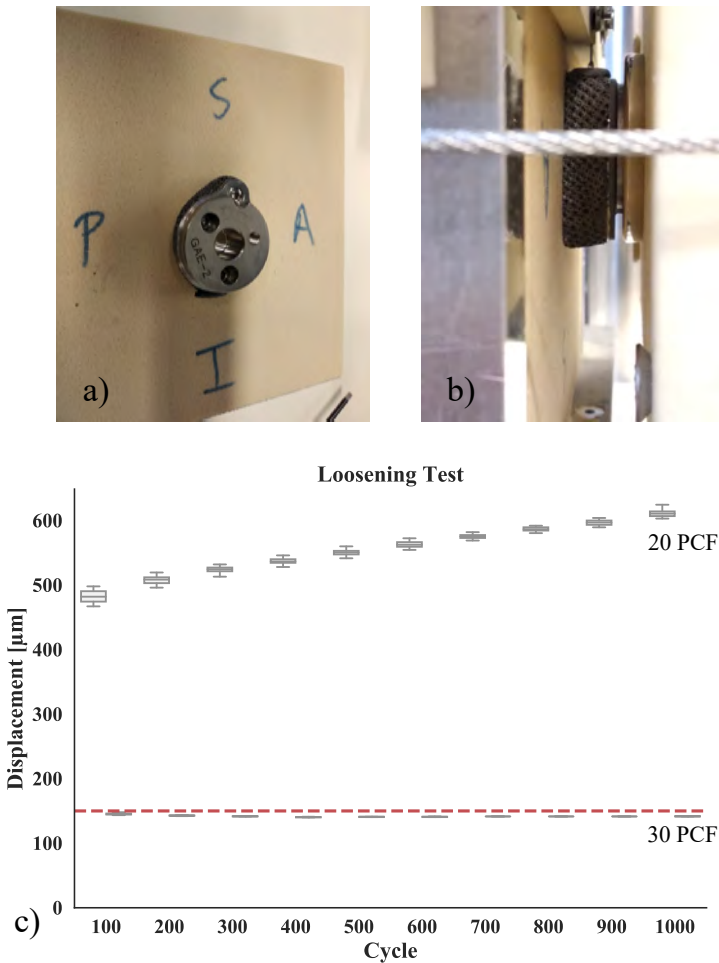


Figure 6.3: Loosening set-up: preliminary experiment. a) A trial implant was designed and printed to assess the impact of bone quality on the stability. b) A DVRT was used to measure baseplate displacement along the S-I direction. c) Displacement results for the 20 and 30 PCF foam blocks; the red line represents the 150 μm bone ingrowth threshold.

For the in-house assembly of the set-up, given the lack of a bi-axial loading machine, a pulley-mass system was used to generate the compressive load (Figure 6.2-a), while a dynamic uniaxial testing system (Electroforce 3330, TA Instruments, New Castle, US) applied the cyclic shear load (Figure 6.2-b). A

single gage-type differential variable reluctance transducer (DVRT, Model MG-DVRT, Microstrain, Burlington, VT) was placed in contact with the baseplate component to measure the displacements (Figure 6.2-c).

In a preliminary experiment, needed to demonstrate the correct operating of the set-up, a trial implant was designed and printed for the test (Figure 6.3). To assess the impact of bone quality on the prosthesis fixation, the implant was inserted into foam blocks with different densities, 20 and 30 PCF, representing respectively the low and high limits of the material properties for human cancellous bone. DVRT peak/valley data were acquired every 100 cycles and the displacement calculated as the average of the superior and inferior motion of the baseplate (Figure 6.3-b).

The results of the preliminary work show that that the fixation of the glenoid baseplate is sensitive to the quality of the bone, and confirm the ability of the experiment to provide useful information on the mechanical characterization of custom implants. In the future, the set-up can be used to extensively test design variations, (type, number and length of the screws, lateralization of the baseplate), and compare the displacement outcomes with other commercial implants or to assess if a certain configuration provides the initial stability necessary to achieve biological ingrowth (150 μm threshold). Moreover, those additional data will be useful to validate novel *in-silico* models, giving more strength to their predictive power also in a pre-clinical setting.

Assessment of scapular cortical thickness using statistical models

In the context of a personalized approach, computer aided technologies have a fundamental role in the acquisition of patient-specific information that is required to tailor a certain clinical treatment to the patient needs. In Chapter 4, a combined SSM including morphological and bone quality knowledge of the scapula was created to support the design of standard implants. The tool can be used for automatically generating a large population of scapulae and deducing statistics on the cortex, thus helping with the identification of the regions with best bone stock when planning the supporting screws.

However, it is recognized that additional steps are necessary to include the cortical thickness information, and more in general other bone quality features such as bone strength, into the optimization of screw proposal. During the course of the research, some work was done to bridge this gap.

In particular, a proof-of-concept study was set up to correlate screw fixation parameters, i.e. torque and compression force, to bone quality features, i.e. cortical thickness and bone densities around the screw, as described in [124]. In this first study, an experimental set-up was built to measure insertion force and torque in artificial bone samples of different quality, in order to estimate ranges

of optimal surgical values and give guidelines to maximize screw fixation and therefore initial implant stability (Figure 6.4-a). Insertion torque was measured till bone breaking and a mathematical model, based on linear regression, was fitted to the maximum values. The three experimentally investigated parameters were used as predictors of the torque: bone density, cortical thickness and intra-osseous screw length.

The obtained relationship linking tightening torque to cortical thickness, bone density and intra-osseous screw length should be helpful to further improve the optimal number and position of the screws that stabilize the baseplate of reversed shoulder prostheses. The analysis also showed that bone density is the parameter, among the ones investigated, which has the biggest impact on the resulting torque. This suggests that surgeons, when looking for suitable screw positions, should first consider trajectories along which bone density is the highest.

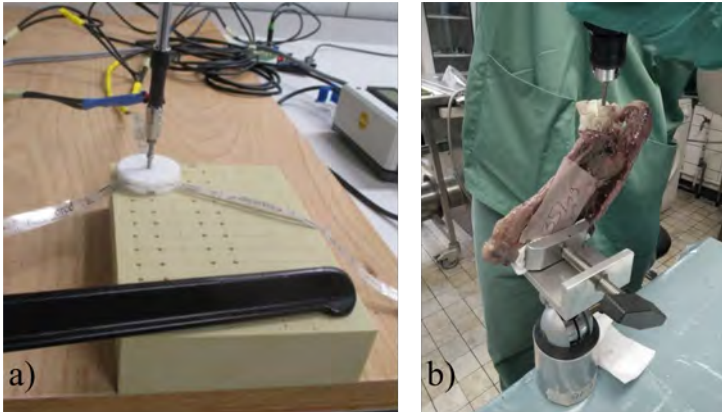


Figure 6.4: Screw fixation parameters, i.e. insertion torque and compression load, were measured using a custom-made set up in artificial (a) and cadaveric bones (b).

In an attempt to extend this conclusion to human models, torque measurements were also performed on 9 fresh-frozen cadaveric scapulae (Figure 6.4-b). While the test setup was successful in measuring the fixation parameters of the screws, due to the large variability of the samples (age, gender, pathological conditions), it was not possible to correlate CT information to the fixation parameters. Future work should focus on collecting more samples to create and validate a model for screw fixation prediction also in human bone.

Estimation of screw fixation from CT-data could be used to compare different screw positions and to provide a basis for the estimation of implant fixation using multiple screws. However, major fundamental research, which could also make use of more advanced technology such as machine learning, is still necessary to develop and validate a screw fixation model based on bone quality features.

Automated landmarking for muscle elongation measurement during RSA

The automated workflow introduced in Chapter 5 extends the current potentialities of the Materialise planner, allowing for a guided placement of the humeral component and an accurate measurement of muscle length variations after virtually implanting a prosthesis. With its clinical applicability being proven, surgeons can use this tool to gain more insight into the effect of implant positioning, trying to limit complications and maximize the postoperative functional patient outcome.

However, as previously mentioned, a major weakness is represented by the missing link between preoperative measurements and postoperative outcome. In fact, while the advancement of the technologies allows clinicians to extract multiple parameters, surgeons are not yet able to predict the functional results of a treatment. Bridging this gap should be the main goal of future works. In particular, regression models could be developed from retrospective datasets and evaluated through preoperative planning data and postoperative patient results, such as satisfaction scores or clinical complications.

With respect to the tools introduced in this thesis, additional research should focus on finding a potential correlation between measured deltoid elongation and postoperative RSA complications, such as joint instability and acromion fractures. In particular, joint instability is reported as the most common problem following RSA and can be caused by insufficient muscle tensioning or elongation [14, 165, 175]. In a possible application, muscle elongation measurements, together with other preoperative data (implant position, bone dimensions), could be included in a model to predict the risk of shoulder instability. A similar approach could be followed to predict acromion fracture risk.

A correlation between preoperative planning and clinical outcomes would not only increase the utility (and possible adoption) of preoperative systems, but also help clinicians to establish guidelines when deciding on the optimal position of an implant.

6.4 Conclusion

In this research, a major step was taken into the direction of a more personalized approach to Reverse Shoulder Arthroplasty, in which the surgical management, i.e. implant design and position, is adapted to the patient-specific characteristics and preoperative condition. Firstly, we applied a FE-based workflow to support the design of custom implants by predicting the initial stability, i.e. micromotion at the bone-implant interface. Secondly, we used a statistical shape model to combine the information of scapula bone morphology and cortical thickness in a novel tool, whose aim is to test the congruency of a new implant designs in a generated virtual population. Thirdly, we developed an automated method to indicate muscle attachment points and measure deltoid and rotator cuff elongations during pre-operative planning, and we demonstrated its usability in a clinical setting. Overall, by applying those methods in the clinical practice, design and planning process could be automated and standardized, thus reducing costs and lead times.

Besides the engineering improvements to the state-of-the-art, this thesis contributed to bridge the gap between fundamental research at the university and product development in a medical device company. The methods developed in this thesis not only underwent a scientific evaluation, but most of them were also transferred into commercial software or used as supporting tools in specific company processes, thus being subjected to additional operational requirements.

Thanks to the novel methods presented in this thesis, we expect in the future a wider adoption of the personalized approach in reverse shoulder arthroplasty, with important benefits both for surgeons and patients.

Chapter 7

Conclusiones

En esta investigación, se dio un paso importante en la dirección de un enfoque más personalizado de la artroplastia inversa de hombro, en el que el manejo quirúrgico, es decir, el diseño y la posición del implante, se adapta a las características específicas del paciente y al estado preoperatorio. En primer lugar, aplicamos un flujo de trabajo basado en EF para respaldar el diseño de implantes personalizados mediante la predicción de la estabilidad inicial, es decir, el micromovimiento en la interfaz hueso-implante. En segundo lugar, utilizamos un modelo estadístico de forma para combinar la información de la morfología del hueso de la escápula y el grosor cortical en una herramienta novedosa, cuyo objetivo es probar la congruencia de un nuevo diseño de implante en una población virtual generada. En tercer lugar, desarrollamos un método automatizado para indicar los puntos de inserción de los músculos y medir el alargamiento del deltoides y del manguito rotador durante la planificación preoperatoria, y demostramos su utilidad en un entorno clínico. En general, al aplicar esos métodos en la práctica clínica, el proceso de diseño y planificación podría automatizarse y estandarizarse, reduciendo así los costos y los plazos de entrega.

Además de las mejoras de ingeniería al estado de la técnica, esta tesis contribuyó a cerrar la brecha entre la investigación fundamental en la universidad y el desarrollo de productos en una empresa de dispositivos médicos. Los métodos desarrollados en esta tesis no solo fueron sometidos a una evaluación científica, sino que la mayoría de ellos también fueron transferidos a software comercial o utilizados como herramientas de soporte en procesos específicos de la empresa, siendo así sujetos a requisitos operativos adicionales.

Gracias a los métodos novedosos presentados en esta tesis, esperamos en el

futuro una adopción más amplia del abordaje personalizado en la artroplastia inversa de hombro, con importantes beneficios tanto para cirujanos como para pacientes.

Bibliography

- [1] Arthritis of the Shoulder - OrthoInfo - AAOS. <https://www.orthoinfo.org/en/diseases--conditions/arthritis-of-the-shoulder/>.
- [2] Avascular Necrosis (Osteonecrosis). <https://www.webmd.com/arthritis/avascular-necrosis-osteonecrosis-symptoms-treatments>. Library Catalog: www.webmd.com.
- [3] Mimics, Mimics Innovation Suite, Materialise NV, Heverlee, Belgium,. <http://biomedical.materialise.com/mimics>.
- [4] Virtual population analysis improves orthopedic implant design. https://www.odtmag.com/issues/2015-08-01/view_columns/virtual-population-analysis-improves-orthopedic-implant-design/. Library Catalog: www.odtmag.com.
- [5] X-ray of rheumatoid arthritis of the shoulder of a 28 year old woman, licensed under cc attribution 4.0 unported, 2016. https://commons.wikimedia.org/wiki/File:X-ray_of_rheumatoid_arthritis_of_the_shoulder.jpg.
- [6] US and European Markets for joint arthroplasty products. <https://pharmastore.informa.com/product/u-s-and-european-markets-for-joint-arthroplasty-products/>, 2016.
- [7] Global Shoulder Arthroplasty (Reverse Total Shoulder Arthroplasty, Total Shoulder Arthroplasty, Revision Shoulder Arthroplasty, Shoulder Resurfacing, Hemiarthroplasty) Market 2019-2023 - ResearchAndMarkets.com. <https://www.businesswire.com/news/home/20190801005893/en/Global-Shoulder-Arthroplasty-Reverse-Total-Shoulder-Arthroplasty>, Aug. 2019. Library Catalog: www.businesswire.com.

- [8] ABLER, D., BERGER, S., TERRIER, A., BECCE, F., FARRON, A., AND BÜCHLER, P. A statistical shape model to predict the premorbid glenoid cavity. *Journal of Shoulder and Elbow Surgery* 27, 10 (2018), 1800–1808.
- [9] ALETAHA, D., AND SMOLEN, J. S. Diagnosis and management of rheumatoid arthritis: A review. *Journal of the American Medical Association* 320, 13 (10 2018), 1360–1372.
- [10] ANGLIN, C., WYSS, U. P., AND PICHORA, D. R. Mechanical testing of shoulder prostheses and recommendations for glenoid design. *Journal of Shoulder and Elbow Surgery* 9, 4 (2000), 323–331.
- [11] ASTM. *Standard specification for cast cobalt-chromium-molybdenum alloy for surgical implant applications*. American Society for Testing and Materials International, 1997.
- [12] ASTM. *Standard practice for finite element analysis (FEA) of non-modular metallic orthopaedic hip femoral stems*. American Society for Testing and Materials International, 2013.
- [13] ASTM. *Standard Test Methods for Dynamic Evaluation of Glenoid Loosening Or Disassociation*. American Society for Testing and Materials International, 2014.
- [14] BARCO, R., SAVVIDOU, O. D., SPERLING, J. W., SANCHEZ-SOTELO, J., AND COFIELD, R. H. Complications in reverse shoulder arthroplasty. *EFORT Open Reviews* 1, 3 (2016), 72–80.
- [15] BARUI, S., CHATTERJEE, S., MANDAL, S., KUMAR, A., AND BASU, B. Microstructure and compression properties of 3D powder printed Ti-6Al-4V scaffolds with designed porosity: experimental and computational analysis. *Materials Science and Engineering: C* 70 (2017), 812–823.
- [16] BAULOT, E., SIRVEAUX, F., AND BOILEAU, P. Grammont’s idea: the story of paul Grammont’s functional surgery concept and the development of the reverse principle. *Clinical Orthopaedics and Related Research* 469, 9 (2011), 2425–2431.
- [17] BERGER, N. M., CRAIG, E. V., AND PETRIGLIANO, F. A. The use of a custom glenoid component for the treatment of severe glenoid bone loss in reverse total shoulder arthroplasty. *Techniques in Shoulder & Elbow Surgery* 15, 2 (2014), 51–54.
- [18] BERHOUE, J., GULOTTA, L., CHEN, X., DINES, D., WARREN, R., AND KONTAXIS, A. Neutral glenoid alignment in reverse shoulder arthroplasty does not guarantee decreased risk of impingement. *Journal of Orthopaedic Research* 36, 4 (2018), 1213–1219.

- [19] BESL, P. J., AND MCKAY, N. D. Method for registration of 3-D shapes. In *Sensor fusion IV: control paradigms and data structures* (1992), vol. 1611, International Society for Optics and Photonics, pp. 586–606.
- [20] BOAMPONG, D., GREEN, S., AND UNSWORTH, A. N+ ion implantation of Ti6Al4V alloy and UHMWPE for total joint replacement application. *Journal of Applied Biomaterials and Biomechanics* 1, 3 (2003), 164–171.
- [21] BOHSALI, K. I., BOIS, A. J., AND WIRTH, M. A. Complications of shoulder arthroplasty. *Journal of Bone and Joint Surgery* 99, 3 (2017), 256–269.
- [22] BOILEAU, P. Complications and revision of reverse total shoulder arthroplasty. *Orthopaedics & Traumatology: Surgery & Research* 102, 1 (2016), S33–S43.
- [23] BOILEAU, P., WATKINSON, D. J., HATZIDAKIS, A. M., AND BALG, F. Grammont reverse prosthesis: design, rationale, and biomechanics. *Journal of Shoulder and Elbow Surgery* 14, 1 (2005), S147–S161.
- [24] BONARETTI, S., SEILER, C., BOICHON, C., REYES, M., AND BÜCHLER, P. Image-based vs. mesh-based statistical appearance models of the human femur: implications for finite element simulations. *Medical Engineering & Physics* 36, 12 (2014), 1626–1635.
- [25] BOSELLI, K. J., AHMAD, C. S., AND LEVINE, W. N. Treatment of glenohumeral arthrosis. *The American Journal of Sports Medicine* 38, 12 (2010), 2558–2572.
- [26] BREMEN, S., MEINERS, W., AND DIATLOV, A. Selective laser melting: a manufacturing technology for the future? *Laser Technik Journal* 9, 2 (2012), 33–38.
- [27] BURTON, W. S., SINTINI, I., CHAVARRIA, J. M., BROWNHILL, J. R., AND LAZ, P. J. Assessment of scapular morphology and bone quality with statistical models. *Computer Methods in Biomechanics and Biomedical Engineering* 22, 4 (2019), 341–351.
- [28] BYUN, J. W., SHIM, J.-H., SHIN, W. J., AND CHO, S. Y. Rapid progressive atypical atraumatic osteonecrosis of humeral head: a case report. *Korean Journal of Anesthesiology* 66, 5 (2014), 398.
- [29] CAMPOCHIARO, G., REBUZZI, M., BAUDI, P., AND CATANI, F. Complex proximal humerus fractures: Hertel’s criteria reliability to predict head necrosis. *Musculoskeletal Surgery* 99, 1 (2015), 9–15.

- [30] CASIER, S. J., VAN DEN BROECKE, R., VAN HOUCKE, J., AUDENAERT, E., DE WILDE, L. F., AND VAN TONGEL, A. Morphologic variations of the scapula in 3-dimensions: a statistical shape model approach. *Journal of Shoulder and Elbow Surgery* 27, 12 (2018), 2224–2231.
- [31] CHAE, S.-W., KIM, S.-Y., LEE, H., YON, J.-R., LEE, J., AND HAN, S.-H. Effect of baseplate size on primary glenoid stability and impingement-free range of motion in reverse shoulder arthroplasty. *BMC Musculoskeletal Disorders* 15, 1 (2014), 417.
- [32] CHAE, S.-W., LEE, H., KIM, S. M., LEE, J., HAN, S.-H., AND KIM, S.-Y. Primary stability of inferior tilt fixation of the glenoid component in reverse total shoulder arthroplasty: a finite element study. *Journal of Orthopaedic Research* 34, 6 (2016), 1061–1068.
- [33] CHALLONER, D. R., AND SENATE, U. Medical devices and the public's health: the FDA 510 (k) clearance process at 35 years. *Written Statement before the Committee on Health, Education, Labor, and Pensions US Senate, Institute of Medicine of the National Academics, Washington* (2011).
- [34] CHALMERS, P. N., AND KEENER, J. D. Expanding roles for reverse shoulder arthroplasty. *Current Reviews in Musculoskeletal Medicine* 9, 1 (2016), 40–48.
- [35] CHAMMAA, R., URI, O., AND LAMBERT, S. Primary shoulder arthroplasty using a custom-made hip-inspired implant for the treatment of advanced glenohumeral arthritis in the presence of severe glenoid bone loss. *Journal of Shoulder and Elbow Surgery* 26, 1 (2017), 101–107.
- [36] CHANG, I.-R., AND VARACALLO, M. Anatomy, shoulder and upper limb, glenohumeral joint. *StatPearls* (2019).
- [37] CHILLEMI, C., AND FRANCESCHINI, V. Shoulder Osteoarthritis. *Arthritis* 2013 (2013).
- [38] CHO, H. J., MOREY, V., KANG, J. Y., KIM, K. W., AND KIM, T. K. Prevalence and risk factors of spine, shoulder, hand, hip, and knee osteoarthritis in community-dwelling Koreans older than age 65 years. *Clinical Orthopaedics and Related Research* 473, 10 (2015), 3307–3314.
- [39] CHRISTIE, M. J., BARRINGTON, S. A., BRINSON, M. F., RUHLING, M. E., AND DEBOER, D. K. Bridging massive acetabular defects with the triflange cup: 2-to 9-year results. *Clinical Orthopaedics and Related Research (1976-2007)* 393 (2001), 216–227.

- [40] CODSI, M. J., BENNETTS, C., POWELL, K., AND IANNOTTI, J. P. Locations for screw fixation beyond the glenoid vault for fixation of glenoid implants into the scapula: an anatomic study. *Journal of Shoulder and Elbow Surgery* 16, 3 (2007), S84–S89.
- [41] COOTES, T., BALDOCK, E., AND GRAHAM, J. An introduction to active shape models. *Image Processing and Analysis 243657* (2000), 223–248.
- [42] COOTES, T. F., AND TAYLOR, C. J. Statistical models of appearance for medical image analysis and computer vision. In *Medical Imaging 2001: Image Processing* (2001), vol. 4322, International Society for Optics and Photonics, pp. 236–248.
- [43] CUFF, D. J., PUPELLO, D. R., SANTONI, B. G., CLARK, R. E., AND FRANKLE, M. A. Reverse shoulder arthroplasty for the treatment of rotator cuff deficiency: a concise follow-up, at a minimum of 10 years, of previous reports. *Journal of Bone and Joint Surgery* 99, 22 (2017), 1895–1899.
- [44] DAALDER, M. A., VENNE, G., SHARMA, V., RAINBOW, M., BRYANT, T., AND BICKNELL, R. T. Trabecular bone density distribution in the scapula relevant to reverse shoulder arthroplasty. *Journal of Shoulder and Elbow Surgery open access* 2, 3 (2018), 174–181.
- [45] DANCKAERS, F., HUYSMANS, T., LACKO, D., LEDDA, A., VERWULGENT, S., VAN DONGEN, S., AND SIJBERS, J. Correspondence preserving elastic surface registration with shape model prior. In *2014 22nd International Conference on Pattern Recognition* (2014), IEEE, pp. 2143–2148.
- [46] DAVIES, R., TWINING, C., AND TAYLOR, C. *Statistical models of shape: Optimisation and evaluation*. Springer Science & Business Media, 2008.
- [47] DE BOER, F. A., AND HUIJSMANS, P. E. Use of a 3D-Printed custom reverse shoulder arthroplasty. *Techniques in Orthopaedics* 35, 1 (2020), 38–41.
- [48] DE WILDE, L., AUDENAERT, E., BARBAIX, E., AUDENAERT, A., AND SOUDAN, K. Consequences of deltoid muscle elongation on deltoid muscle performance: a computerised study. *Clinical Biomechanics* 17, 7 (2002), 499–505.
- [49] DEBEER, P., BERGHS, B., POULIART, N., VAN DEN BOGAERT, G., VERHAEGEN, F., AND NIJS, S. Treatment of severe glenoid deficiencies in reverse shoulder arthroplasty: the glenius glenoid reconstruction system experience. *Journal of Shoulder and Elbow Surgery* 28, 8 (2019), 1601–1608.

- [50] DENARD, P. J., LEDERMAN, E., PARSONS, B. O., AND ROMEO, A. A. Finite element analysis of glenoid-sided lateralization in reverse shoulder arthroplasty. *Journal of Orthopaedic Research* 35, 7 (2017), 1548–1555.
- [51] DENARD, P. J., PROVENCHER, M. T., LÄDERMANN, A., ROMEO, A. A., PARSONS, B. O., AND DINES, J. S. Version and inclination obtained with 3-dimensional planning in total shoulder arthroplasty: do different programs produce the same results? *Journal of Shoulder and Elbow Surgery Open Access* 2, 4 (2018), 200–204.
- [52] DEORE, V. T., GRIFFITHS, E., AND MONGA, P. Shoulder arthroplasty—past, present and future. *Journal of Arthroscopy and Joint Surgery* 5, 1 (2018), 3–8.
- [53] DHARIA, M., AND MANI, S. Impact of screw preload on primary stability in reverse shoulder arthroplasty. In *Orthopaedic Proceedings* (2019), vol. 101, The British Editorial Society of Bone & Joint Surgery, pp. 48–48.
- [54] DHARIA, M. A., BISCHOFF, J. E., AND SCHNEIDER, D. Impact of modeling assumptions on stability predictions in reverse total shoulder arthroplasty. *Frontiers in Physiology* 9 (2018), 1116.
- [55] DINES, D. M., GULOTTA, L., CRAIG, E. V., AND DINES, J. S. Novel solution for massive glenoid defects in shoulder arthroplasty: a patient-specific glenoid vault reconstruction system. *American Journal of Orthopedics* 46, 2 (2017), 104–108.
- [56] DISTEFANO, J. G., PARK, A. Y., NGUYEN, T.-Q. D., DIEDERICHS, G., BUCKLEY, J. M., AND MONTGOMERY III, W. H. Optimal screw placement for base plate fixation in reverse total shoulder arthroplasty. *Journal of Shoulder and Elbow Surgery* 20, 3 (2011), 467–476.
- [57] DRAKE, G. N., O’CONNOR, D. P., AND EDWARDS, T. B. Indications for reverse total shoulder arthroplasty in rotator cuff disease. *Clinical Orthopaedics and Related Research* 468, 6 (2010), 1526–1533.
- [58] DUBROW, S., STREIT, J. J., MUH, S., SHISHANI, Y., AND GOBEZIE, R. Acromial stress fractures: correlation with acromioclavicular osteoarthritis and acromiohumeral distance. *Orthopedics* 37, 12 (2014), e1074–e1079.
- [59] ECKLUND, K. J., LEE, T. Q., TIBONE, J., AND GUPTA, R. Rotator cuff tear arthropathy. *JAAOS-Journal of the American Academy of Orthopaedic Surgeons* 15, 6 (2007), 340–349.
- [60] ELHASSAN, B., OZBAYDAR, M., HIGGINS, L. D., AND WARNER, J. J. Glenoid reconstruction in revision shoulder arthroplasty. *Clinical Orthopaedics and Related Research* 466, 3 (2008), 599–607.

- [61] ELWELL, J., CHOI, J., AND WILLING, R. Quantifying the competing relationship between adduction range of motion and baseplate micromotion with lateralization of reverse total shoulder arthroplasty. *Journal of Biomechanics* 52 (2017), 24–30.
- [62] ERICKSON, B. J., CHALMERS, P. N., DENARD, P., LEDERMAN, E., HORNEFF, G., WERNER, B. C., PROVENCHER, M. T., AND ROMEO, A. A. Does commercially available shoulder arthroplasty preoperative planning software agree with surgeon measurements of version, inclination and subluxation? *Journal of Shoulder and Elbow Surgery* (2020).
- [63] FAMILIARI, F., ROJAS, J., NEDIM DORAL, M., HURI, G., AND MCFARLAND, E. G. Reverse total shoulder arthroplasty. *EFORT Open Reviews* 3, 2 (2018), 58–69.
- [64] FAVARD, L., LEVIGNE, C., NEROT, C., GERBER, C., DE WILDE, L., AND MOLE, D. Reverse prostheses in arthropathies with cuff tear: are survivorship and function maintained over time? *Clinical Orthopaedics and Related Research* 469, 9 (2011), 2469–2475.
- [65] FAVRE, P., AND HENDERSON, A. D. Prediction of stemless humeral implant micromotion during upper limb activities. *Clinical Biomechanics* 36 (2016), 46–51.
- [66] FAVRE, P., PERALA, S., VOGEL, P., FUCENTESE, S. F., GOFF, J. R., GERBER, C., AND SNEDEKER, J. G. In vitro assessments of reverse glenoid stability using displacement gages are misleading—recommendations for accurate measurements of interface micromotion. *Clinical Biomechanics* 26, 9 (2011), 917–922.
- [67] FEELEY, B. T., GALLO, R. A., AND CRAIG, E. V. Cuff tear arthropathy: current trends in diagnosis and surgical management. *Journal of Shoulder and Elbow Surgery* 18, 3 (2009), 484–494.
- [68] FORMAINI, N. T., EVERDING, N. G., LEVY, J. C., SANTONI, B. G., NAYAK, A. N., AND WILSON, C. Glenoid baseplate fixation using hybrid configurations of locked and unlocked peripheral screws. *Journal of Orthopaedics and Traumatology* 18, 3 (2017), 221–228.
- [69] FRANKLE, M. A., TERAMOTO, A., LUO, Z.-P., LEVY, J. C., AND PUPELLO, D. Glenoid morphology in reverse shoulder arthroplasty: classification and surgical implications. *Journal of Shoulder and Elbow Surgery* 18, 6 (2009), 874–885.
- [70] GEE, E. C., HANSON, E. K., AND SAITHNA, A. Reverse shoulder arthroplasty in rheumatoid arthritis: a systematic review. *The Open Orthopaedics Journal* 9 (2015), 237.

- [71] GRAHAM, P. Post-traumatic arthritis of the shoulder. *Orthopaedic Nursing* 38, 6 (2019), 398–400.
- [72] GRASSI, L., VÄÄNÄNEN, S. P., RISTINMAA, M., JURVELIN, J. S., AND ISAKSSON, H. Prediction of femoral strength using 3d finite element models reconstructed from DXA images: validation against experiments. *Biomechanics and Modeling in Mechanobiology* 16, 3 (2017), 989–1000.
- [73] GUERY, J., FAVARD, L., SIRVEAUX, F., OUDET, D., MOLE, D., AND WALCH, G. Reverse total shoulder arthroplasty: survivorship analysis of eighty replacements followed for five to ten years. *Journal of Bone and Joint Surgery* 88, 8 (2006), 1742–1747.
- [74] GUNTHER, S. B., AND LYNCH, T. L. Total shoulder replacement surgery with custom glenoid implants for severe bone deficiency. *Journal of Shoulder and Elbow Surgery* 21, 5 (2012), 675–684.
- [75] HAMID, N., CONNOR, P. M., FLEISCHLI, J. F., AND D’ALESSANDRO, D. F. Acromial fracture after reverse shoulder arthroplasty. *American Journal of Orthopedics (Belle Mead NJ)* 40, 7 (2011), E125–E129.
- [76] HARMAN, M., FRANKLE, M., VASEY, M., AND BANKS, S. Initial glenoid component fixation in “reverse” total shoulder arthroplasty: a biomechanical evaluation. *Journal of Shoulder and Elbow Surgery* 14, 1 (2005), S162–S167.
- [77] HOENECKE JR, H. R., FLORES-HERNANDEZ, C., AND D’LIMA, D. D. Reverse total shoulder arthroplasty component center of rotation affects muscle function. *Journal of Shoulder and Elbow Surgery* 23, 8 (2014), 1128–1135.
- [78] HOENIG, M. P., LOEFFLER, B., BROWN, S., PEINDL, R., FLEISCHLI, J., CONNOR, P., AND D’ALESSANDRO, D. Reverse glenoid component fixation: is a posterior screw necessary? *Journal of Shoulder and Elbow Surgery* 19, 4 (2010), 544–549.
- [79] HOFFELNER, T., MORODER, P., AUFFARTH, A., TAUBER, M., AND RESCH, H. Outcomes after shoulder arthroplasty revision with glenoid reconstruction and bone grafting. *International Orthopaedics* 38, 4 (2014), 775–782.
- [80] HOLLIS, R., AND YAMAGUCHI, K. Avascular necrosis of the shoulder. *Seminars in Arthroplasty* 19, 1 (Mar. 2008), 19–22.
- [81] HOLZBAUR, K. R., MURRAY, W. M., AND DELP, S. L. A model of the upper extremity for simulating musculoskeletal surgery and analyzing

- neuromuscular control. *Annals of Biomedical Engineering* 33, 6 (2005), 829–840.
- [82] HOPKINS, A. R., HANSEN, U. N., BULL, A. M., EMERY, R., AND AMIS, A. A. Fixation of the reversed shoulder prosthesis. *Journal of Shoulder and Elbow Surgery* 17, 6 (2008), 974–980.
- [83] IANNOTTI, J., BAKER, J., RODRIGUEZ, E., BREMS, J., RICCHETTI, E., MESIHA, M., AND BRYAN, J. Three-dimensional preoperative planning software and a novel information transfer technology improve glenoid component positioning. *Journal of Bone and Joint Surgery* 96, 9 (2014), e71.
- [84] IANNOTTI, J. P., AND FRANGIAMORE, S. J. Fate of large structural allograft for treatment of severe uncontained glenoid bone deficiency. *Journal of Shoulder and Elbow Surgery* 21, 6 (2012), 765–771.
- [85] IANNOTTI, J. P., WEINER, S., RODRIGUEZ, E., SUBHAS, N., PATTERSON, T. E., JUN, B. J., AND RICCHETTI, E. T. Three-dimensional imaging and templating improve glenoid implant positioning. *Journal of Bone and Joint Surgery* 97, 8 (2015), 651–658.
- [86] JARRETT, C. D., BROWN, B. T., AND SCHMIDT, C. C. Reverse shoulder arthroplasty. *Orthopedic Clinics* 44, 3 (2013), 389–408.
- [87] JASTY, M., BRAGDON, C., BURKE, D., O’CONNOR, D., LOWENSTEIN, J., AND HARRIS, W. H. In vivo skeletal responses to porous-surfaced implants subjected to small induced motions. *Journal of Bone and Joint Surgery* 79, 5 (1997), 707–714.
- [88] JOBIN, C. M., BROWN, G. D., BAHU, M. J., GARDNER, T. R., BIGLIANI, L. U., LEVINE, W. N., AND AHMAD, C. S. Reverse total shoulder arthroplasty for cuff tear arthropathy: the clinical effect of deltoid lengthening and center of rotation medialization. *Journal of Shoulder and Elbow Surgery* 21, 10 (2012), 1269–1277.
- [89] JOHNSON, V. L., AND HUNTER, D. J. The epidemiology of osteoarthritis. *Best Practice & Research Clinical Rheumatology* 28, 1 (2014), 5–15.
- [90] KAPTEIN, B., AND VAN DER HELM, F. Estimating muscle attachment contours by transforming geometrical bone models. *Journal of Biomechanics* 37, 3 (2004), 263–273.
- [91] KARELSE, A., LEURIDAN, S., VAN TONGEL, A., DEBEER, P., VAN DER SLOTEN, J., DENIS, K., AND DE WILDE, L. F. Consequences of reaming with flat and convex reamers for bone volume and surface area

- of the glenoid; a basic science study. *Journal of Orthopaedic Surgery and Research* 10, 1 (2015), 181.
- [92] KERR, R., RESNICK, D., PINEDA, C., AND HAGHIGHI, P. Osteoarthritis of the glenohumeral joint: a radiologic-pathologic study. *American Journal of Roentgenology* 144, 5 (1985), 967–972.
- [93] KWON, Y. W., POWELL, K. A., YUM, J. K., BREMS, J. J., AND IANNOTTI, J. P. Use of three-dimensional computed tomography for the analysis of the glenoid anatomy. *Journal of Shoulder and Elbow Surgery* 14, 1 (2005), 85–90.
- [94] LÄDERMANN, A., DENARD, P. J., BOILEAU, P., FARRON, A., DERANSART, P., AND WALCH, G. What is the best glenoid configuration in onlay reverse shoulder arthroplasty? *International Orthopaedics* 42, 6 (2018), 1339–1346.
- [95] LÄDERMANN, A., EDWARDS, T. B., AND WALCH, G. Arm lengthening after reverse shoulder arthroplasty: a review. *International Orthopaedics* 38, 5 (2014), 991–1000.
- [96] LAMECKER, H., SEEBASS, M., HEGE, H.-C., AND DEUFLHARD, P. A 3D statistical shape model of the pelvic bone for segmentation. In *Medical Imaging 2004: Image Processing* (2004), vol. 5370, International Society for Optics and Photonics, pp. 1341–1351.
- [97] LEHTINEN, J. T., TINGART, M. J., APRELEVA, M., AND WARNER, J. J. Total, trabecular, and cortical bone mineral density in different regions of the glenoid. *Journal of Shoulder and Elbow Surgery* 13, 3 (2004), 344–348.
- [98] MA, J., WANG, A., LIN, F., WESARG, S., AND ERDT, M. Nonlinear statistical shape modeling for ankle bone segmentation using a novel kernelized robust PCA. In *International Conference on Medical Image Computing and Computer-Assisted Intervention* (2017), Springer, pp. 136–143.
- [99] MARRA, M. A., VANHEULE, V., FLUIT, R., KOOPMAN, B. H., RASMUSSEN, J., VERDONSCHOT, N., AND ANDERSEN, M. S. A subject-specific musculoskeletal modeling framework to predict in vivo mechanics of total knee arthroplasty. *Journal of Biomechanical Engineering* 137, 2 (2015).
- [100] MATHEWS, S., BURKHARD, M., SERRANO, N., LINK, K., HÄUSLER, M., FRATER, N., FRANKE, I., BISCHOFBERGER, H., BUCK, F. M., GASCHO, D., ET AL. Glenoid morphology in light of anatomical and reverse total shoulder arthroplasty: a dissection-and 3D-CT-based study

- in male and female body donors. *BMC Musculoskeletal Disorders* 18, 1 (2017), 1–11.
- [101] MATIAS, R., ANDRADE, C., AND VELOSO, A. P. Accuracy of a transformation method to estimate muscle attachments based on three bony landmarks. *Computer Methods in Biomechanics and Biomedical Engineering* 14, 01 (2011), 73–78.
- [102] MCFARLAND, E. G., HURI, G., HYUN, Y. S., PETERSEN, S. A., AND SRIKUMARAN, U. Reverse total shoulder arthroplasty without bone-grafting for severe glenoid bone loss in patients with osteoarthritis and intact rotator cuff. *Journal of Bone and Joint Surgery* 98, 21 (2016), 1801.
- [103] MENGE, T. J., BOYKIN, R. E., BYRAM, I. R., AND BUSHNELL, B. D. A comprehensive approach to glenohumeral arthritis. *Southern medical journal* 107, 9 (2014), 567–573.
- [104] MERRILL, A., GUZMAN, K., AND MILLER, S. L. Gender differences in glenoid anatomy: an anatomic study. *Surgical and Radiologic Anatomy* 31, 3 (2009), 183–189.
- [105] MILLETT, P. J., GOBEZIE, R., AND BOYKIN, R. E. Shoulder osteoarthritis: diagnosis and management. *American Family Physician* 78, 5 (2008), 605–611.
- [106] MINNEMA, J., VAN EIJNATTEN, M., KOUW, W., DIBLEN, F., MENDRIK, A., AND WOLFF, J. Ct image segmentation of bone for medical additive manufacturing using a convolutional neural network. *Computers in biology and medicine* 103 (2018), 130–139.
- [107] MORGAN, S. J., FURRY, K., PAREKH, A. A., AGUDELO, J. F., AND SMITH, W. R. The deltoid muscle: an anatomic description of the deltoid insertion to the proximal humerus. *Journal of Orthopaedic Trauma* 20, 1 (2006), 19–21.
- [108] MUCCIOLI, G. M. M., FRATINI, S., RINALDI, V. G., CAMMISA, E., ALESI, D., DI SARSINA, T. R., LULLINI, G., GUERRA, E., AND ZAFFAGNINI, S. Anatomic shoulder arthroplasty: Causes and indications to surgery. In *Shoulder Arthroplasty*. Springer, 2020, pp. 47–52.
- [109] MUKAKA, M. M. A guide to appropriate use of correlation coefficient in medical research. *Malawi medical journal* 24, 3 (2012), 69–71.
- [110] MUTSVANGWA, T., WASSWA, W., BURDIN, V., BOROTIKAR, B., AND DOUGLAS, T. S. Interactive patient-specific 3D approximation of scapula

- bone shape from 2D X-ray images using landmark-constrained statistical shape model fitting. In *2017 39th Annual International Conference of the IEEE Engineering in Medicine and Biology Society (EMBC)* (2017), IEEE, pp. 1816–1819.
- [111] NATIONS, U. World population to 2300. *United Nations: New York, NY* (2004).
- [112] NEER 2ND, C., CRAIG, E., AND FUKUDA, H. Cuff-tear arthropathy. *The Journal of Bone and Joint surgery. American volume* 65, 9 (1983), 1232–1244.
- [113] NOOTHOUT, J. M., DE VOS, B. D., WOLTERINK, J. M., LEINER, T., AND IŠGUM, I. CNN-based landmark detection in cardiac CTA scans. *arXiv preprint arXiv:1804.04963* (2018).
- [114] NORRIS, T. R., KELLY, J. D., HUMPHREY, C. S., ET AL. Management of glenoid bone defects in revision shoulder arthroplasty: a new application of the reverse total shoulder prosthesis. *Techniques in Shoulder & Elbow Surgery* 8, 1 (2007), 37–46.
- [115] ÖZMANEVRA, R., AND KAYA, E. Anterior deltoid insertion distance to various bony landmarks before and after humeral head lateralization. *Acta Medica Alanya* 3, 1, 17–20.
- [116] PARSONS, M., GREENE, A., POLAKOVIC, S., BYRAM, I., CHEUNG, E., JONES, R., PAPANDREA, R., YOUNDERIAN, A., WRIGHT, T., FLURIN, P.-H., ET AL. Assessment of surgeon variability in preoperative planning of reverse total shoulder arthroplasty: a quantitative comparison of 49 cases planned by 9 surgeons. *Journal of Shoulder and Elbow Surgery* (2020).
- [117] PARVIZI, J., AND KIM, G. K. Chapter 196 - Rotator Cuff Tear. In *High Yield Orthopaedics*, J. Parvizi and G. K. Kim, Eds. W.B. Saunders, Philadelphia, Jan. 2010, pp. 408–410.
- [118] PAYER, C., ŠTERN, D., BISCHOF, H., AND URSCHLER, M. Regressing heatmaps for multiple landmark localization using CNNs. In *International Conference on Medical Image Computing and Computer-Assisted Intervention* (2016), Springer, pp. 230–238.
- [119] PELLIKAAN, P., VAN DER KROGT, M., CARBONE, V., FLUIT, R., VIGNERON, L., VAN DEUN, J., VERDONSCHOT, N., AND KOOPMAN, H. F. Evaluation of a morphing based method to estimate muscle attachment sites of the lower extremity. *Journal of Biomechanics* 47, 5 (2014), 1144–1150.

- [120] PETERSSON, C. J. Degeneration of the gleno-humeral joint: an anatomical study. *Acta Orthopaedica Scandinavica* 54, 2 (1983), 277–283.
- [121] PITOCCHI, J., PLESSERS, K., WIRIX-SPEETJENS, R., DEBEER, P., VAN LENTHE, G. H., JONKERS, I., PÉREZ, M. A., AND VANDER SLOTEN, J. Automated muscle elongation measurement during reverse shoulder arthroplasty planning. *Journal of Shoulder and Elbow Surgery* (2020).
- [122] PITOCCHI, J., WESSELING, M., VAN LENTHE, G. H., AND PÉREZ, M. A. Finite element analysis of custom shoulder implants provide accurate prediction of initial stability. *Mathematics* 8, 7 (2020), 1113.
- [123] PITOCCHI, J., WIRIX-SPEETJENS, R., VAN LENTHE, G. H., AND PÉREZ, M. Á. Integration of cortical thickness data in a statistical shape model of the scapula. *Computer Methods in Biomechanics and Biomedical Engineering* (2020), 1–7.
- [124] PITOCCHI, J., WIRIX-SPEETJENS, R., VAN LENTHE, G. H., AND PEREZ, M. A. Measuring tightening torque and force of non-locking screws for reverse shoulder prosthesis. In *Orthopaedic Proceedings* (2020), vol. 102, The British Editorial Society of Bone & Joint Surgery, pp. 75–75.
- [125] PLESSERS, K., BERGHE, P. V., VAN DIJCK, C., WIRIX-SPEETJENS, R., DEBEER, P., JONKERS, I., AND VANDER SLOTEN, J. Virtual reconstruction of glenoid bone defects using a statistical shape model. *Journal of Shoulder and Elbow Surgery* 27, 1 (2018), 160–166.
- [126] PLESSERS, K., VERHAEGEN, F., VAN DIJCK, C., WIRIX-SPEETJENS, R., DEBEER, P., JONKERS, I., AND VANDER SLOTEN, J. Automated quantification of glenoid bone defects using 3-dimensional measurements. *Journal of Shoulder and Elbow Surgery* (2020).
- [127] POLTARETSKYI, S., CHAOUI, J., MAYYA, M., HAMITOUCHE, C., BERCIK, M., BOILEAU, P., AND WALCH, G. Prediction of the pre-morbid 3D anatomy of the proximal humerus based on statistical shape modelling. *The bone & joint journal* 99, 7 (2017), 927–933.
- [128] PREVRHAL, S., ENGELKE, K., AND KALENDER, W. A. Accuracy limits for the determination of cortical width and density: the influence of object size and CT imaging parameters. *Physics in Medicine & Biology* 44, 3 (1999), 751.
- [129] REDERT, A., KAPTEIN, B., REINDERS, M., VAN DEN EELAART, I., AND HENDRIKS, E. Extraction of semantic 3D models of human faces from stereoscopic image sequences. *Acta Stereologica* 18 (1999), 255–264.

- [130] ROCHE, C. P., DIEP, P., HAMILTON, M., CROSBY, L. A., FLURIN, P.-H., WRIGHT, T. W., ZUCKERMAN, J. D., AND ROUTMAN, H. D. Impact of inferior glenoid tilt, humeral retroversion, bone grafting, and design parameters on muscle length and deltoid wrapping in reverse shoulder arthroplasty. *Bulletin of the Hospital for Joint Diseases* 71, 4 (2013).
- [131] RODRÍGUEZ, J. A., ENTEZARI, V., IANNOTTI, J. P., AND RICCHETTI, E. T. Pre-operative planning for reverse shoulder replacement: the surgical benefits and their clinical translation. *Annals OF Joint* 4, 1 (2019).
- [132] SALHI, A., BURDIN, V., MUTSVANGWA, T., SIVARASU, S., BROCHARD, S., AND BOROTIKAR, B. Subject-specific shoulder muscle attachment region prediction using statistical shape models: A validity study. In *2017 39th Annual International Conference of the IEEE Engineering in Medicine and Biology Society (EMBC)* (2017), IEEE, pp. 1640–1643.
- [133] SAMITIER, G., ALENTORN-GELI, E., TORRENS, C., AND WRIGHT, T. W. Reverse shoulder arthroplasty. Part 1: systematic review of clinical and functional outcomes. *International Journal of Shoulder Surgery* 9, 1 (2015), 24.
- [134] SANCHEZ-SOTELO, J., COFIELD, R. H., AND ROWLAND, C. M. Shoulder hemiarthroplasty for glenohumeral arthritis associated with severe rotator cuff deficiency. *Journal of Bone and Joint Surgery* 83, 12 (2001), 1814–1822.
- [135] SARKALKAN, N., WEINANS, H., AND ZADPOOR, A. A. Statistical shape and appearance models of bones. *Bone* 60 (2014), 129–140.
- [136] SAUL, K. R., HU, X., GOEHLER, C. M., VIDT, M. E., DALY, M., VELISAR, A., AND MURRAY, W. M. Benchmarking of dynamic simulation predictions in two software platforms using an upper limb musculoskeletal model. *Computer Methods in Biomechanics and Biomedical Engineering* 18, 13 (2015), 1445–1458.
- [137] SCALISE, J. J., BRYAN, J., POLSTER, J., BREMS, J. J., AND IANNOTTI, J. P. Quantitative analysis of glenoid bone loss in osteoarthritis using three-dimensional computed tomography scans. *Journal of Shoulder and Elbow Surgery* 17, 2 (2008), 328–335.
- [138] SCALISE, J. J., AND IANNOTTI, J. P. Bone grafting severe glenoid defects in revision shoulder arthroplasty. *Clinical Orthopaedics and Related Research* 466, 1 (2008), 139–145.

- [139] SCHROEDER, W. J., LORENSEN, B., AND MARTIN, K. *The visualization toolkit: an object-oriented approach to 3D graphics*. Kitware, 2004.
- [140] SCHULTZ, C., RODRIGUEZ-OLIVARES, R., BOSMANS, J., LEFEVRE, T., DE SANTIS, G., BRUINING, N., COLLAS, V., DEZUTTER, T., BOSMANS, B., RAHHAB, Z., ET AL. Patient-specific image-based computer simulation for the prediction of valve morphology and calcium displacement after TAVI with the Medtronic CoreValve and the Edwards SAPIEN valve. *EuroIntervention* 11, 9 (2016), 1044–1052.
- [141] SEIM, H., KAINMUELLER, D., HELLER, M., ZACHOW, S., AND HEGE, H.-C. Automatic extraction of anatomical landmarks from medical image data: An evaluation of different methods. In *2009 IEEE International Symposium on Biomedical Imaging: From Nano to Macro* (2009), IEEE, pp. 538–541.
- [142] SHETH, U., AND SALTZMAN, M. Reverse total shoulder arthroplasty: Implant design considerations. *Current Reviews in Musculoskeletal Medicine* 12, 4 (2019), 554–561.
- [143] SHIELDS, E., KOUeiter, D. M., AND WIATER, J. M. Rate of improvement in outcomes measures after reverse total shoulder arthroplasty: A longitudinal study with 2-year follow-up. *Journal of Shoulder and Elbow Arthroplasty* 3 (2019), 2471549219861446.
- [144] SINTINI, I., BURTON, W. S., SADE SR, P., CHAVARRIA, J. M., AND LAZ, P. J. Investigating gender and ethnicity differences in proximal humeral morphology using a statistical shape model. *Journal of Orthopaedic Research®* 36, 11 (2018), 3043–3052.
- [145] SMITHERS, C. J., YOUNG, A. A., AND WALCH, G. Reverse shoulder arthroplasty. *Current Reviews in Musculoskeletal Medicine* 4, 4 (2011), 183.
- [146] SONG, J., CHANG, R. W., AND DUNLOP, D. D. Population impact of arthritis on disability in older adults. *Arthritis Care & Research: Official Journal of the American College of Rheumatology* 55, 2 (2006), 248–255.
- [147] SPRENGEL, R., ROHR, K., AND STIEHL, H. S. Thin-plate spline approximation for image registration. In *Proceedings of 18th Annual International Conference of the IEEE Engineering in Medicine and Biology Society* (1996), vol. 3, IEEE, pp. 1190–1191.
- [148] STOFFELEN, D. V., ERAly, K., AND DEBEER, P. The use of 3D printing technology in reconstruction of a severe glenoid defect: a case report with 2.5 years of follow-up. *Journal of Shoulder and Elbow Surgery* 24, 8 (2015), e218–e222.

- [149] STOLK, J., JANSSEN, D., HUISKES, R., AND VERDONSCHOT, N. Finite element-based preclinical testing of cemented total hip implants. *Clinical Orthopaedics and Related Research (1976-2007)* 456 (2007), 138–147.
- [150] STROUD, N., DIPAOLO, M. J., FLURIN, P.-H., ROCHE, C. P., ET AL. Reverse shoulder glenoid loosening: an evaluation of the initial fixation associated with six different reverse shoulder designs. *Bulletin of the NYU Hospital for Joint Diseases* 71, 2 (2013), S12.
- [151] SUAREZ, D., VAN DER LINDEN, J., VALSTAR, E., BROOMANS, P., POORT, G., ROZING, P., AND VAN KEULEN, F. Influence of the positioning of a cementless glenoid prosthesis on its interface micromotions. *Proceedings of the Institution of Mechanical Engineers, Part H: Journal of Engineering in Medicine* 223, 7 (2009), 795–804.
- [152] SUAREZ, D. R., VALSTAR, E. R., ROZING, P. M., AND VAN KEULEN, F. Fracture risk and initial fixation of a cementless glenoid implant: The effect of numbers and types of screws. *Proceedings of the Institution of Mechanical Engineers, Part H: Journal of Engineering in Medicine* 227, 10 (2013), 1058–1066.
- [153] THON, S. G., SEIDL, A. J., BRAVMAN, J. T., MCCARTY, E. C., SAVOIE, F. H., AND FRANK, R. M. Advances and update on reverse total shoulder arthroplasty. *Current Reviews in Musculoskeletal Medicine* 13, 1 (2020), 11–19.
- [154] TITCHENER, A., TAMBE, A., AND CLARK, D. Reverse shoulder arthroplasty: is reverse the way forward? *Bone & Joint* 360 6, 4 (2017), 2–7.
- [155] TREECE, G. M., GEE, A. H., MAYHEW, P., AND POOLE, K. E. High resolution cortical bone thickness measurement from clinical CT data. *Medical Image Analysis* 14, 3 (2010), 276–290.
- [156] VAN DEN BROECK, J., VEREECKE, E., WIRIX-SPEETJENS, R., AND VANDER SLOTEN, J. Segmentation accuracy of long bones. *Medical Engineering & Physics* 36, 7 (2014), 949–953.
- [157] VANDEN BERGHE, P., DEMOL, J., GELAUDE, F., AND VANDER SLOTEN, J. Virtual anatomical reconstruction of large acetabular bone defects using a statistical shape model. *Computer Methods in Biomechanics and Biomedical Engineering* 20, 6 (2017), 577–586.
- [158] VICECONTI, M., PAPPALARDO, F., RODRIGUEZ, B., HORNER, M., BISCHOFF, J., AND TSHINANU, F. M. In silico trials: Verification, validation and uncertainty quantification of predictive models used in the regulatory evaluation of biomedical products. *Methods* (2020).

- [159] VICTOR, J., VAN DONINCK, D., LABEY, L., INNOCENTI, B., PARIZEL, P., AND BELLEMANS, J. How precise can bony landmarks be determined on a CT scan of the knee? *The knee* 16, 5 (2009), 358–365.
- [160] VIRANI, N. A., HARMAN, M., LI, K., LEVY, J., PUPELLO, D. R., AND FRANKLE, M. A. In vitro and finite element analysis of glenoid bone/baseplate interaction in the reverse shoulder design. *Journal of Shoulder and Elbow Surgery* 17, 3 (2008), 509–521.
- [161] V&V40, A. Assessing credibility of computational modeling through verification and validation: application to medical devices. *The American Society of Mechanical Engineers* (2018).
- [162] WALCH, G., BACLE, G., LADERMANN, A., NOVE-JOSSERAND, L., AND SMITHERS, C. J. Do the indications, results, and complications of reverse shoulder arthroplasty change with surgeon’s experience? *Journal of Shoulder and Elbow Surgery* 21, 11 (2012), 1470–1477.
- [163] WALKER, M., BROOKS, J., WILLIS, M., AND FRANKLE, M. How reverse shoulder arthroplasty works. *Clinical Orthopaedics and Related Research* 469, 9 (2011), 2440–2451.
- [164] WARFIELD, S. K., ZOU, K. H., AND WELLS, W. M. Validation of image segmentation and expert quality with an expectation-maximization algorithm. In *International Conference on Medical Image Computing and Computer-Assisted Intervention* (2002), Springer, pp. 298–306.
- [165] WERNER, C., STEINMANN, P., GILBART, M., AND GERBER, C. Treatment of painful pseudoparesis due to irreparable rotator cuff dysfunction with the delta III reverse-ball-and-socket total shoulder prosthesis. *Journal of Bone and Joint Surgery* 87, 7 (2005), 1476–1486.
- [166] WERTHEL, J.-D., SCHOCH, B. S., VAN VEEN, S. C., ELHASSAN, B. T., AN, K.-N., COFIELD, R. H., AND SPERLING, J. W. Acromial fractures in reverse shoulder arthroplasty: a clinical and radiographic analysis. *Journal of Shoulder and Elbow Arthroplasty* 2 (2018).
- [167] WESTERMANN, R. W., PUGELY, A. J., MARTIN, C. T., GAO, Y., WOLF, B. R., AND HETTRICH, C. M. Reverse shoulder arthroplasty in the United States: a comparison of national volume, patient demographics, complications, and surgical indications. *The Iowa Orthopaedic Journal* 35 (2015), 1.
- [168] WIEDING, J., SOUFFRANT, R., FRITSCHKE, A., MITTELMEIER, W., AND BADER, R. Finite element analysis of osteosynthesis screw fixation in the bone stock: an appropriate method for automatic screw modelling. *PloS one* 7, 3 (2012).

- [169] WILLIAMS JR, G. R., AND IANNOTTI, J. P. Options for glenoid bone loss: composites of prosthetics and biologics. *Journal of Shoulder and Elbow Surgery* 16, 5 (2007), S267–S272.
- [170] WRIGHT, J., POTTS, C., SMYTH, M. P., FERRARA, L., SPERLING, J. W., AND THROCKMORTON, T. W. A quantitative analysis of the effect of baseplate and glenosphere position on deltoid lengthening in reverse total shoulder arthroplasty. *International Journal of Shoulder Surgery* 9, 2 (2015), 33.
- [171] WYLIE, J. D., AND TASHJIAN, R. Z. Planning software and patient-specific instruments in shoulder arthroplasty. *Current Reviews in Musculoskeletal Medicine* 9, 1 (2016), 1–9.
- [172] ZHANG, J., HISLOP-JAMBRICH, J., AND BESIER, T. F. Predictive statistical models of baseline variations in 3-D femoral cortex morphology. *Medical Engineering & Physics* 38, 5 (2016), 450–457.
- [173] ZHANG, Y., AHN, P. B., FITZPATRICK, D. C., HEINER, A. D., POGGIE, R. A., AND BROWN, T. D. Interfacial frictional behavior: cancellous bone, cortical bone, and a novel porous tantalum biomaterial. *Journal of Musculoskeletal Research* 3, 04 (1999), 245–251.
- [174] ZHENG, Y., LIU, D., GEORGESCU, B., NGUYEN, H., AND COMANICIU, D. 3D deep learning for efficient and robust landmark detection in volumetric data. In *International Conference on Medical Image Computing and Computer-Assisted Intervention* (2015), Springer, pp. 565–572.
- [175] ZUMSTEIN, M. A., PINEDO, M., OLD, J., AND BOILEAU, P. Problems, complications, reoperations, and revisions in reverse total shoulder arthroplasty: a systematic review. *Journal of Shoulder and Elbow Surgery* 20, 1 (2011), 146–157.

This is curriculum

Personal Data

Name: Jonathan Pitocchi
Date of birth: 11th of June, 1992
Place of birth: Citta' di Castello, Italy

Work address: Materialise nv, Technologielaan 15 - 3001
Leuven - Belgium
Email: jonathan.pitocchi@materialise.be
Alt. email: jonathan.pitocchi@gmail.com

Education & Experience

2017:2020 PhD candidate University of Zaragoza and KU
Leuven
2017:2020 Research Engineer at Materialise n.v.
2017: Intern at "Istituto Ortopedico Rizzoli",
Bologna, Italy
2014:2017 Master of Biomedical Engineer, University of
Bologna
2011:2014 Bachelor of Biomedical Engineer, University of
Bologna

Publications

Publications in International Peer Reviewed Journals

Pitocchi, J., Wirix-Speetjens, R., van Lenthe, G. H., and Pérez, M. Á. Integration of cortical thickness data in a statistical shape model of the scapula. *Computer Methods in Biomechanics and Biomedical Engineering* (2020), 1–7

Pitocchi, J., Wesseling, M., van Lenthe, G. H., and Pérez, M. Á. Finite Element Analysis of Custom Shoulder Implants Provides Accurate Prediction of Initial Stability. *Mathematics* 8, 7 (2020), 1113

Pitocchi, J., Plessers, K., Wirix-Speetjens, R., Debeer, P., van Lenthe, G. H., Jonkers, I., Pérez, M. Á., and Vander Sloten, J. Automated muscle elongation measurement during reverse shoulder arthroplasty planning. *Journal of Shoulder and Elbow Surgery* (2020)

Schileo, E., **Pitocchi, J.**, Falcinelli, C., and Taddei, F. Cortical bone mapping improves finite element strain prediction accuracy at the proximal femur. *Bone* (2020), 115348

Nasello, G., Vautrin A., **Pitocchi J.**, Wesseling M., Kuiper J. H., Pérez, M. Á., Garcia-Aznar J. M. Mechano-driven regeneration predicts response variations in large animal model based on scaffold implantation site and individual mechano-sensitivity. *Bone* submitted June 2020

Meeting abstracts, presented at international scientific conferences and symposia, published or not published in proceedings or journals

Pitocchi, J., Plessers, K., Wesseling, M., van Lenthe, G. H., and Pérez, M. Á. Automatic muscle elongation measurement during shoulder arthroplasty planning. (2020). *International Society for Computer Assisted Orthopaedic Surgery*, Brest, 10-13 June.

Pitocchi, J., Wirix-Speetjens, R., van Lenthe, G. H., and Pérez, M. Á. Measuring tightening torque and force of nonlocking screws for reverse shoulder prosthesis. (2019). *32nd Annual Congress International Society for Technology in Arthroplasty*, Toronto, 2-5 October.

Pitocchi, J., Wirix-Speetjens, R., van Lenthe, G. H., and Pérez, M. Á. Virtual assessment of reverse shoulder implant fixation through statistical model and finite element analysis. (2019). *25th Congress of the European Society of*

Biomechanics, Vienna, 7-10 July.

Pitocchi, J., Vanden Berghe P., Pérez, M. Á., and Wirix-Speetjens, R. Integration of Cortical Thickness data in a Statistical Shape Model of the Scapula. (2018). *Virtual Physiological Human Conference*, Zaragoza, 5-7 September.

Pitocchi, J., Vanden Berghe P., Wirix-Speetjens, R., and Pérez, M. Á. Predicting micro-motion for custom shoulder implants: a finite element model sensitivity analysis. (2018). *8th World Congress of Biomechanics*, Dublin, 8-12 July.

FACULTY OF ENGINEERING SCIENCE
DEPARTMENT OF MECHANICAL ENGINEERING
BIOMECHANICS SECTION
Celestijnenlaan 300C box 2419
B-3001 Leuven
jonathan.pitocchi@kuleuven.be
<https://www.mech.kuleuven.be/en/bme>

